Zero mean curvature surfaces of Bonnet-type

Cho, Joseph

(Degree)
博士（理学）

(Date of Degree)
2019-09-25

(Date of Publication)
2020-09-01

(Resource Type)
doctoral thesis

(Report Number)
甲第7583号

(URL)
https://hdl.handle.net/20.500.14094/D1007583

博　士　論　文

Zero mean curvature surfaces of Bonnet-type

(ボネ型平均曲率零曲面)

令和元年 7 月

神戸大学大学院理学研究科

CHO JOSEPH

Contents

Abstract

This thesis concerns planar curvature lines of zero mean curvature surfaces in various space-forms. Using an analytic approach, we give the classification of maximal surfaces and timelike minimal surfaces with planar curvature lines, which this thesis refers to as zero mean curvature surfaces of Bonnet-type. In addition, we establish the existence of deformations consisting exactly of all surfaces in each class, while the singularities appearing on these surfaces are recognized. In the timelike minimal case, we give a further characterization of Bonnet-type surfaces using the generating null curves. Then in the discrete setting, we establish a relationship between plane symmetry and line symmetry appearing on a discrete minimal surface, and give numerical examples of discrete minimal surfaces with non-trivial topology. Finally, we provide an elementary introduction to Lorentz-Möbius geometry.

Acknowledgements

First, I would like to thank my supervisor Professor Wayne Rossman for his guidance in my research. His seemingly endless patience with me and encouragement was not only what made this thesis possible but also a source for inspiration for me to envision myself staying in research. I cannot thank him enough for being the exemplary researcher that I one day aspire to be.

I would also like to express my gratitude to Professor Seong-Deog Yang for giving me an opportunity to continue my career that seemed all but over. Furthermore, I am very grateful to Professor Francis Burstall and Professor Udo Hertrich-Jeromin for the insightful conversations and explanations that helped me grasp and appreciate the beauty in this field.

I have had amazing opportunities to meet and discuss mathematics with wonderful mathematicians, and I am thankful to them for the utterly enjoyable conversations that deepened my knowledge and appreciation of the field: Shintaro Akamine, Callum Kemp, Katrin Leschke, Christian Müller, Kosuke Naokawa, Yuta Ogata, Mason Pember, Denis Polly, Kentaro Saji, Gudrun Szewieczek, and Masashi Yasumoto. Especially, I am grateful to Yuta Ogata for being the first one to reach out to me in Kobe, resulting in many late night conversations that ended up developing into research projects. I also thank Mason Pember not only for introducing me to sphere geometries and showing immense patience through all my questions, but also for his wonderful friendship.

I am grateful to the support I received during my doctoral program: Japanese government scholarship from Ministry of Education, Culture, Sports, Science and Technology (MEXT); JSPS/FWF Bilateral Joint Project I3809-N32 "Geometric shape generation"; and Grant-in-Aid for JSPS Fellows No. 19J10679.

My life would be nowhere near where it is now without the amazing love shown by my parents time and time again. Thank you.

Finally, I would like to thank God for his faithfulness throughout the years of me playing hide-and-seek with Him. It was His divine and unrelenting love that made all this possible.

Chapter 1

Introduction

Minimal surfaces with planar curvature lines in the Euclidean 3-space were first considered by Bonnet in [20], where he found the family of surfaces defined by

$$\begin{pmatrix} \cos(im)x + \sin(im)\sin(ix)\cos(y) \\ i\sin(im)x + \cos(im)\cos(ix)\sin(y) \\ \cos(ix)\cos(y) \end{pmatrix} \tag{1.1}$$

for a some constant $m \in \mathbb{R}$, now commonly referred to as *Bonnet's minimal surfaces*. (Note that one obtains a catenoid when $m = 0$.) However, he did not note the Enneper surface defined in [41] also has planar curvature lines (cf. [88, p. 164]).

On the other hand, the study of minimal surfaces was greatly aided by the Weierstrass representation formula for minimal surfaces [114], which we recall below.

Fact 1.1. *Any minimal surface $f : \Sigma \subset \mathbb{C} \to \mathbb{R}^3$ can be locally represented as*

$$f = \operatorname{Re} \int \Big(1 - h^2, i(1 + h^2), 2h\Big)\, \eta \, \mathrm{d}z$$

over a simply-connected domain Σ on which h is meromorphic, while η and $h^2\eta$ are holomorphic.

Using the Weierstrass data $(h, \eta\,\mathrm{d}z)$ and the representation, one can give a classification of minimal surfaces with planar curvature lines, which this thesis refers to as *minimal surfaces of Bonnet-type*, as follows:

Fact 1.2 ([20, 41])**.** *A minimal surface of Bonnet-type in Euclidean space $\mathbb{R}^3$ must be a piece of one, and only one, of*

- *plane* $(0, 1\,\mathrm{d}z)$,
- *catenoid* $(e^z, e^{-z}\,\mathrm{d}z)$,
- *Enneper surface* $(z, 1\,\mathrm{d}z)$, *or*
- *one of the Bonnet's minimal surfaces* $\{(e^z + t, e^{-z}\,\mathrm{d}z), t > 0\}$,

up to isometries and homotheties of $\mathbb{R}^3$.

Remark 1.3. The Weierstrass representation gives a parametrization of a minimal surface; therefore, Weierstrass data for a surface is not unique. Hence, the Weierstrass data for Bonnet's minimal surfaces given in Fact 1.2 do not give the parametrization found by Bonnet (1.1). To get the parametrization of Bonnet's minimal surface given in (1.1), one needs to use the Weierstrass data $(-e^{-t}\coth(z/2), -2e^{t}\sinh^2(z/2)\,\mathrm{d}z)$.

Classically, minimal surfaces of Bonnet-type were studied by looking at their Gauss maps. A planar curvature line on a minimal surface is mapped to a planar curve on the sphere under the Gauss map, i.e. the image is contained in a circle. Hence, if a surface admits one family of planar curvature lines, then these curvature lines are mapped onto circles on the sphere under the Gauss map. However, Gauss map is a conformal transformation, implying that the image of the curvature lines in the other family under the Gauss map must meet the circles orthogonally. Using this fact, one can show that then the curvature lines in the other family are also mapped to circles under the Gauss map, telling us that one family of curvatures is planar if and only if the other family of curvature lines is planar. Therefore, to classify all the minimal surfaces of Bonnet-type, one needs to look at all the *orthogonal system of circles* on the sphere. (For more information, see [88, Section 2.6].) The fact that planar curvature lines on a minimal surface corresponds to an orthogonal system of circles on the sphere via the Gauss map gives us two interesting characterizations of minimal surfaces of Bonnet-type.

1.1 Thomsen surfaces

Thomsen studied minimal surfaces that are also affine minimal, a class of surfaces now often referred to as Thomsen surfaces. In his work [109], he mentioned that the asymptotic coordinate lines on Thomsen surfaces are mapped to an orthogonal system of circles on the sphere via the Gauss map. Given a minimal surface parametrized by curvature lines with Weierstrass data $(h, \eta\,\mathrm{d}z)$, an isometric (i.e. sharing the same first fundamental form) *conjugate minimal surface* parametrized by asymptotic coordinate lines can be obtained from the Weierstrass data $(h, i\eta\,\mathrm{d}z)$. Therefore, from Thomsen's observation, one can deduce the following fact mentioned by Blaschke:

Fact 1.4 ([12, p. 190])**.** *Minimal surfaces of Bonnet-type are exactly the conjugate minimal surface of Thomsen surfaces.*

In fact, it was the work on Thomsen surfaces in [9, 104] that showed the following:

Fact 1.5. *There exists a deformation consisting exactly of all Thomsen surfaces (see Figure 1.1).*

By considering the conjugate minimal surfaces of Thomsen surfaces, one can also obtain a deformation consisting exactly of all minimal surfaces of Bonnet type (see Figure 1.2).

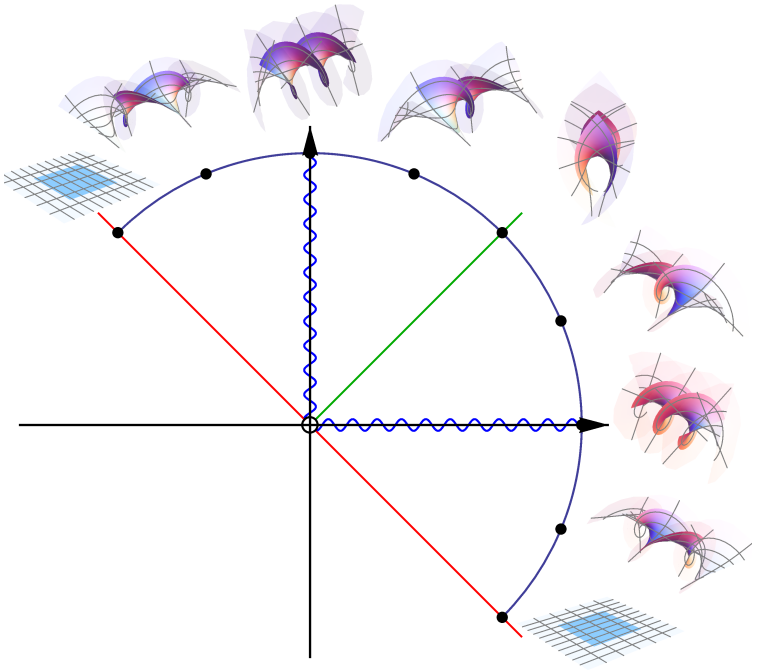

Figure 1.1: Deformation consisting exactly of Thomsen surfaces.

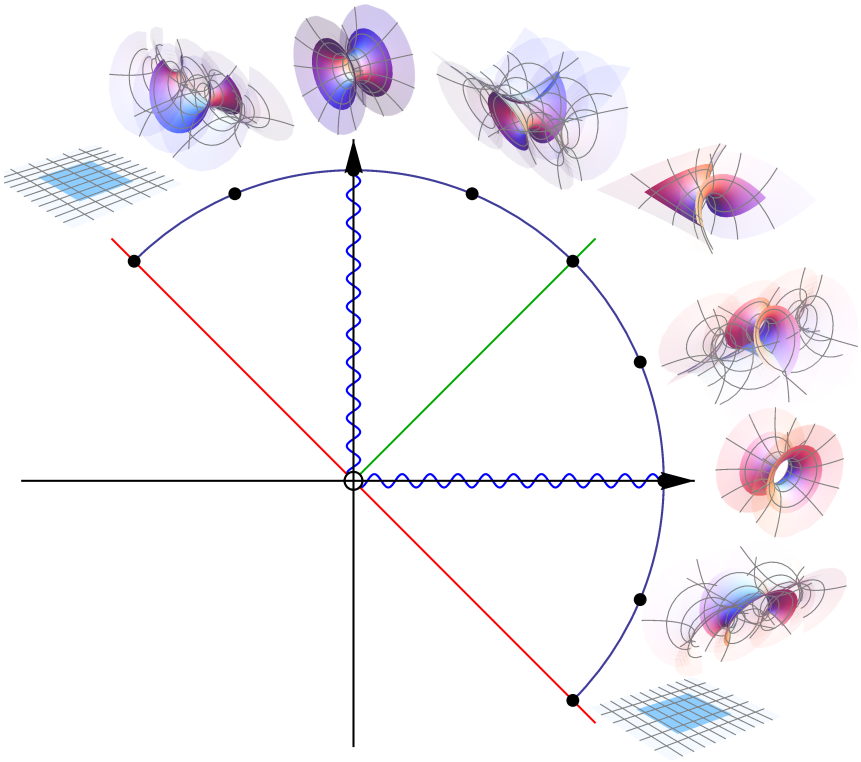

Figure 1.2: Deformation consisting exactly of minimal surfaces of Bonnet-type.

1.2 Goursat transformations

One consequence of the Weierstrass representation is that a minimal surface is the real part of a holomorphic null curve in $\mathbb{C}^3$. Therefore, given a minimal surface and its corresponding holomorphic null curve, one can consider applying an orthogonal transformation of $\mathbb{C}^3$ to the holomorphic null curve to get another holomorphic null curve. Taking the real part of the new holomorphic null curve results in a new minimal surface, called the Goursat transformation of the given minimal surface [50, 51].

On the other hand, minimal surfaces are isothermic surfaces, i.e. they admit conformal curvature line coordinates; hence, one can consider their Christoffel transformations, first defined in [30].

Fact 1.6 ([30])**.** *$f : \Sigma \to \mathbb{R}^3$ is an isothermic surface if and only if there is a surface $f^* : \Sigma \to \mathbb{R}^3$ such that f and f^**

(1) have parallel tangent planes,

(2) have the same conformal structure on Σ, and

(3) induce opposite orientations on Σ.

We call f^* a Christoffel transform *of f.*

The symmetricity of the above conditions implies that f^* is also an isothermic surface, and that Christoffel transformations are involutive, i.e. $(f^*)^* = f$ up to homotheties and isometries of $\mathbb{R}^3$. Minimal surfaces can be characterized via Christoffel transformations as isothermic surfaces whose Christoffel transformations are their corresponding Gauss maps. Therefore, one way of understanding Weierstrass representations is to consider the following recipe:

(1) Take a holomorphic function $h : \Sigma \to \mathbb{C}$.

(2) For a stereographic projection $St : \mathbb{S}^2 \to \mathbb{C}$, the holomorphicity of h implies the isothermicity of $St^{-1} \circ h : \Sigma \to \mathbb{S}^2$.

(3) Then $f : \Sigma \to \mathbb{R}^3$ defined as

$$f := (St^{-1} \circ h)^* = \int (1 - h^2, i(1 + h^2), 2h) \frac{1}{h_z} \, \mathrm{d}z$$

becomes a minimal surface with isothermic coordinates $z = u + iv$.

In fact, it is known through works such as [93, Lemma 2.18] that the Goursat transformation of a minimal surface is equivalent to keeping the Hopf differential the same while applying a Möbius transformation to the Gauss map. Generalizing this to isothermic surfaces, a Goursat transformation of isothermic surfaces was defined by Hertrich-Jeromin as follows:

Definition 1.7 ([53, 54])**.** Let $f : \Sigma \to \mathbb{R}^3$ be an isothermic surface and $\mu : \mathbb{R}^3 \cup \{\infty\} \to \mathbb{R}^3 \cup \{\infty\}$ be a Möbius transformation. Then a new isothermic surface $\tilde{f}$ defined by

$$\tilde{f} := (\mu \circ f^*)^*$$

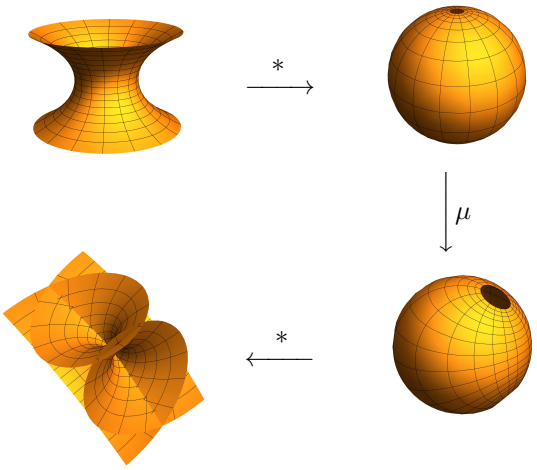

Figure 1.3: Goursat transformation of a catenoid

is called a *Goursat transform* of f.

Möbius transformations map spheres to spheres, circles to circles, and keep orthogonality intact. Therefore, given an orthogonal system of circles on a sphere, one can apply a Möbius transformation to get a different orthogonal system of circles. As a result, a Goursat transform of a minimal surface of Bonnet-type is again a minimal surface of Bonnet-type, a fact also mentioned in [93, Satz 2.23] (see also Figure 1.3). In fact, one can characterize minimal surfaces of Bonnet-type as Goursat transformations of the catenoid.

1.3 Summary

This thesis treats the different aspects of planar curvature lines on zero mean curvature surfaces in various spaceforms. Chapters 2 and 3 consider zero mean curvature surfaces of Bonnet-type in Minkowski 3-space. The techniques used in these chapters are based heavily on work by Abresch, Walter, and Wente, used to study cmc tori admitting one system of planar curvature lines [1, 112, 116, 117]. These techniques were also applied to study minimal surfaces of Bonnet-type in [29].

Chapter 2 considers spacelike zero mean curvature surfaces, also known as maximal surfaces, with planar curvature lines, called *maximal surfaces of Bonnet-type* in this thesis. The classification of such surfaces was given in [76, 82]; this thesis introduces a different method to obtain the classification, modeled after the works of [1, 112, 116, 117]. In fact, this thesis shows that the method introduced easily gives the existence of a deformation consisting exactly of all maximal surfaces of Bonnet-type. Furthermore, maximal surfaces can be extended to the idea of *maxfaces*, which are maximal surfaces admitting certain non-degenerate singularities, defined in [110]. Considering maximal surfaces of Bonnet-type as maxfaces, the singularities appearing on these surfaces are completely recognized; in addition, an example of a maxface having cuspidal butterflies and cuspidal S_1^- singularities is given (see [7, 8] for more information on these singularities). Finally, through a known

relationship between maximal surfaces of Bonnet-type and maximal Thomsen surfaces (those maximal surfaces that are also affine minimal) [82], similar to the relationship between their Euclidean counterparts, we obtain a result on the existence of a deformation and recognition of singularities of maximal Thomsen surfaces. The content in Chapter 2 is based on joint work with Yuta Ogata, and is published in [28].

Chapter 3 shifts its attention to timelike zero mean curvature surfaces, also called timelike minimal surfaces having planar curvature lines, which this thesis refers to as *timelike minimal surfaces of Bonnet-type*. Timelike minimal surfaces distinguish themselves from minimal surfaces in Euclidean 3-space and maximal surfaces in Minkowski 3-space in that they admit a different type of coordinates, called the *null coordinates* [115]. In addition to the results on the classification, deformation, and singularities, this thesis considers a characterization of timelike minimal surfaces of Bonnet-type via the null coordinates. By doing so, the relationship between timelike minimal surfaces of Bonnet-type and timelike Thomsen surfaces, timelike minimal surfaces that are also affine minimal defined in [81], is explored. The content in Chapter 3 is based on joint work with Shintaro Akamine and Yuta Ogata, and is published in [4, 5].

In Chapter 4, the attention shifts to discrete minimal surfaces with symmetries. In the smooth case, the Schwarz reflection principle states that if a minimal surface has a planar curvature line along which the normal lines are also contained in the same plane, then the minimal surface is symmetric with respect to the plane. Furthermore, a given minimal surface has a planar symmetry along a curvature line if and only if the corresponding conjugate minimal surface has a line symmetry along the corresponding asymptotic coordinate line. On the other hand, discrete isothermic minimal surfaces were defined via discrete isothermic surface theory, as discrete Christoffel transformations of discrete isothermic surfaces whose images are contained in a sphere [17]. Also, using a concept of parallel transformation for circular nets, mean curvature was defined via the discrete Steiner's formula (see [95, 105], for example), and it was shown that the discrete isothermic minimal surface defined via Christoffel duality indeed has zero mean curvature. Recently, a concept of edge-constraint nets was defined in [59], and as an application, the associated family of discrete isothermic minimal surfaces was developed, where discrete asymptotic minimal surfaces arise as conjugate surface of discrete isothermic minimal surface. This chapter considers discrete isothermic minimal surfaces having planar symmetry and explores its relationship with the conjugate discrete asymptotic minimal surface. Using the symmetry properties, new examples of discrete isothermic minimal surfaces having high degrees of symmetry are numerically created. The content in Chapter 4 is based on the joint work with Wayne Rossman and Seong-Deog Yang.

Finally, Chapter 5 deals with preparatory materials to unify the arguments found in Chapters 2 and 3 for maximal surfaces and timelike minimal surfaces. The similarity of the arguments and the results suggest that maximal surfaces and timelike minimal surfaces of Bonnet-type can be treated uniformly, and the Lorentz-Möbius geometry of $\mathbb{R}^{3,2}$ is explored as a candidate for such unification. Spacelike and timelike isothermic surfaces were explored in the context of Lorentz-Möbius geometry in works such as [37, 38, 107, 113]; however, the work [24] suggests that the metric induced on the surface does not play a role in the

theory of isothermic surfaces. After showing that Minkowski 3-space, de Sitter 3-space, and anti-de Sitter 3-space can be unified under the lightcone model of Lorentz-Möbius geometry, analogous to the lightcone model of Möbius geometry developed first by Darboux [33, Chapitre VI], we explore how the different types of spheres are represented in this model. As an application, we see how the induced metric of a given surface can be identified via the causality of the vector representing the tangent plane congruence.

Chapter 2

Maximal surfaces of Bonnet-type

The classification of maximal surfaces of Bonnet-type in Minkowski 3-space $\mathbb{R}^{2,1}$ has not been given until recently [76]. Leite developed an approach using orthogonal systems of circles on the hyperbolic 2-space $\mathbb{H}^2$, and used the fact that families of planar curvature lines transform into orthogonal families of circles on $\mathbb{H}^2$ under its analogue of the Gauss map. Then she obtained the data for the following Weierstrass-type representation for maximal surfaces as first stated in [70], later refined to include singularities in [110].

Fact 2.1 (Weierstrass-type representation theorem for maximal surfaces)**.** *Any conformal maximal surface $f : \Sigma \subset \mathbb{C} \to \mathbb{R}^{2,1}$ can be locally represented as*

$$f = \operatorname{Re} \int (1 + h^2, i(1 - h^2), -2h)\eta \, \mathrm{d}z$$

over a simply-connected domain Σ on which h is meromorphic, while η and $h^2\eta$ are holomorphic.

Note here that for a conformal maximal surface with Weierstrass data $(h, \eta \, \mathrm{d}z)$, one obtains the associated family of maximal surfaces via Weierstrass data $(h, \lambda^{-2}\eta \, \mathrm{d}z)$ for $\lambda \in \mathbb{S}^1 = \{\lambda \in \mathbb{C} : |\lambda|^2 = 1\}$. Using the above representation, Leite produced the following classification and their respective Weierstrass data $(h, \eta \, \mathrm{d}z)$.

Fact 2.2 ([76])**.** *A maximal surface in Minkowski 3-space $\mathbb{R}^{2,1}$ with planar curvature lines must be a piece of one, and only one of*

- *plane, with Weierstrass data $(0, 1 \, \mathrm{d}z)$,*
- *Enneper surface of first kind, with Weierstrass data $(z, 1 \, \mathrm{d}z)$,*
- *Enneper surface of second kind, with Weierstrass data $\left(\frac{1-z}{1+z}, -\frac{(1+z)^2}{2} \, \mathrm{d}z\right)$, or one member of its associated family,*
- *catenoid of first kind, with Weierstrass data $(e^z, e^{-z} \, \mathrm{d}z)$,*

- *catenoid of second kind, with Weierstrass data* $\left(\frac{1-e^z}{1+e^z}, -1-\cosh z\,\mathrm{d}z\right)$, *or*
- *one surface in the Bonnet family, with Weierstrass data* $\{(e^z+t, e^{-z}\,\mathrm{d}z), t>0\}$

up to isometries and homotheties of $\mathbb{R}^{2,1}$.

To study maximal surfaces of Bonnet-type, we start by proposing an alternative method to using Leite's method. In Section 2.1, we closely follow the method used in [29], which was modeled after techniques used in [1], [9], [112], and [116]. First, we obtain and solve a system of partial differential equations for the metric function using the zero mean curvature condition and the planar curvature line condition. Then, from the metric function, we find the normal vector to the surface by using the notion of axial directions. From the normal vector, we recover the Weierstrass data and the parametrizations of maximal surfaces of Bonnet-type, allowing us to obtain a complete classification (see Theorem 2.16).

In fact, the axial directions play a crucial role in this chapter, as they allow us not only to further classify maximal Bonnet-type surfaces into three types, but also to attain deformations consisting of the surfaces under consideration. In Section 2.2, we investigate those deformations, and show that there exists a single continuous deformation consisting exactly of the maximal surfaces of Bonnet-type (see Theorem 2.17, Fig. 2.4, and Fig. 2.5).

On the other hand, the notion of maxfaces as maximal surfaces in $\mathbb{R}^{2,1}$ with singularities was introduced in [110], and various types of singularities appearing on maximal surfaces have been studied in various works [43, 47, 69, 71, 91, 110]. Since the singularities of maximal catenoids and the maximal Enneper-type surface were investigated in [47, 71, 110], in Section 2.3, we recognize the types of singularities for maximal Bonnet-type surfaces using the criteria introduced in [110], [47], and [91], and specify the types of singularities appearing in maximal surfaces of Bonnet-type (see Theorem 2.20, Fig. 2.6, and Fig. 2.7).

Finally in Section 2.4, we apply the results in Section 2.2 and Section 2.3 to maximal surfaces that are also affine minimal surfaces. Thomsen studied minimal surfaces in $\mathbb{R}^3$ that are also affine minimal surfaces, and mentioned that such surfaces are conjugate surfaces of minimal surfaces of Bonnet-type [109]. Manhart has shown that the analogous result holds true for the maximal case in $\mathbb{R}^{2,1}$ [82], and we use that result to consider the deformations and singularities of maximal surfaces that are also affine minimal surfaces (see Corollary 2.23, Corollary 2.24, Fig. 2.8, and Fig. 2.9).

2.1 Classification of maximal surfaces of Bonnet-type

In this section, we would like to obtain a complete classification of maximal surfaces of Bonnet-type by using the Weierstrass-type representation. We use an alternative method to orthogonal systems of cycles to recover the Weierstrass data as follows: First, from the zero mean curvature condition and planar curvature line condition, we obtain and solve a system of partial differential equations for the metric function. Then using the explicit solutions for the metric function, we recover the Weierstrass data and the parametrization by calculating the unit normal vector.

2.1.1 Maximal surface theory

Let $\mathbb{R}^{2,1}$ be Minkowski 3-space with Lorentzian metric

$$\langle (x_1, x_2, x_0), (y_1, y_2, y_0) \rangle := x_1 y_1 + x_2 y_2 - x_0 y_0.$$

In addition, let Σ be a simply-connected domain with coordinates $(u, v) \in \Sigma \subset \mathbb{R}^2$. Throughout the paper, we identify $\mathbb{R}^2$ with the set of complex numbers $\mathbb{C}$ via $(u, v) \leftrightarrow z := u + iv$ where $i = \sqrt{-1}$. Let $X : \Sigma \to \mathbb{R}^{2,1}$ be a conformally immersed spacelike surface. Since $X(u, v)$ is conformal, the induced metric $\mathrm{d}s^2$ is represented as

$$\mathrm{d}s^2 = \rho^2 \left(\mathrm{d}u^2 + \mathrm{d}v^2\right)$$

for some function $\rho : \Sigma \to \mathbb{R}_+$, where $\mathbb{R}_+$ is the set of positive real numbers.

We choose the timelike unit normal vector field $N : \Sigma \to \mathbb{H}^2$ of X, where $\mathbb{H}^2$ is the two-sheeted hyperboloid in $\mathbb{R}^{2,1}$ (cf. [110, (1.2)]), i.e.

$$\mathbb{H}^2 = \mathbb{H}^2_+ \cup \mathbb{H}^2_-$$

for

$$\mathbb{H}^2_+ := \{x \in \mathbb{R}^{2,1} : \langle x, x \rangle = -1, x_0 > 0\} \quad \text{and} \quad \mathbb{H}^2_- := \{x \in \mathbb{R}^{2,1} : \langle x, x \rangle = -1, x_0 < 0\}.$$

Now, let $X(u, v)$ be a non-planar umbilic-free maximal surface on the domain Σ. By [16, Lemma 2.3.2] (see also [13, 14]), we may then further assume that (u, v) are conformal curvature line (or isothermic) coordinates, and that the Hopf differential factor

$$Q := \langle X_{zz}, N \rangle = -\frac{1}{2}$$

without loss of generality. Hence, the Gauss-Weingarten equations for the maximal case are the following:

$$\begin{cases} X_{uu} = \frac{\rho_u}{\rho} X_u - \frac{\rho_v}{\rho} X_v + N, \\ X_{vv} = -\frac{\rho_u}{\rho} X_u + \frac{\rho_v}{\rho} X_v - N, \\ X_{uv} = \frac{\rho_v}{\rho} X_u + \frac{\rho_u}{\rho} X_v, \\ N_u = \frac{1}{\rho^2} X_u, \\ N_v = -\frac{1}{\rho^2} X_v, \end{cases} \tag{2.1}$$

while the integrability condition, or the Gauss equation, becomes

$$\rho \cdot \Delta \rho - (\rho_u^2 + \rho_v^2) + 1 = 0$$

where $\Delta = \partial_u^2 + \partial_v^2$. Finally, changing $Q \mapsto \lambda^{-2} Q$ for $\lambda \in \mathbb{S}^1 \subset \mathbb{C}$, we obtain the associated family of $X(u, v)$. In particular, if $\lambda^{-2} = \pm i$ then the new surface is called the *conjugate* of the original surface.

2.1.2 Planar curvature line condition and analytic classification

Now, we impose the planar curvature line condition on a maximal surface. First, we consider the relationship between the planar curvature line condition and the metric function.

Lemma 2.3. *For a non-planar umbilic-free maximal surface $X(u,v)$, the following statements are equivalent:*

(1) u-curvature lines are planar.

(2) v-curvature lines are planar.

(3) $\rho_{uv} = 0$.

Proof. Since (u,v) are conformal curvature line coordinates, u-curvature lines are planar if and only if

$$\det(X_u, X_{uu}, X_{uuu}) = 0.$$

The Gauss-Weingarten equation (2.1) tells us that

$$X_{uuu} = \frac{\rho_{uu}\rho - \rho_v^2 + 1}{\rho^2} X_u - \frac{\rho_u\rho_v + \rho_{uv}\rho}{\rho^2} X_v + \frac{\rho_u}{\rho} N.$$

Therefore, we have that

$$\det(X_u, X_{uu}, X_{uuu}) = \rho_{uv}\rho.$$

Since $\rho : \Sigma \to \mathbb{R}_+$, we have that u-curvature lines are planar if and only if $\rho_{uv} = 0$. Similarly, one can calculate that v-curvature lines are planar if and only if $\rho_{uv} = 0$. □

Therefore, finding all non-planar umbilic-free maximal surfaces of Bonnet-type is equivalent to finding solutions to the following system of partial differential equations:

$$\begin{cases} \rho \cdot \Delta\rho - (\rho_u^2 + \rho_v^2) + 1 = 0 & \text{(Gauss equation for maximal surfaces)}, \quad (2.2a) \\ \rho_{uv} = 0 & \text{(planar curvature line condition)}. \quad (2.2b) \end{cases}$$

To solve the above system, we note that (2.2a) and (2.2b) can be reduced to a system of ordinary differential equations as follows.

Lemma 2.4. *For a solution $\rho : \Sigma \to \mathbb{R}_+$ to* (2.2a) *and* (2.2b)*, there exist real-valued functions $f(u)$ and $g(v)$ such that*

$$\begin{cases} \rho_u = f(u), & (2.3a) \\ \rho_v = g(v). & (2.3b) \end{cases}$$

Furthermore, $\rho(u,v)$ can be explicitly written in terms of $f(u)$ and $g(v)$ as follows:

Case (1): *If $\Delta\rho$ is nowhere zero on Σ,*

$$\rho(u,v) = \frac{f(u)^2 + g(v)^2 - 1}{f_u(u) + g_v(v)}, \quad (2.4)$$

where $f(u)$ and $g(v)$ satisfy the following system of ordinary differential equations:

$$\begin{cases} (f_u(u))^2 = (d-c)f(u)^2 + c & \text{(2.5a)} \\ f_{uu}(u) = (d-c)f(u) & \text{(2.5b)} \\ (g_v(v))^2 = (c-d)g(v)^2 + d & \text{(2.5c)} \\ g_{vv}(v) = (c-d)g(v) & \text{(2.5d)} \end{cases}$$

for real constants c and d such that $c^2 + d^2 \neq 0$.

Case (2): *If $\Delta\rho \equiv 0$ on Σ, i.e. $\Delta\rho$ is identically zero on Σ,*

$$\rho(u, v) = (\cos\phi) \cdot u + (\sin\phi) \cdot v. \tag{2.6}$$

where $f(u) = \sin\phi$ and $g(v) = \cos\phi$ for some constant $\phi \in [0, 2\pi)$.

Proof. By integrating Equation (2.2b) with respect to v, we obtain

$$\rho_u = C_1(u)$$

for some integral constant $C_1(u)$. Similarly, we get $\rho_v = C_2(v)$ for some integral constant $C_2(v)$ by integrating (2.2b) with respect to u. Define $f(u) := C_1(u)$ and $g(v) := C_2(v)$ to get (2.3). Inputing (2.3) to (2.2a), we get

$$\rho \cdot (f_u(u) + g_v(v)) - (f(u)^2 + g(v)^2) + 1 = 0.$$

To prove the first case, first assume that $\Delta\rho$ is not identically equal to zero. Then we can choose a point (u_0, v_0) such that $\rho(u_0, v_0) \neq 0$, implying that we can choose a neighborhood $\Sigma \subset \mathbb{R}^2$ of (u_0, v_0) such that $\Delta\rho$ is nowhere zero on Σ. Since $\Delta\rho = f_u + g_v \not\equiv 0$,

$$\rho(u, v) = \frac{f(u)^2 + g(v)^2 - 1}{f_u(u) + g_v(v)},$$

i.e. we have (2.4). Then from (2.3a), we have

$$f = \rho_u = \frac{2ff_u(f_u + g_v) - (f^2 + g^2 - 1)f_{uu}}{(f_u + g_v)^2}$$

or

$$\begin{aligned} 0 &= f(f_u + g_v)^2 - 2ff_u(f_u + g_v) + (f^2 + g^2 - 1)f_{uu} \\ &= ff_u^2 + 2ff_ug_v + fg_v^2 - 2ff_u^2 - 2ff_ug_v + (f^2 + g^2 - 1)f_{uu} \\ &= f(g_v^2 - f_u^2) + (f^2 + g^2 - 1)f_{uu}. \end{aligned} \tag{2.7}$$

After multiplying both sides by $\frac{2f_u}{(f^2+g^2-1)^2}$, we have that

$$0 = \frac{2f_uf_{uu}(f^2 + g^2 - 1) - (f_u^2 - g_v^2) \cdot 2ff_u}{(f^2 + g^2 - 1)^2} = \left(\frac{f_u^2 - g_v^2}{f^2 + g^2 - 1}\right)_u.$$

Integrating both sides with respect to u, we obtain that

$$\frac{f_u^2 - g_v^2}{f^2 + g^2 - 1} = k_1(v) \tag{2.8}$$

for some $k_1(v)$. Substituting $k_1(v)$ for (2.7), we have that

$$0 = -fk_1(v)(f^2 + g^2 - 1) + f_{uu}(f^2 + g^2 - 1) = (f^2 + g^2 - 1)(f_{uu} - fk_1(v)).$$

Since $f^2 + g^2 - 1 \neq 0$, we have that $f_{uu} = k_1(v)f$, implying that $k_1(v) = \tilde{c} \in \mathbb{R}$ is a constant, i.e.

$$f_{uu} = \tilde{c}f. \tag{2.9}$$

Multiplying both sides of (2.9) with $2f_u$ and integrating with respect to u gives us that

$$f_u^2 = \tilde{c}f^2 + c$$

for some constant c.

On the other hand, from (2.3b), we have

$$g = \rho_v = \frac{2gg_v(f_u + g_v) - (f^2 + g^2 - 1)g_{vv}}{(f_u + g_v)^2}$$

or

$$\begin{aligned} 0 &= g(f_u + g_v)^2 - 2gg_v(f_u + g_v) + (f^2 + g^2 - 1)g_{vv} \\ &= gf_u^2 + 2gf_ug_v + gg_v^2 - 2gf_ug_v - 2gg_v^2 + (f^2 + g^2 - 1)g_{vv} \\ &= g(f_u^2 - g_v^2) + (f^2 + g^2 - 1)g_{vv}. \end{aligned} \tag{2.10}$$

Substituting (2.8) with $k_1(v) = \tilde{c}$ into (2.10), we get that

$$0 = \tilde{c}g(f^2 + g^2 - 1) + (f^2 + g^2 - 1)g_{vv} = (f^2 + g^2 - 1)(g_{vv} + \tilde{c}g).$$

Again. since $f^2 + g^2 - 1 \neq 0$, we have that

$$g_{vv} = -\tilde{c}g. \tag{2.11}$$

Multiplying both sides of (2.11) with $2g_v$ and integrating with respect to v gives us that

$$g_v^2 = -\tilde{c}g^2 + d$$

for some constant d. Now, from (2.8),

$$\tilde{c}(f^2 + g^2 - 1) = f_u^2 - g_v^2 = \tilde{c}f^2 + c + \tilde{c}g^2 - d = \tilde{c}(f^2 + g^2 - 1) + \tilde{c} + c - d,$$

implying that $\tilde{c} = d - c$, giving us (2.5). Lastly, $c = d = 0$ implies $f(u)$ and $g(v)$ are both constants by (2.5), a contradiction since we assumed that $\Delta\rho \not\equiv 0$.

Now assume that $\Delta\rho$ is identically equal to zero on some simply-connected domain $\Sigma \subset \mathbb{R}^2$. Since $\Delta\rho = f_u(u) + g_v(v) \equiv 0$, $f(u)^2 + g(v)^2 = 1$ for all u and v. This implies that both $f(u)$ and $g(v)$ are constant, and we can set $f := \cos\phi$ and $g := \sin\phi$ for some constant $\phi \in [0, 2\pi)$. Solving (2.3a) and (2.3b), we obtain (2.6). □

We would now like to solve for $f(u)$ and $g(v)$ satisfying (2.5a)–(2.5d) in Case (1). First, assume that $c = d$. Then (2.5a) and (2.5c) imply that $c = d > 0$ and that

$$f(u) = \pm\sqrt{c}\,u + \tilde{C}_1 \quad \text{and} \quad g(v) = \pm\sqrt{d}\,v + \tilde{C}_2 \tag{2.12}$$

for some real constants of integration $\tilde{C}_1$ and $\tilde{C}_2$. Now assuming that $c \neq d$, we can explicitly solve for $f(u)$ and $g(v)$ to find that

$$\begin{aligned} f(u) &= C_1 e^{\sqrt{d-c}\,u} + C_2 e^{-\sqrt{d-c}\,u}, \quad 4(c-d)C_1C_2 = c, \\ g(v) &= C_3 e^{\sqrt{c-d}\,v} + C_4 e^{-\sqrt{c-d}\,v}, \quad 4(d-c)C_3C_4 = d, \end{aligned} \tag{2.13}$$

where $C_1, \ldots, C_4 \in \mathbb{C}$ are constants of integration. Furthermore since $f(u)$ and $g(v)$ are real-valued functions, $C_1, \ldots, C_4$ must satisfy

$$\begin{cases} C_1, C_2 \in \mathbb{R} \text{ and } C_3 = \overline{C_4}, & \text{if } d > c, \\ C_1 = \overline{C_2} \text{ and } C_3, C_4 \in \mathbb{R}, & \text{if } c > d, \end{cases}$$

where $\bar{\cdot}$ denotes the complex conjugation.

To explicitly solve for $f(u)$ and $g(v)$ and hence $\rho(u, v)$, we first need to consider the initial conditions of $f(u)$ and $g(v)$. We identify the exact conditions for $f(u)$ and $g(v)$ having a zero, and derive the appropriate initial conditions in the following series of lemmas.

Lemma 2.5. *$f(u)$ (resp. $g(v)$) satisfying (2.5a)–(2.5d) has a zero if and only if either $c > 0$ or $f(u) \equiv 0$ (resp. $d > 0$ or $g(v) \equiv 0$).*

Proof. If $c = d$, then the statement is trivial by (2.12); hence, we may assume $c \neq d$. To prove the necessary condition, since $f \equiv 0$ case is trivial, assume that $c > 0$, and we show that there is some real u_0 such that $f(u + 0) = 0$. If $d > c$, then it is easy to check that for

$$u_0 := \frac{\log c - \log(4(d-c)C_1^2)}{2\sqrt{d-c}}$$

we get $f(u_0) = 0$ by (2.13).

Now assume $c > d$. Then since

$$C_1 = \frac{c}{4(c-d)C_2} = \frac{c}{4(c-d)\overline{C_1}},$$

we may write $C_1 = \sqrt{\frac{c}{4(c-d)}}e^{i\theta}$ and $C_2 = \sqrt{\frac{c}{4(c-d)}}e^{-i\theta}$ for some constant $\theta \in \mathbb{R}$. By letting

$$u_0 := \frac{\frac{\pi}{2} - \theta}{\sqrt{c-d}},$$

we have $f(u_0) = 0$ again by (2.13).

To show the sufficient condition, suppose there is some u_0 such that $f(u_0) = 0$. By (2.5a), $(f_u(u_0))^2 = c \geq 0$. If $c = 0$, then, (2.13) gives us

$$f(u) = C_1 e^{\sqrt{d}u} + C_2 e^{-\sqrt{d}u}$$

for some complex constants C_1 and C_2 where $d \cdot C_1 C_2 = 0$. Since $d \neq 0$, without loss of generality, let $C_2 = 0$. From $f(u_0) = 0$, we get $C_1 e^{\sqrt{d}u_0} = 0$. Therefore, $C_1 = 0$, and we have $f(u) \equiv 0$.

The statement regarding $g(v)$ is proven analogously. □

Lemma 2.6. *$f(u)$ (resp. $g(v)$) has no zero if and only if either $c < 0$ or $f(u) = \pm e^{\sqrt{d}u}$ where $d > 0$ (resp. $d < 0$ or $g(v) = \pm e^{\sqrt{c}u}$ where $c > 0$).*

Proof. Note that by the previous lemma and the fact that $c < 0$ implies $f(u) \not\equiv 0$, we only need to show that $f(u) \not\equiv 0$ and $c = 0$ if and only if $f(u) = C_1 e^{\sqrt{d}u}$ for $C_1 = \pm 1$ and $d > 0$.

First, suppose that $f(u) \not\equiv 0$ and $c = 0$. Then, similar to the proof of the previous lemma,

$$f(u) = C_1 e^{\sqrt{d}u}$$

for some complex constant C_1. Since $f(u) \not\equiv 0$, $C_1 \neq 0$. In addition, since $f(u)$ is real, C_1 is real, and $d > 0$. Finally, by shifting parameters, we may assume that $C_1 = \pm 1$.

Now assume that $f(u) = \pm e^{\sqrt{d}u}$ for $d > 0$. Then $f(u) \not\equiv 0$ trivially. Furthermore, (2.5b) implies that $c \cdot (\pm e^{\sqrt{d}u}) = 0$ for all u. Hence, $c = 0$. □

Lemma 2.7. *At least one of $f(u)$ or $g(v)$ must have a zero.*

Proof. Without loss of generality, suppose that $f(u)$ does not have a zero. Hence, by the previous lemma, $c < 0$ or $f(u) = \pm e^{\sqrt{d}u}$ where $d > 0$. If $f(u) = \pm e^{\sqrt{d}u}$ with $d > 0$, $g(v)$ must have a zero by Lemma 2.5.

Now suppose $c < 0$. Then, by (2.5a), $d - c > 0$. If $d < 0$, then (2.5c) implies $c - d > 0$, a contradiction; hence, $d \geq 0$. If $d = 0$, direct calculation shows that either $g(v) \equiv 0$ or $g(v) = C_2 e^{\sqrt{c}u}$ where $C_2 \neq 0$ and $c > 0$. However, since we assumed $c < 0$, it must follow that $g(v) \equiv 0$ or $d > 0$. Hence, $g(v)$ must have a zero. □

Exchanging the roles of u and v, if necessary, we may assume without loss of generality that g has a zero, and we may further assume that $g(0) = 0$ by shifting parameters. By considering the fact that we may switch the roles of $f(u)$ and $g(v)$, we only need to consider the following five cases:

$c > 0, d > 0$	$c > 0, g(v) \equiv 0$	$f(u) = \pm e^{\sqrt{d}u}, d > 0$	$c < 0, d > 0$	$c < 0, g(v) \equiv 0$

(2.14)

It should be noted that in the cases considered (2.14), $d \geq 0$, and that $d = 0$ if and only if $g(v) \equiv 0$. For the third case, since $c = 0$, $g(v) = \sin(\sqrt{d}v)$. By letting $v \mapsto -v$, we see that the plus or minus condition on $f(u)$ may be dropped, allowing us to assume that $f(u) = e^{\sqrt{d}u}$. Finally, we prove the following statement regarding the initial condition of $f(u)$.

Lemma 2.8. *For the cases* (2.14)*, there is some* u_0 *such that* $f(u_0) = 1$*.*

Proof. It is easy to check that the statement holds if $c = d$ via (2.12); hence, assume $c \neq d$. From (2.13), since $c \neq 0$ implies C_1 and C_2 are non-zero, we let

$$C_2 = \frac{c - d + \sqrt{d(d-c)}}{2(c-d)}.$$

If $d - c > 0$, then since $d \geq 0$, $f(u)$ is real-valued such that $f(0) = 1$. Since $c < 0$ implies that $d - c > 0$, assume $c > 0$ and $d - c < 0$. Then direct calculation shows that C_1 is the complex conjugate of C_2 implying that $f(u)$ is equal to its own conjugate. Therefore, $f(u)$ is real-valued such that $f(0) = 1$. □

Therefore, through shifting parameters, we may assume that $f(0) = 1$ and $g(0) = 0$. Using these initial conditions, we arrive at the following explicit solutions for $f(u)$ and $g(v)$.

Proposition 2.9. *For a non-planar maxface* $X(u, v)$ *with planar curvature lines, the real-analytic solution* $\rho : \mathbb{R}^2 \to \mathbb{R}$ *of* (2.2a) *and* (2.2b) *is precisely given as follows:*

Case (1) *If* $\Delta\rho \not\equiv 0$*, i.e.* $\Delta\rho$ *is not identically equal to zero, then*

$$\rho(u, v) = \frac{f(u)^2 + g(v)^2 - 1}{f_u(u) + g_v(v)},$$

with

$$f(u) = \begin{cases} \cosh\left(\sqrt{d-c}\,u\right) + \dfrac{\sqrt{d}}{\sqrt{d-c}} \sinh\left(\sqrt{d-c}\,u\right), & \text{if } c \neq d \\ \sqrt{d}u + 1, & \text{if } c = d \end{cases}$$
$$g(v) = \begin{cases} \dfrac{\sqrt{d}}{\sqrt{d-c}} \sin\left(\sqrt{d-c}\,v\right), & \text{if } c \neq d \\ \sqrt{d}v, & \text{if } c = d \end{cases} \tag{2.15}$$

where $c^2 + d^2 \neq 0$ *and* $d \geq 0$*.*

Case (2) *If* $\Delta\rho \equiv 0$*, then for some constant* ϕ *such that* $\phi \in [0, 2\pi)$*,*

$$\rho(u, v) = (\cos\phi) \cdot u + (\sin\phi) \cdot v.$$

Proof. Solving (2.5a)–(2.5d) for $f(u)$ and $g(v)$ with initial conditions $f(0) = 1$ and $g(0) = 0$, and considering the change in parameter $u \mapsto -u$ or $v \mapsto -v$, if necessary, gives the explicit solutions in (2.15).

Now we wish to see that the domain of $\rho(u, v)$ can be extended to $\mathbb{R}^2$ globally. If $c = d$, then this is a direct result of applying the solution in (2.15). Therefore, assume $c \neq d$. Then by (2.5a) and (2.5c), we have

$$f_u^2 - g_v^2 = (d - c)(f^2 + g^2 - 1).$$

implying that

$$\rho(u,v) = \frac{f(u)^2 + g(v)^2 - 1}{f_u(u) + g_v(v)} = \frac{f_u(u) - g_v(v)}{d - c}.$$

Therefore, the real-analyticity of $f(u)$ and $g(v)$ implies that the domain of $\rho(u,v)$ can be extended to $\mathbb{R}^2$ globally. □

Remark 2.10. We make a few important remarks about Proposition 2.9:

- In the statement of Proposition 2.9, we now allow ρ to map into $\mathbb{R}$ as opposed to $\mathbb{R}_+$, i.e. ρ may have zeroes, or even be negative. By doing so, we now consider $X(u,v)$ as *maxfaces*, defined in [110] as a class of maximal surfaces with singularities (see also [47]).
- In (2.15), we allow $d - c < 0$. However, even in such case, by using the identities

  $$\cosh(\sqrt{d-c}\,u) = \cos(\sqrt{c-d}\,u) \quad \text{and} \quad \sinh(\sqrt{d-c}\,u) = i\sin(\sqrt{c-d}\,u)$$

  we see that $f(u)$ and $g(v)$ are real-valued analytic functions.
- For case (2) in Proposition 2.9, we may use an associated family's parameter $\lambda \in \mathbb{S}^1 \subset \mathbb{C}$ instead of ϕ through appropriate coordinate change shown below:

  $$\begin{cases} \tilde{u} := \cos\phi \cdot u + \sin\phi \cdot v, & \tilde{v} := -\sin\phi \cdot u + \cos\phi \cdot v \\ \lambda := e^{-i\phi}, & \tilde{Q} := -\frac{1}{2}\lambda^{-2} = \lambda^{-2}Q. \end{cases}$$

  However, it should be noted that while the coordinate change $(u,v) \mapsto (\tilde{u},\tilde{v})$ and parameter change $\phi \mapsto \lambda$ preserve the conformal structure, it does not hold the curvature line coordinates such that $Q \mapsto \tilde{Q}$.

Note that for all cases, the metric function $\rho(u,v)$ is always bounded for all $(u,v) \in \mathbb{R}^2$, and we now have the following theorem. Note that $u \leftrightarrow v$, used as a subscript in Figure 2.1, means the role of u and v are switched, up to shift of parameters.

Theorem 2.11. *Let $X(u,v)$ be a non-planar maxface in $\mathbb{R}^{2,1}$ with isothermic coordinates (u,v) such that the induced metric $\mathrm{d}s^2 = \rho^2 \cdot (\mathrm{d}u^2 + \mathrm{d}v^2)$. Then X has planar curvature lines if and only if $\rho(u,v)$ satisfies Proposition 2.9. Furthermore, for different values of (c,d) or λ as in Remark 2.10, the surface $X(u,v)$ has the following properties based on Fig. 2.1:*

Case (1) *If $\Delta\rho \not\equiv 0$, when (c,d) lies on*

- ①*: X is not periodic in the u-direction, but constant in the v-direction,*
- ②, ③*, or* ④*: X is not periodic in the u-direction, but periodic in the v-direction,*
- ⑤*: X is not periodic in both the u-direction and the v-direction,*
- ⑥*: X is periodic in the u-direction, but constant in the v-direction.*

Case (2) *If $\Delta\rho \equiv 0$, when λ lies on*

- ⑦*: X is a surface of revolution,*
- ⑧*: X is a surface in the associated family of* ⑦*.*

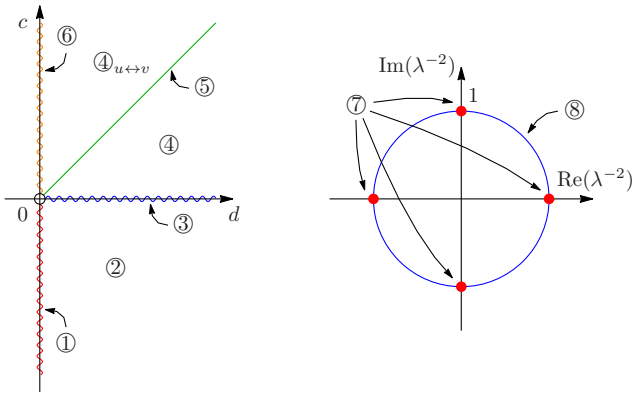

Figure 2.1: The classification diagrams of non-planar maxfaces of Bonnet-type.

2.1.3 Axial directions and normal vector

To find the parametrizations of the surfaces considered, we would like to recover the Weierstrass data from the metric function as follows: We first show the existence of a unique constant direction for surfaces under consideration called the *axial direction*, and use it to calculate the unit normal vector. Then from the unit normal vector, we recover the Weierstrass data. First, we show the existence of the axial direction in the following proposition.

Proposition 2.12. *If there exists u_0 (resp. v_0) such that $f(u_0) \neq 0$ (resp. $g(v_0) \neq 0$) in Proposition 2.9, then there exists a unique non-zero constant vector $\vec{v}_1$ (resp. $\vec{v}_2$) such that*

$$\langle m(u,v), \vec{v}_1 \rangle = \langle m_v(u,v), \vec{v}_1 \rangle = 0 \quad (\textit{resp. } \langle n(u,v), \vec{v}_2 \rangle = \langle n_u(u,v), \vec{v}_2 \rangle = 0),$$

where $m = \rho^{-2}(X_u \times X_{uu})$ (resp. $n = \rho^{-2}(X_v \times X_{vv})$) and

$$\vec{v}_1 := \frac{(\rho_u)^2 - \rho \cdot \rho_{uu}}{\rho^2} X_u - \frac{\rho_u \rho_v}{\rho^2} X_v + \frac{\rho_u}{\rho} N \tag{2.16}$$

$$(\textit{resp. } \vec{v}_2 := -\frac{\rho_u \rho_v}{\rho^2} X_u + \frac{(\rho_v)^2 - \rho \cdot \rho_{vv}}{\rho^2} X_v - \frac{\rho_v}{\rho} N).$$

If $\vec{v}_1$ and $\vec{v}_2$ both exist, then they are orthogonal to each other. We call $\vec{v}_1$ and $\vec{v}_2$ the axial directions *of $X(u,v)$.*

Proof. From (2.1),

$$m = \frac{1}{\rho^2} X_v - \frac{\rho_v}{\rho} N. \tag{2.17}$$

However, it is easy to show that

$$m_u = -\frac{\rho_u}{\rho} m$$

using (2.2). Therefore, m and m_u are parallel.

On the other hand, direct calculation shows that

$$m_v = -\frac{\rho_u}{\rho^3} X_u + \frac{\rho_{uu}\rho - \rho_u^2}{\rho^2} N \tag{2.18}$$

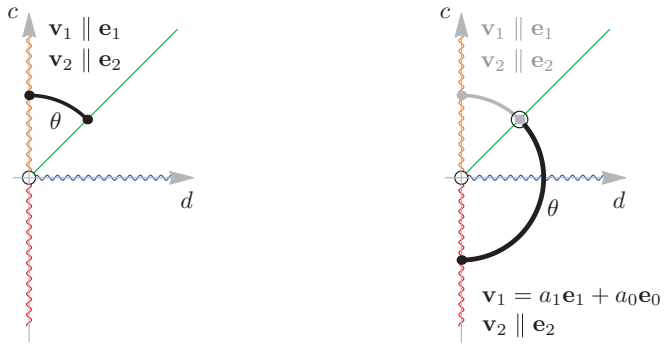

Figure 2.2: Choice of parameter and axial directions for cases (1a) and (1b).

and

$$m_{vv} = \frac{2\rho_u\rho_v}{\rho^4}X_u - \frac{\rho_{uu}\rho}{\rho^4}X_v + \frac{2\rho_u^2\rho_v - \rho\rho_{uu}\rho_v}{\rho^3}N,$$

implying that

$$\det(m, m_v, m_{vv}) = 0.$$

Since $f(u)$ is not identically equal to zero, let u_0 be a constant such that $f(u_0) \neq 0$. Then, for all v, $m(u_0, v)$ and $m_v(u_0, v)$ are linearly independent. Therefore, $\vec{v}_1$ such that

$$\langle m(u_0, v), \vec{v}_1\rangle = \langle m_v(u_0, v), \vec{v}_1\rangle = 0$$

is unique up to scaling. However, the direction of m is independent of u; therefore, such $\vec{v}_1$ is unique for all u and v. The analogous statement for $\vec{v}_2$ is shown similarly. □

Since $\vec{v}_1$ and $\vec{v}_2$ are constant, we use (2.2a), (2.2b), (2.4), and (2.5a)–(2.5d) to calculate that

$$\langle \vec{v}_1, \vec{v}_1\rangle = c, \quad \langle \vec{v}_2, \vec{v}_2\rangle = d, \tag{2.19}$$

implying that the axial directions of the surface has the following causalities: if $d > 0$,

- both $\vec{v}_1$ and $\vec{v}_2$ are spacelike if $c > 0$,
- $\vec{v}_1$ is lightlike, but $\vec{v}_2$ is spacelike if $c = 0$, or
- $\vec{v}_1$ is timelike, but $\vec{v}_2$ is spacelike if $c < 0$.

Note that if $d = 0$, then $g(v) \equiv 0$, implying that $\vec{v}_2$ does not exist. By aligning the axial directions with coordinate axes of the ambient space, we now calculate the unit normal vector.

First, assume $\Delta\rho \not\equiv 0$. Since the definition of $f(u)$ and $g(v)$ depend on the signature of $c - d$, we consider each case separately.

Case (1a)

Assume first that $d - c \leq 0$ (see left side of Fig. 2.2). Then $\vec{v}_1$ and $\vec{v}_2$ are both spacelike, and we align the axial directions so that $\vec{v}_1$ and $\vec{v}_2$ are parallel to $\mathbf{e}_1$ and $\mathbf{e}_2$, respectively,

where $\mathbf{e}_i$ are the unit vectors in the x_i-direction for $i = 1, 2, 0$. Then, we may calculate the unit normal vector as follows.

Lemma 2.13. *Let $N(u, v) = (N_1, N_2, N_0)$ be the unit normal vector to the surface $X(u, v)$ satisfying case (1) of Proposition 2.9. If $c - d \geq 0$, then, the unit normal vector is given by*

$$N(u, v) = \left(-\frac{1}{\sqrt{c}} \frac{\rho_u}{\rho}, -\frac{1}{\sqrt{d}} \frac{\rho_v}{\rho}, \sqrt{\frac{1}{c} \frac{(\rho_u)^2}{\rho^2} + \frac{1}{d} \frac{(\rho_v)^2}{\rho^2} + 1} \right).$$

Proof. Since $\langle m, \vec{v}_1 \rangle = 0$, (2.1) and (2.17) implies that

$$N_1 = \tilde{D}_1(u) \frac{1}{\rho}$$

for some function $\tilde{D}_1(u)$. Furthermore, from $\langle m_v, \vec{v}_1 \rangle = 0$, using (2.1) and (2.18), we may show that

$$N_1 = \tilde{D}_2(v) \frac{\rho_u}{\rho}$$

for some function $\tilde{D}_2(v)$. Therefore, $\tilde{D}_1(u) = \tilde{D}_2(v)\rho_u = D_1\rho_u$ for some constant D_1.

Now $c > d \geq 0$ implies that there is some u_0 such that $f(u_0) = 0$. Then, $\langle m, X_u \rangle = \langle m_v, X_u \rangle$ on (u_0, v), and it follows that $X_u(u_0, v) \in \operatorname{span}\{\mathbf{e}_1\}$. Therefore,

$$\rho^2 = \|X_u(u_0, v)\|^2 = ((X_1(u_0, v))_u)^2 = \rho^2 (D_1)^2 c.$$

Similarly, by letting $\vec{v}_2 = \mathbf{e}_2$, we understand that

$$N_2 = \frac{1}{\sqrt{d}} \frac{\rho_v}{\rho}.$$

Finally, use the fact that N is a unit normal vector to get the desired conclusion. □

Now, let $d = r \cos\theta$ and $c = r \sin\theta$ for $\theta \in \left[\frac{\pi}{4}, \frac{\pi}{2}\right]$ (see left side of Fig. 2.2). Since r is a homothety factor of domain (u, v)-plane by (2.15), we may assume $r = 1$. Using the above lemma, we may find the normal vector $N^\theta(u, v)$ dependent on θ. On the other hand, since the meromorphic function $h(u, v)$ of the Weierstrass data is equal to the normal vector function under stereographic projection, and since $Q = -\frac{1}{2}(h_u - ih_v)\eta = -\frac{1}{2}$,

$$h(u, v) = \frac{1}{1 - N_0(u, v)} (N_1(u, v) + iN_2(u, v)), \quad \eta(u, v) = \frac{1}{h_u - ih_v}.$$

Therefore, using $N^\theta(u,v)$, we calculate that for $\theta \in \left[\frac{\pi}{4}, \frac{\pi}{2}\right]$,

$$\begin{aligned} h^\theta(z) &= \begin{cases} \dfrac{A_2 \tan\left(\frac{1}{2}(A_1 z + A_3)\right)}{A_1}, & \text{if } \theta \neq \frac{\pi}{4} \\ 2^{-1/4} z + 1, & \text{if } \theta = \frac{\pi}{4} \end{cases} \\ \eta^\theta(z) &= \begin{cases} \dfrac{\cos^2\left(\frac{1}{2}(A_1 z + A_3)\right)}{A_2}, & \text{if } \theta \neq \frac{\pi}{4} \\ 2^{-3/4}, & \text{if } \theta = \frac{\pi}{4} \end{cases} \end{aligned} \tag{2.20}$$

where $A_1(\theta) = \sqrt{\sin\theta - \cos\theta}$, $A_2(\theta) = \sqrt{\cos\theta} + \sqrt{\sin\theta}$, and $A_3(\theta) = \tan^{-1}\left(\sqrt{\tan\theta - 1}\right)$.

Case (1b)

Now assume that $d - c > 0$ (see right side of Fig. 2.2). Then, since the causality of $\vec{v}_1$ changes while that of $\vec{v}_2$ is always spacelike, we let

$$\vec{v}_1 = a_1 \mathbf{e}_1 + a_0 \mathbf{e}_0 \tag{2.21}$$

for some real constants a_0 and a_1, while we let $\vec{v}_2$ be parallel to $\mathbf{e}_2$. To calculate the unit normal vector N for this case, we first need the following lemma.

Lemma 2.14. *Let $N(u,v) = (N_1, N_2, N_0)$ be the unit normal vector to the surface $X(u,v)$ satisfying case (1) of Proposition 2.9. If $d - c > 0$, then*

$$a_1 N_1 - a_0 N_0 = -\frac{\sqrt{a_1^2 - a_0^2}}{\sqrt{c}} \frac{\rho_u}{\rho}, \quad N_2 = -\frac{1}{\sqrt{d}} \frac{\rho_v}{\rho} \tag{2.22}$$

where a_1 and a_0 are as in (2.21).

Proof. Employing similar techniques to those used in the proof of Lemma 2.13 implies that

$$a_1 N_1 - a_0 N_0 = D_2 \cdot \frac{\rho_u}{\rho}. \tag{2.23}$$

for some constant D_2. To find D_2 in (2.23), consider the following system of equations,

$$\begin{cases} c = \|((\rho_u)^2 - \rho \cdot \rho_{uu}) N_u + \rho_u \rho_v N_v + \frac{\rho_u}{\rho} N\|^2 \\ a_1 N_1 - a_0 N_0 = D_2 \cdot \frac{\rho_u}{\rho} \\ N_1^2 + \frac{1}{d} \frac{\rho_v^2}{\rho^2} - N_0^2 = -1 \end{cases}$$

where the first equation comes from (2.1), (2.16), and (2.19). Since D_2 is constant, we may solve for D_2 at the point $\left(0, \frac{\pi}{2\sqrt{d-c}}\right)$ to get (2.22). □

Since N is unit length, (2.22) lets us calculate the normal of the surface for any given a_0, a_1, c, and d. Similar to the previous case, let $d = \cos\theta$ and $c = \sin\theta$ for $\theta \in \left[-\frac{\pi}{2}, \frac{\pi}{4}\right)$, and further let

$$a_0 = \sqrt{\cos\theta - \sin\theta}, \quad a_1 = \sqrt{\cos\theta}.$$

Now, we calculate the normal vector, and find that for $\theta \in \left[-\frac{\pi}{2}, \frac{\pi}{4}\right)$,

$$h^\theta(z) = \frac{B_2 e^{B_1 z} - 1}{B_2 - 1}, \quad \eta^\theta(z) = \frac{(B_2 - 1)e^{-B_1 z}}{2B_1 B_2} \tag{2.24}$$

where $B_1(\theta) = \sqrt{\cos\theta - \sin\theta}$ and $B_2(\theta) = 1 + \sqrt{1 - \tan\theta}$.

Case (2)

Finally, we consider the case when $\Delta\rho \equiv 0$. By Remark 2.10, we only need to consider $\rho(u, v) = u$, and then utilize the parameter $\lambda \in \mathbb{S}^1 \subset \mathbb{C}$ for the associated family for $\eta(u, v)$. First we assume that the lightlike axis $\vec{v}_1 = \mathbf{e}_1 + \mathbf{e}_0$. Then similar to the previous cases,

$$N_1 - N_0 = D_3 \cdot \frac{\rho_u}{\rho} = D_3 \cdot \frac{1}{u}$$

for some real constant D_3. By applying the scaling of u, without loss of generality, we can assume $D_3 = -1$. Now since $\rho(u, v) = u$ is independent of v, we notice that $N(u, v)$ has the form of $N(u, v) = \big(N_1(u),\ 0,\ N_0(u)\big) \cdot T(v)$ for a specific isometry transform $T(v) \in \mathrm{SO}_{2,1}$ keeping the lightlike axis $\mathbf{e}_1 + \mathbf{e}_0$. Thus we get the following:

Lemma 2.15. *For case (2) in Proposition 2.9, the unit normal vector N of $\tilde{X}$ is given by*

$$\begin{aligned} N(u, v) &= \left(\frac{u^2 - 1}{2u},\ 0,\ \frac{u^2 + 1}{2u}\right) \cdot \begin{pmatrix} 1 - \frac{v^2}{2} & v & -\frac{v^2}{2} \\ -v & 1 & -v \\ \frac{v^2}{2} & -v & 1 + \frac{v^2}{2} \end{pmatrix} \\ &= \left(\frac{u^2 + v^2 - 1}{2u},\ -\frac{v}{u},\ \frac{u^2 + v^2 + 1}{2u}\right). \end{aligned}$$

Using the above proposition, we obtain the following Weierstrass data, up to the homothety of domain:

$$\tilde{h}(z) = -\frac{1 + z}{-1 + z}, \quad \tilde{\eta}(z) = \frac{1}{4}(-1 + z)^2. \tag{2.25}$$

By changing data $(\tilde{h}, \tilde{\eta}) \mapsto (\tilde{h}, \lambda^{-2}\tilde{\eta})$, we get all maxfaces in case (2) with parameter $\lambda \in \mathbb{S}^1$.

Since the data obtained all satisfy the meromorphicity and holomorphicity conditions, we may use the Weierstrass-type representation for maxfaces to obtain the following parametrizations.

Theorem 2.16. *If $X(u, v)$ is a non-planar maxface of Bonnet-type in $\mathbb{R}^{2,1}$, then the surface*

is given by the following parametrization on its domain for some $\theta \in \left[-\frac{\pi}{2}, \frac{\pi}{2}\right]$*:*

$$X^\theta(u,v) = \begin{cases} \begin{pmatrix} \frac{(A_1^2+A_2^2)A_1u+(A_1^2-A_2^2)\sin(A_1u+A_3)\cosh(A_1v)+(A_2^2-A_1^2)\sin A_3}{2A_1^3A_2} \\ \frac{(A_2^2-A_1^2)A_1v-(A_1^2+A_2^2)\cos(A_1u+A_3)\sinh(A_1v)}{2A_1^3A_2} \\ \frac{\cos(A_1u+A_3)\cosh(A_1v)-\cos A_3}{A_1^2} \end{pmatrix}^t, \\ \qquad\qquad \text{if } \theta \in \left(\frac{\pi}{4}, \frac{\pi}{2}\right] \\ \begin{pmatrix} \frac{e^{-B_1u}\left\{\left(B_2(B_2(e^{2B_1}-1)+2)-2\right)\cos(B_1v)-2e^{B_1u}\left(B_1B_2u+B_2-1\right)\right\}}{2(B_1)^2B_2(B_2-1)} \\ \frac{e^{-B_1u}\left\{(B_2e^{2B_1u}-B_2+2)\sin(B_1v)-2B_1ve^{B_1u}\right\}}{2(B_1)^2(B_2-1)} \\ -\frac{B_1B_2u+e^{-B_1u}\cos(B_1v)-1}{(B_1)^2B_2} \end{pmatrix}^t, \\ \qquad\qquad \text{if } \theta \in \left[-\frac{\pi}{2}, \frac{\pi}{4}\right) \\ \frac{1}{\sqrt{2}}\left(\hat{u}-\hat{u}\hat{v}^2+\frac{1}{3}\hat{u}^3-\frac{4}{3},\ -\hat{v}+\hat{u}^2\hat{v}-\frac{1}{3}\hat{v}^3,\ -\hat{u}^2+\hat{v}^2+1\right), \\ \qquad\qquad \text{if } \theta = \frac{\pi}{4} \end{cases} \tag{2.26}$$

where $(\hat{u}, \hat{v})$ *is given by* $u = 2^{1/4}(\hat{u}-1)$ *and* $v = 2^{1/4}\hat{v}$*, and*

$$\begin{cases} A_1(\theta) = \sqrt{\sin\theta - \cos\theta}, A_2(\theta) = \sqrt{\cos\theta} + \sqrt{\sin\theta}, A_3(\theta) = \tan^{-1}\left(\sqrt{\tan\theta - 1}\right) \\ B_1(\theta) = \sqrt{\cos\theta - \sin\theta}, B_2(\theta) = 1 + \sqrt{1-\tan\theta}; \end{cases}$$

or for some $\lambda^{-2} \in \mathbb{S}^1$*,*

$$\tilde{X}^\lambda(u,v) = \frac{\mathrm{Re}(\lambda^{-2})}{2}\begin{pmatrix} u - uv^2 + \frac{1}{3}u^3 \\ 2uv \\ -u - uv^2 + \frac{1}{3}u^3 \end{pmatrix}^t - \frac{\mathrm{Im}(\lambda^{-2})}{2}\begin{pmatrix} v + u^2v - \frac{1}{3}v^3 \\ -u^2 + v^2 \\ -v + u^2v - \frac{1}{3}v^3 \end{pmatrix}^t \tag{2.27}$$

up to isometries and homotheties of $\mathbb{R}^{2,1}$*. In fact, it must be a piece of one, and only one, of the following:*

- *maximal Enneper-type surface* (E) *with Weierstrass data* $(2^{-1/4}z + 1, 2^{-3/4}\,\mathrm{d}z)$*,* $(\theta = \frac{\pi}{4})$*,*
- *maximal catenoid with lightlike axis* ($\mathrm{C_L}$) *with Weierstrass data*

  $$\left(-\frac{1+z}{-1+z}, \frac{1}{4}(-1+z)^2\,\mathrm{d}z\right),$$

  or a member of its associated family $(\lambda \in \mathbb{S}^1)$*,*
- *maximal catenoid with spacelike axis* ($\mathrm{C_S}$) *with Weierstrass data*

$\left(\tan\left(\frac{1}{4}(\pi+2z)\right), \frac{1}{2}(1-\sin z)\,\mathrm{d}z\right)$, $(\theta=\frac{\pi}{2})$,

- *maximal catenoid with timelike axis* $(\mathrm{C_T})$ *with Weierstrass data* $\left(e^z, \frac{1}{2}e^{-z}\,\mathrm{d}z\right)$, $(\theta=-\frac{\pi}{2})$,

- *maximal Bonnet-type surface with lightlike axial direction* $(\mathrm{B_L})$ *with Weierstrass data* $\left(2e^z-1, \frac{1}{4}e^{-z}\,\mathrm{d}z\right)$, $(\theta=0)$,

- *maximal Bonnet-type surface with spacelike axial direction* $(\mathrm{B_S})$ *with Weierstrass data*

$$\left\{\left(\frac{A_2\tan\left(\frac{1}{2}(A_1z+A_3)\right)}{A_1}, \frac{\cos^2\left(\frac{1}{2}(A_1z+A_3)\right)}{A_2}\,\mathrm{d}z\right) : \theta\in\left(\tfrac{\pi}{4},\tfrac{\pi}{2}\right)\right\}, \textit{ or}$$
$$\left\{\left(\frac{B_2e^{B_1z}-1}{B_2-1}, \frac{(B_2-1)e^{-B_1z}}{2B_1B_2}\,\mathrm{d}z\right) : \theta\in\left(0,\tfrac{\pi}{4}\right)\right\},$$

- *or maximal Bonnet-type surface with timelike axial direction* $(\mathrm{B_T})$ *with Weierstrass data*

$$\left\{\left(\frac{B_2e^{B_1z}-1}{B_2-1}, \frac{(B_2-1)e^{-B_1z}}{2B_1B_2}\,\mathrm{d}z\right) : \theta\in\left(-\tfrac{\pi}{2},0\right)\right\}.$$

Moreover, $X^\theta(u,v)$ *is continuous at every point* (u,v) *with respect to the parameter* θ*.*

Note that by (2.19), we see that the different classes of maximal Bonnet-type surfaces mentioned in [76] have a geometric meaning; namely, the causal character of the axial directions are different. Finally, it should be noted that a catenoid with timelike axis is indeed a limiting case of maximal Bonnet-type surfaces with timelike axial direction, while a catenoid with spacelike axis is a limiting case of maximal Bonnet-type surfaces with spacelike axial direction.

2.2 Deformation of maximal surfaces of Bonnet-type

Now, we show that all maxfaces of Bonnet-type can be conjoined by a single continuous deformation. However, as seen in the previous section, the Weierstrass data and the parametrizations of such surfaces depended on two separate parameters θ and λ. Therefore, we need to show that there exists a deformation consisting of maxfaces of Bonnet-type that connects the surfaces in each parameter family. In addition, it must be verified that the plane can also be attained as a limit of such surfaces.

Therefore, in this section, we explain how all the maxfaces of Bonnet-type can be joined by a series of continuous deformations. We consider a deformation to be "continuous" with respect to a parameter, if the deformation dependent on the parameter converges uniformally over compact subdomains component-wise. In fact, it will be enough to show that each component function in the parametrization is continuous for the parameter at any point (u,v) in the domain.

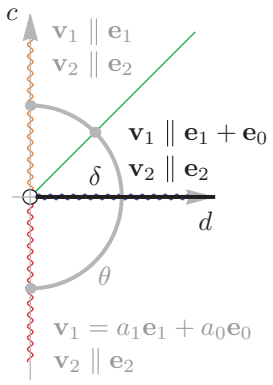

Figure 2.3: Choice of parameter and axial directions for deformation to the catenoid with lightlike axis.

2.2.1 Deformation to the maximal catenoid with lightlike axis

First, we will show that there exists a deformation between a maximal Bonnet-type surface with lightlike axial direction and a maximal catenoid with lightlike axis. Assume $c = 0$ and $d > 0$ (see Fig. 2.3). Then by (2.19), $\vec{v}_1$ is a lightlike axial direction while $\vec{v}_2$ is a spacelike axial direction. Therefore, align the vectors as $\vec{v}_1 \parallel \mathbf{e}_1 + \mathbf{e}_0$ and $\vec{v}_2 \parallel \mathbf{e}_2$.

Then by Lemma 2.14, $N_1 - N_0 = -\frac{\rho_u}{\rho}$, and $N_2 = -\frac{1}{\delta}\frac{\rho_v}{\rho}$ where $\delta = \sqrt{d}$. Again using the unit normal vector, we calculate the following Weierstrass data:

$$h^{\delta}_{\mathrm{C_L}}(z) = \frac{(\delta+1)e^{\delta z} - 1}{(\delta-1)e^{\delta z} + 1}, \quad \eta^{\delta}_{\mathrm{C_L}}(z) = \frac{\left(1 + (\delta-1)e^{\delta z}\right)^2}{4\delta^2 e^{\delta z}}.$$

Note that

$$h^{\delta}_{\mathrm{C_L}}(z)\Big|_{\delta=1} = h^{\theta}(z)\Big|_{\theta=0}, \quad \eta^{\delta}_{\mathrm{C_L}}(z)\Big|_{\delta=1} = \eta^{\theta}(z)\Big|_{\theta=0},$$
$$\lim_{\delta\searrow 0} h^{\delta}_{\mathrm{C_L}}(z) = \tilde{h}(z), \quad \lim_{\delta\searrow 0} \eta^{\delta}_{\mathrm{C_L}}(z) = \tilde{\eta}(z).$$

In addition, by using the Weierstrass-type representation theorem,

$$X^{\delta}_{\mathrm{C_L}}(u,v) = \begin{pmatrix} \frac{e^{-\delta u}\left\{((\delta^2+1)e^{2\delta u}-1)\cos(\delta v) - \delta(2u+\delta)e^{\delta u}\right\}}{2\delta^3} \\ \frac{e^{\delta u}\sin(\delta v) - \delta v}{\delta^2} \\ \frac{e^{-\delta u}\left\{-((\delta^2-1)e^{2\delta u}+1)\cos(\delta v) - \delta(2u-\delta)e^{\delta u}\right\}}{2\delta^3} \end{pmatrix}^t$$

for $\delta > 0$. Since

$$X^{\delta}_{\mathrm{C_L}}(u,v)\Big|_{\delta=1} = X^{\theta}(u,v)\Big|_{\theta=0}, \quad \lim_{\delta\searrow 0} X^{\delta}_{\mathrm{C_L}}(u,v) = \tilde{X}^{\lambda}(u,v)\Big|_{\lambda=1},$$

$X^{\delta}_{\mathrm{C_L}}(u,v)$ is a continuous deformation from maximal Bonnet-type surface with lightlike axial direction ($\mathrm{B_L}$) to the maximal catenoid with lightlike axis ($\mathrm{C_L}$) (or maximal Enneper-type surface of second kind).

2.2.2 Deformation to the plane

Now, we show that there exists a deformation connecting maximal catenoid with spacelike axis to the plane. Up to this point, to solve the system of ordinary differential equations (2.5a)–(2.5d), we assumed that $\rho_u(0,v) = f(0) = 1$, and $\rho_v(u,0) = g(0) = 0$. However, since $\rho(u,v) \equiv 1$ for the plane, we must consider different initial conditions for $f(u)$ and $g(v)$. Therefore, we use the result from Lemma 2.5 and consider the surfaces corresponding to case (1a), to assume that $f(0) = 0$ and $g(0) = 0$. Solving (2.5a)–(2.5d) similarly, we get

$$f_{\mathrm{P}}(u) = \frac{\sqrt{c}}{\sqrt{c-d}} \sin\left(\sqrt{c-d}\, u\right), \quad g_{\mathrm{P}}(v) = \frac{\sqrt{d}}{\sqrt{c-d}} \sinh\left(\sqrt{c-d}\, v\right)$$

where $c^2 + d^2 \neq 0$.

Since we assumed each of $f(u)$ and $g(v)$ has a zero, both axial directions are spacelike, and we may use Lemma 2.13 to calculate the unit normal vector. After letting $\sqrt{c} = \cos\psi$ and $\sqrt{d} = \sin\psi$, we calculate the Weierstrass data as

$$h^{\psi}_{\mathrm{P}}(z) = \frac{\sqrt{\cos 2\psi}}{\cos\psi - \sin\psi} \tan\left(\frac{\sqrt{\cos 2\psi}}{2}(z + S^{\psi})\right)$$
$$\eta^{\psi}_{\mathrm{P}}(z) = \frac{1}{\cos\psi + \sin\psi} \cos^2\left(\frac{\sqrt{\cos 2\psi}}{2}(z + S^{\psi})\right)$$

for $\psi \in \left(-\frac{\pi}{4}, 0\right]$, where the factor for shifting parameter $S^{\psi} = 2\psi + \frac{\pi}{2}$ was chosen so that

$$h^{\psi}_{\mathrm{P}}(z)\Big|_{\psi=0} = h^{\theta}(z)\Big|_{\theta=\frac{\pi}{2}}, \quad \eta^{0}_{\mathrm{P}}(z)\Big|_{\psi=0} = \eta^{\theta}(z)\Big|_{\theta=\frac{\pi}{2}}.$$

Using the Weierstrass-type representation theorem, and multiplying by a homothety factor $\cos 2\psi$, we find that

$$X^{\psi}_{\mathrm{P}}(u,v) = \begin{cases} \begin{pmatrix} \frac{u\cos\psi\sqrt{\cos 2\psi} - \sin\psi \sin\left((u+S^{\psi})\sqrt{\cos 2\psi}\right)\cosh\left(v\sqrt{\cos 2\psi}\right)}{\sqrt{\cos 2\psi}} \\ \frac{v\sin\psi\sqrt{\cos 2\psi} - \cos\psi\cos\left((u+S^{\psi})\sqrt{\cos 2\psi}\right)\sinh\left(v\sqrt{\cos 2\psi}\right)}{\sqrt{\cos 2\psi}} \\ \cos\left((u+S^{\psi})\sqrt{\cos 2\psi}\right)\cosh\left(v\sqrt{\cos 2\psi}\right) \end{pmatrix}^{t}, & \text{if } \psi \neq -\frac{\pi}{4} \\ \left(\sqrt{2}u, -\sqrt{2}v, 1\right), & \text{if } \psi = -\frac{\pi}{4} \end{cases}$$

for $\psi \in \left[-\frac{\pi}{4}, 0\right]$, where $X^{\psi}_{\mathrm{P}}(u,v)\Big|_{\psi=-\frac{\pi}{4}} = \lim_{\psi\searrow -\frac{\pi}{4}} X^{\psi}_{\mathrm{P}}(u,v)$. Since

$$X^{\psi}_{\mathrm{P}}(u,v)\Big|_{\psi=0} = X^{\theta}(u,v)\Big|_{\theta=\frac{\pi}{2}},$$

$X^{\psi}_{\mathrm{P}}(u,v)$ defines a continuous deformation from the maximal catenoid with spacelike axis ($\mathrm{C_S}$) to the plane (P). In summary, we get the following theorem.

Theorem 2.17. *There exists a continuous deformation consisting precisely of the maxfaces of Bonnet-type (see Fig. 2.4 and Fig. 2.5).*

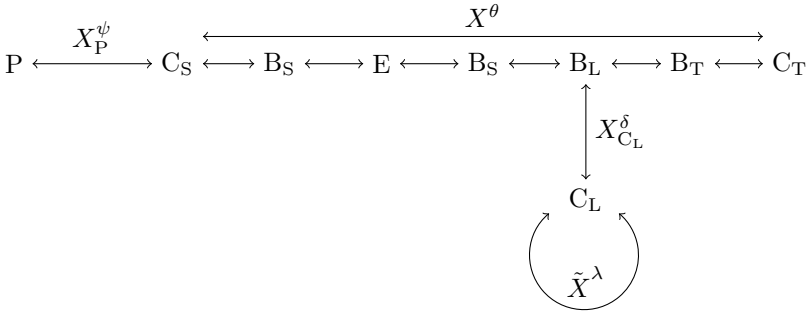

Figure 2.4: Diagram of deformations connecting maxfaces of Bonnet-type.

2.3 Singularities of maximal Bonnet-type surfaces

As mentioned in Remark 2.10, *maxfaces* was introduced as a class of maximal surfaces with singularities in [110]. In this section, we investigate the types of singularities appearing on maxfaces of Bonnet-type. Since the types of singularities of maximal catenoids and maximal Enneper-type surfaces have been investigated [47, 71, 110], we focus on recognizing the types of singularities on maximal Bonnet-type surfaces.

Let $S(X) := \{(u, v) \in \mathbb{R}^2 : \rho(u, v) = 0\}$ be the singular set. Then using the explicit solution of the metric function in Proposition 2.9, we understand that the singular set becomes 1-dimensional. To recognize the types of singularities of maximal Bonnet-type surfaces, we refer to the following results from [47, 91, 110].

Fact 2.18. *Let $X(u, v) : \Sigma \to \mathbb{R}^{2,1}$ be a maxface with Weierstrass data $(h, \eta\, \mathrm{d}z)$. Then, a point $p \in \Sigma$ is a singular point if and only if $|h(p)| = 1$. Furthermore, for*

$$\varphi := \frac{h_z}{h^2\eta}, \quad \phi := \frac{h}{h_z}\varphi_z, \quad \Phi := \frac{h}{h_z}\phi_z,$$

the image of X around a singular point p is locally diffeomorphic to

- *a cuspidal edge if and only if $\operatorname{Re}\varphi \neq 0$ and $\operatorname{Im}\varphi \neq 0$ at p,*
- *a swallowtail if and only if $\varphi \in \mathbb{R} \setminus \{0\}$ and $\operatorname{Re}\phi \neq 0$ at p,*
- *a cuspidal cross cap if and only if $\varphi \in i\,\mathbb{R} \setminus \{0\}$ and $\operatorname{Im}\phi \neq 0$ at p, or*
- *a cuspidal S^-_1 singularity if and only if $\varphi \in i\,\mathbb{R} \setminus \{0\}$, $\phi \in \mathbb{R} \setminus \{0\}$, and $\operatorname{Im}\Phi \neq 0$ at p.*

To make the calculations simpler, from Lemma 2.14, assume that $c = t^2 - 1$ and $d = t^2$ for $t > 0$. If we further assume that $a_1 = t$ and $a_0 = 1$, then we obtain the following Weierstrass data:

$$h^t(z) = e^z - t, \quad \eta^t(z) = \frac{e^{-z}}{2} \tag{2.28}$$

after a shift of paramter $u \mapsto u + \log(t + 1)$. Note that this Weierstrass data represents exactly the Bonnet family described in [76], and that all maximal Bonnet-type surfaces are included in this family by Theorem 2.11. Then, for the family,

- If $t > 1$, the surface is a maximal Bonnet-type surface with spacelike axial direction.

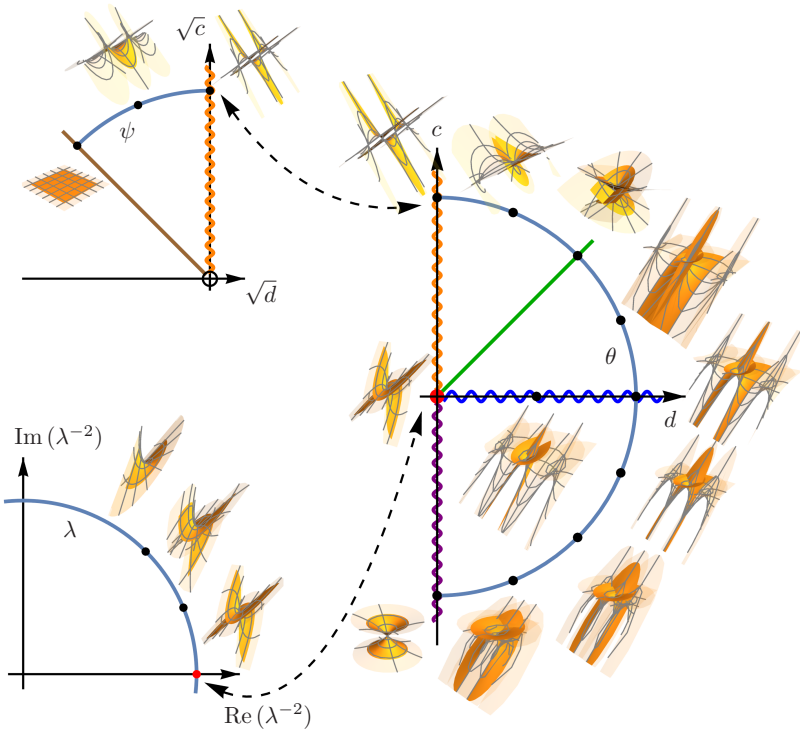

Figure 2.5: Maxfaces of Bonnet-type and their deformations.

- If $t = 1$, the surface is a maximal Bonnet-type surface with lightlike axial direction.
- If $t < 1$, the surface is a maximal Bonnet-type surface with timelike axial direction.

By directly calculating φ, ϕ, and Φ, and using Fact 2.18, we arrive at the following result.

Proposition 2.19. *Let $X^t(u, v)$ be a maximal Bonnet-type surface with the Weierstrass data given in* (2.28)*. The image of X around a singular point $p = (u, v)$ is locally diffeomorphic to the following:*

- *a swallowtail (SW) only at*

$$\begin{array}{lll} 0 < t < 1 & (\mathrm{B_T}): & \left(\log(\oplus\!\!\!\!\ominus\, t + 1), \cos^{-1}(\oplus\!\!\!\!\ominus 1)\right) \\ t = 1 & (\mathrm{B_L}): & (\log 2, \cos^{-1} 1) \\ t > 1 & (\mathrm{B_S}): & (\log(t \pm 1), \cos^{-1} 1), \left(\log \sqrt{t^2 - 1}, \cos^{-1} \sqrt{1 - t^{-2}}\right) \end{array}$$

- *a cuspidal cross cap (CCR) only at*

$$\begin{array}{lll} 0 < t \leq \frac{1}{\sqrt{2}} & (\mathrm{B_T}): & \textit{None} \\ \frac{1}{\sqrt{2}} < t < 1 & (\mathrm{B_T}): & \left(\log\left(\oplus\!\!\!\!\ominus \sqrt{t^2 - \frac{1}{2}} + \sqrt{\frac{1}{2}}\right), \cos^{-1}\left(\oplus\!\!\!\!\ominus \frac{1}{t}\sqrt{t^2 - \frac{1}{2}}\right)\right) \\ t = 1 & (\mathrm{B_L}): & \left(\log \sqrt{2}, \cos^{-1} \frac{1}{\sqrt{2}}\right) \\ t > 1 & (\mathrm{B_S}): & \left(\log\left(\sqrt{t^2 - \frac{1}{2}} \pm \sqrt{\frac{1}{2}}\right), \cos^{-1}\left(\frac{1}{t}\sqrt{t^2 - \frac{1}{2}}\right)\right) \end{array}$$

- *or a cuspidal S_1^- singularity (CS) only at*

$$t = 1/\sqrt{2} \quad (\mathrm{B_T}): \quad \left(-\log(\sqrt{2}), \cos^{-1} 0\right)$$

where $\oplus\!\!\!\!\ominus$ corresponds to each other.

Hence, from the singularity theory point of view, we understand that maximal Bonnet-type surfaces with timelike axial directions can further be classified into the following three types: type 1 ($\mathrm{B_{T1}}$), type 2 ($\mathrm{B_{T2}}$), or type 3 ($\mathrm{B_{T3}}$).

Since maximal Bonnet-type surfaces are periodic in the v-direction, let a single portion of $X(u, v)$ refer to the part of the surface mapped over a single period of v in the domain. Then, in summary, we understand the following theorem concerning the types of singularities on maximal Bonnet-type surfaces.

Theorem 2.20. *Let $X^t(u, v)$ be a maximal Bonnet-type surface with the Weierstrass data given in* (2.28)*. The images of a single portion of X around singular points are locally*

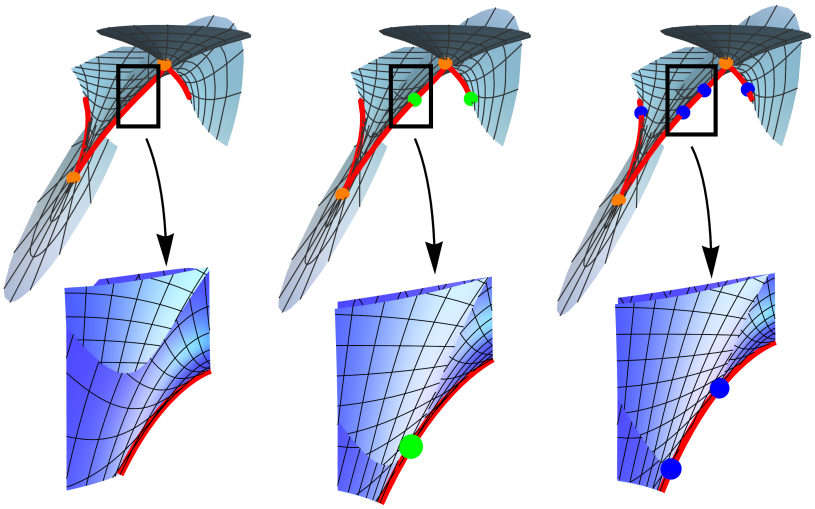

Figure 2.6: Types of singularities for maximal Bonnet-type surfaces with timelike axial directions ($\mathrm{B_{T1}}$, $\mathrm{B_{T2}}$, $\mathrm{B_{T3}}$) where the cuspidal edges are highlighted by a red line, swallowtails by orange points, cuspidal cross caps by blue points, and cuspidal S_1^- singularities by green points.

diffeomorphic to cuspidal edges except at the following number of points.

	type of surface	*# of SW*	*# of CCR*	*# of CS*
$0 < t < 1/\sqrt{2}$	$\mathrm{B_{T1}}$	2	0	0
$t = 1/\sqrt{2}$	$\mathrm{B_{T2}}$	2	0	2
$1/\sqrt{2} < t < 1$	$\mathrm{B_{T3}}$	2	4	0
$t = 1$	$\mathrm{B_L}$	1	2	0
$1 < t$	$\mathrm{B_S}$	4	4	0

Combined with the result in [71], [110], and [47], we obtain the following corollary.

Corollary 2.21. *Let $X(u, v)$ be a maxface of Bonnet-type. If p is a singular point of $X(u, v)$, then the image of X around the singular point p must be locally diffeomorphic to one of the following: conelike singularity, fold singularity, cuspidal edge, swallowtail, cuspidal cross cap, or cuspidal S_1^- singularity.*

2.4 Maximal surfaces that are also affine minimal surfaces

In the Euclidean case, Thomsen studied minimal surfaces in $\mathbb{R}^3$ that are also affine minimal surfaces, those surfaces with zero affine mean curvature surfaces and with indefinite affine metric with respect to the equiaffine structure, called Thomsen surfaces, in [109], and commented on the fact that such surfaces are conjugates of minimal surfaces of Bonnet-type.

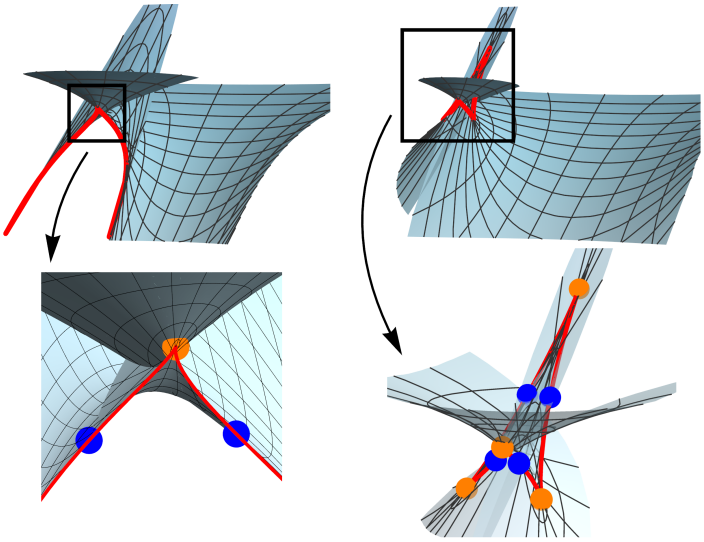

Figure 2.7: Types of singularities for maximal Bonnet-type surfaces with lightlike and space axial directions (B_L, B_S) where the cuspidal edges are highlighted by a red line, swallowtails by orange points, and cuspidal cross caps by blue points.

The analogous statement holds true for maximal surfaces in $\mathbb{R}^{2,1}$ as shown through the following result in [82].

Fact 2.22. *An umbilic-free maximal surface in $\mathbb{R}^{2,1}$ has planar curvature lines if and only if the conjugate surface is an affine minimal surface.*

Therefore, by considering the conjugate surfaces of maximal surfaces of Bonnet-type, we get the following result from Theorem 2.17.

Corollary 2.23 (Corollary to Theorem 2.17)**.** *There exists a continuous deformation consisting precisely of the maximal surfaces that are also affine minimal surfaces.*

Furthermore, by the duality of singularities between conjugate surfaces explored in [110], [69], [47], and [91], we obtain the following classification of singularities on maximal Thomsen-type surfaces.

Corollary 2.24 (Corollary to Theorem 2.20)**.** *Let $Y^t(u,v)$ be a maximal Thomsen-type surface where $Y^t(u,v)$ is the conjugate surface of $X^t(u,v)$ as defined in Theorem 2.20. The images of a single portion of Y around singular points are locally diffeomorphic to cuspidal edges except at the following number of points.*

	# of CCR	*# of SW*	*# of CB*
$0 < t < 1/\sqrt{2}$	2	0	0
$t = 1/\sqrt{2}$	2	0	2
$1/\sqrt{2} < t < 1$	2	4	0
$t = 1$	1	2	0
$1 < t$	4	4	0

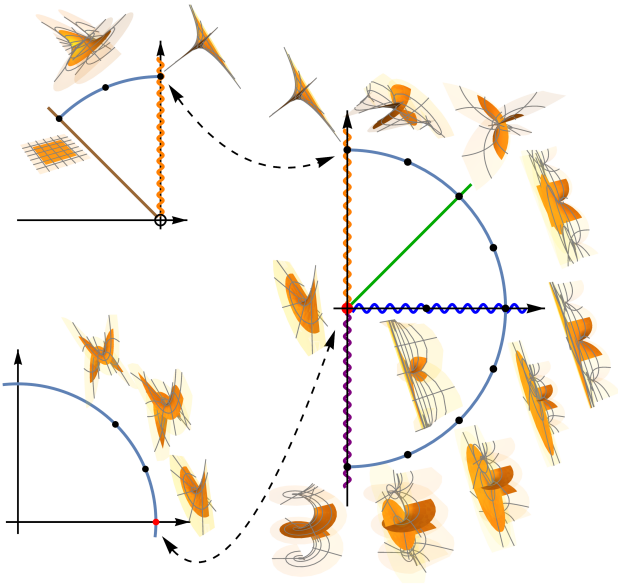

Figure 2.8: Maximal surfaces that are also affine minimal and their deformations.

where CB stands for cuspidal butterfly.

Moreover, if $Y(u, v)$ is a maximal surface that is also an affine minimal surface, then the image of Y around the singular point p must be locally diffeomorphic to one of the following: conelike singularity, fold singularity, cuspidal edge, swallowtail, cuspidal cross cap, or cuspidal butterfly.

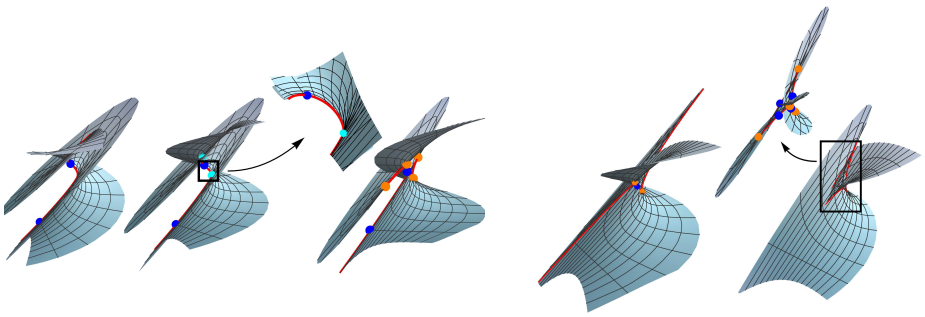

Figure 2.9: Types of singularities for maximal Thomsen-type surfaces where the cuspidal edges are highlighted by a red line, swallowtails by orange points, cuspidal cross caps by blue points, and cuspidal butterflies by cyan points.

Chapter 3

Timelike minimal surfaces of Bonnet-type

In this chapter, we consider the timelike minimal analogue of minimal surfaces of Bonnet-type and Thomsen surfaces in Minkowski 3-space, and clarify their relationship. We first focus on the class of timelike minimal surfaces of Bonnet-type, and consider its classification. To achieve this, we use the following method: First, as in Chapter 2 (see also [1, 116]), using the Lorentz conformal coordinates, we express the timelike minimality condition and the planar curvature line condition via a system of partial differential equations in terms of the Lorentz conformal factor. Then as in Chapter 2 (see also [112, 117]), from the solutions of the system of partial differential equations, we show and utilize the existence of axial directions to recover the Weierstrass data [114] for the Weierstrass-type representation for timelike minimal surfaces given by Konderak [73] (see Fact 3.2). With the Weierstrass data, we give a complete classification of all timelike minimal surfaces of Bonnet-type (see Theorem 3.21).

Then we switch our attention to the class of timelike Thomsen surfaces, defined by Magid in [81] as timelike minimal surfaces that are also affine minimal. In his work, Magid considered the null coordinates representation of timelike minimal surfaces found by McNertney in [84] (see Fact 3.3), where a timelike minimal surface is obtained via two generating null curves. Using this representation, he applied the result given by Manhart in [83] on affine minimal surfaces of particular form, and obtained an explicit parametrization for the generating null curves of timelike Thomsen surfaces.

Therefore, to investigate the relationship between the two classes of timelike minimal surfaces, we now shift the focus to null coordinates. We first characterize timelike minimal surfaces of Bonnet-type in terms of geometric invariants of their generating null curves, called *lightlike curvatures* (see Theorem 3.25). As an application, we obtain deformations of null curves preserving the pseudo-arclength parametrization and the constantness of lightlike curvatures. Then, interpreting Magid's result on timelike Thomsen surfaces in terms of lightlike curvatures, we reveal a surprising relationship between the two classes of timelike minimal surfaces (see Theorem 3.31), surprising since the relationship differs from that of the minimal case in $\mathbb{R}^3$ and the maximal case in $\mathbb{R}^{2,1}$.

Lastly, similar to Chapter 2, we use the axial directions to show that there exists a deformation consisting exactly of all timelike Thomsen surfaces (see Theorem 3.36 and Corollary 3.37). On the other hand, it is possible to consider the singularities appearing on timelike minimal surfaces by viewing the surfaces as *generalized timelike minimal surfaces* as defined in [68, Definition 2.4]. Furthermore, in [108], *minfaces* were defined as a class of timelike minimal surfaces admitting certain types of singularities, a timelike minimal analogue of *maxfaces* defined by Umehara and Yamada in [110, Definition 2.2] for maximal surfaces. It is known that every minface is a generalized timelike minimal surface; however, there exist generalized timelike minimal surfaces that are not minfaces on their domains (see, for example, [68, Example 2.7]). By showing that timelike Thomsen surfaces are minfaces, we recognize the types of singularities appearing on these surfaces, using the criterion introduced in [108] (see Theorem 3.39 and Corollary 3.40).

3.1 Timelike minimal surfaces of Bonnet-type

In this section, we aim to completely classify timelike minimal surfaces of Bonnet-type. To achieve this, we propose the following method: First, we derive a system of partial differential equations for the Lorentz conformal factor from the integrability condition for timelike minimal surfaces and the planar curvature line condition. Then, using the explicit solutions of the Lorentz conformal factor, we calculate the unit normal vector, and then recover the Weierstrass data using the notion of axial directions. In doing so, we show the existence of axial directions for these surfaces; by normalizing these axial directions, we eliminate the freedom of isometry in the ambient space, and complete the classification.

3.1.1 Paracomplex analysis

First, we briefly introduce the set of paracomplex numbers $\mathbb{C}'$, and the theory of paracomplex analysis. For a more detailed introduction, we refer the readers to works such as [3, 62, 73, 120].

We consider the set of paracomplex numbers $\mathbb{C}'$

$$\mathbb{C}' := \{z = x + jy : x, y \in \mathbb{R}\}$$

where j is the imaginary unit such that $j^2 = 1$. Let $z = x + jy$ denote any paracomplex number. We call $\operatorname{Re} z := x$ and $\operatorname{Re} z := y$ the *real* and *imaginary parts* of z, respectively; furthermore, analogous to the set of complex numbers, we use $\bar{z} := x - jy$ to denote the *paracomplex conjugate* of z. In this paper, we denote the *squared norm* of z as $|z|^2 = z\bar{z} = x^2 - y^2$, which may not necessarily be positive.

We also have the paracomplex Wirtinger derivatives $\partial_z := \frac{1}{2}\left(\partial_x + j\partial_y\right)$ and $\partial_{\bar{z}} := \frac{1}{2}\left(\partial_x - j\partial_y\right)$. Given a paracomplex function (typeset using typewriter font throughout the paper) $\mathtt{f} : \mathbb{C}' \to \mathbb{C}'$, we call $\mathtt{f}$ *paraholomorphic* if $\mathtt{f}$ satisfies the Cauchy-Riemann type conditions,

$$\mathtt{f}_{\bar{z}} = \partial_{\bar{z}}\mathtt{f} = 0. \tag{3.1}$$

We define a few elementary paracomplex analytic functions that are used in this paper here via analytically extending the real counterparts. The exponential function $\mathtt{e}^z$ is defined by

$$\mathtt{e}^z := \sum_{n=0}^{\infty} \frac{z^n}{n!}$$

while the circular and hyperbolic functions are defined by

$$\begin{aligned} \mathtt{cosh}\, z &:= \sum_{n=0}^{\infty} \frac{z^{2n}}{(2n)!}, \quad \mathtt{sinh}\, z := \sum_{n=0}^{\infty} \frac{z^{2n+1}}{(2n+1)!}, \\ \mathtt{cos}\, z &:= \sum_{n=0}^{\infty} (-1)^n \frac{z^{2n}}{(2n)!}, \quad \mathtt{sin}\, z := \sum_{n=0}^{\infty} (-1)^n \frac{z^{2n+1}}{(2n+1)!} \end{aligned} \tag{3.2}$$

suggesting that we have the paracomplex version of Euler's formula

$$\mathtt{e}^{jz} = \mathtt{cosh}\, z + j\, \mathtt{sinh}\, z$$

for any z. We also define the hyperbolic tangent and tangent functions by

$$\mathtt{tanh}\, z := \frac{\mathtt{sinh}\, z}{\mathtt{cosh}\, z}, \quad \mathtt{tan}\, z := \frac{\mathtt{sin}\, z}{\mathtt{cos}\, z}.$$

Since these functions are the analytic continuations of the corresponding real hyperbolic tangent and tangent functions, $\mathtt{tanh}\, z$ is defined on $\mathbb{C}'$ but $\mathtt{tan}\, z$ is defined on $\{z \in \mathbb{C}' \mid |\operatorname{Re} z \pm \operatorname{Re} z| < \frac{\pi}{2}\}$.

Remark 3.1. We note here that the definition of circular functions $\mathtt{sin}\, z$ and $\mathtt{cos}\, z$ are different from those in [73]. In [73], these functions were defined via the paracomplex exponential function and the paracomplex Euler's formula; in (3.2), these functions are defined via analytic continuation from the real counterparts.

3.1.2 Timelike minimal surface theory

Let $\mathbb{R}^{2,1}$ be the Minkowski 3-space endowed with Lorentzian metric

$$\langle (\xi_1, \xi_2, \xi_0), (\zeta_1, \zeta_2, \zeta_0) \rangle := \xi_1\zeta_1 + \xi_2\zeta_2 - \xi_0\zeta_0,$$

and let $\mathbb{R}^{1,1}$ denote the Minkowski 2-plane endowed with Lorentzian metric

$$\langle (\xi_1, \xi_0), (\zeta_1, \zeta_0) \rangle := \xi_1\zeta_1 - \xi_0\zeta_0.$$

We identify the set of paracomplex numbers $\mathbb{C}'$ with Minkowski 2-plane $\mathbb{R}^{1,1}$ via $x + jy \leftrightarrow (x, y)$, and we let Σ denote a simply-connected domain with coordinates (x, y) in $\mathbb{R}^{1,1}$.

Let $F : \Sigma \to \mathbb{R}^{2,1}$ be a timelike immersion. As proved in [115, p.13], there always exist null coordinates (u, v) at each point on Σ. Hence, Lorentz conformal coordinates (x, y) also exist, by the relation

$$(x, y) = \left(\frac{u+v}{2}, \frac{u-v}{2} \right),$$

so that the induced metric $\mathrm{d}s^2$ is represented as

$$\mathrm{d}s^2 = \rho^2(\mathrm{d}x^2 - \mathrm{d}y^2) = \rho^2\,\mathrm{d}z\,\mathrm{d}\bar{z} = \rho^2\,\mathrm{d}u\,\mathrm{d}v \tag{3.3}$$

for some function $\rho : \Sigma \to \mathbb{R}_+$, where $\mathbb{R}_+$ is the set of positive real numbers. We choose the spacelike unit normal vector field $N : \Sigma \to \mathbb{S}^{1,1}$, where

$$\mathbb{S}^{1,1} := \{\xi \in \mathbb{R}^{2,1} : \langle \xi, \xi \rangle = 1\}.$$

Timelike minimal surfaces inherit Lorentzian metric from the ambient space; hence, by using paracomplex analysis over the set of paracomplex numbers $\mathbb{C}'$, Konderak has shown that timelike minimal surfaces also admit a Weierstrass-type representation [73] (see also [108, 120]):

Fact 3.2. *Any timelike minimal surface $F : \Sigma \subset \mathbb{C}' \to \mathbb{R}^{2,1}$ can be locally represented as*

$$F(x, y) = \mathrm{Re} \int (2h, 1 - h^2, -j(1 + h^2))\eta\ \mathrm{d}z$$

over a simply-connected domain Σ on which h is parameromorphic, while η and $h^2\eta$ are paraholomorphic. Furthermore, the induced metric of the surface becomes

$$\mathrm{d}s^2 = (1 + |h|^2)^2|\eta|^2(\mathrm{d}x^2 - \mathrm{d}y^2). \tag{3.4}$$

We call $(h, \eta\,\mathrm{d}z)$ the Weierstrass data *of the timelike minimal surface F.*

On the other hand, timelike minimal surfaces admit another representation based on null coordinates, found by McNertney [84]:

Fact 3.3. *Any timelike minimal surface F can be locally written as the sum of two null curves α and β:*

$$F(u, v) = \frac{\alpha(u) + \beta(v)}{2}. \tag{3.5}$$

We call such α and β the generating null curves *of F.*

Remark 3.4. Similar to the minimal surfaces and maximal surfaces cases, timelike minimal surfaces also admit associated families and conjugate timelike minimal surfaces:

- Given a Lorentz conformally parametrized timelike minimal surface F with Weierstrass data $(h, \eta\,\mathrm{d}z)$, we define F^φ to be a member of the *associated family of F* if F^φ is given by the Weierstrass data $(h, \mathsf{e}^{j\varphi}\eta\,\mathrm{d}z)$ for some $\varphi \in \mathbb{R}$ (note that $\mathsf{e}^{j\varphi} \in \mathbb{H}$, where $\mathbb{H} := \{z \in \mathbb{C}' : |z|^2 = 1\}$). However, unlike the minimal surfaces and maximal surfaces cases, the *conjugate timelike minimal surface* of a given timelike minimal surface is not in the associated family: the conjugate timelike minimal surface F^* of F is given by the Weierstrass data $(h, j\eta\,\mathrm{d}z)$.

- Given a timelike minimal surface F generated by null curves $\alpha(u)$ and $\beta(v)$, F^μ is a member of the associated family of F if F^μ is generated by null curves $\mu\,\alpha(u)$ and $\frac{1}{\mu}\beta(v)$ for a fixed $\mu > 0$, while the conjugate timelike minimal surface of F if F^* is generated

by null curves $\alpha(u)$ and $-\beta(v)$. We note that the parameters of the associated family φ and μ are related by $e^{\varphi} = \mu$.

Following [60] (see also [48, 62]), we define the *Hopf pair* of F as

$$Q\,\mathrm{d}u^2 := \langle F_{uu}, N\rangle\,\mathrm{d}u^2, \quad R\,\mathrm{d}v^2 := \langle F_{vv}, N\rangle\,\mathrm{d}v^2$$

using the null coordinates (u, v). In terms of the Lorentz conformal coordinates, the *Hopf differential* $\mathtt{q}\,\mathrm{d}z^2$ of F can be defined from the Hopf pair of F via

$$\mathtt{q}\,\mathrm{d}z^2 = Q\,\mathrm{d}u^2 + R\,\mathrm{d}v^2$$

for some paracomplex-valued function $\mathtt{q}$ where $\mathtt{q} = \frac{Q+R}{2} + j\frac{Q-R}{2}$. We call a point $(x, y) \in \Sigma$ an *umbilic point* of F if $\mathtt{q} = 0$ on (x, y), and a *quasi-umbilic point* of F if $\mathtt{q} \neq 0$ but $QR = 0$ on (x, y) (see also [62, Remark 4.3] or [31, Definition 1.1]). Since the Gaussian curvature at umbilic and quasi-umbilic points vanishes, we call them *flat points*.

Following [48, Definition 3.1] (see also [49]), we say that (x, y) are *isothermic* (or conformal curvature line) coordinates of F if $\mathtt{q}$ is real on Σ; we say that (x, y) are *anti-isothermic* (or conformal asymptotic line) coordinates if $\mathtt{q}$ is pure imaginary on Σ. For a non-planar timelike minimal surface without flat points on Σ, it is known that there exist either isothermic or anti-isothermic coordinates (x, y) [48].

Remark 3.5. One can also characterize the existence of isothermic or anti-isothermic coordinates on any timelike minimal surface by examining the sign of the Gaussian curvature (see [80, p.629] or [3, Theorem 3.4]).

Since we are interested in timelike minimal surfaces of Bonnet-type, we assume that the mean curvature $H \equiv 0$ on the domain. Furthermore we require that F is without flat points and has negative Gaussian curvature on its domain, so that F admits isothermic coordinates. Note that by doing this, we exclude the case when F is a timelike plane as well. Then an analogous result to [16, Lemma 1.1] for isothermic timelike surfaces implies that we may assume $\mathtt{q} = -\frac{1}{2}$. Calculating the Gauss-Weingarten equations then gives us

$$\begin{cases} F_{xx} = F_{yy} = -N + \frac{\rho_x}{\rho} F_x + \frac{\rho_y}{\rho} F_y, \\ F_{xy} = \frac{\rho_y}{\rho} F_x + \frac{\rho_x}{\rho} F_y, \\ N_x = \frac{1}{\rho^2} F_x, \\ N_y = -\frac{1}{\rho^2} F_y, \end{cases} \tag{3.6}$$

while the Gauss equation (or the integrability condition) becomes

$$\rho \cdot \Box\rho - ({\rho_x}^2 - {\rho_y}^2) - 1 = 0,$$

where $\Box := \partial_x^2 - \partial_y^2$ is the d'Alembert operator.

3.1.3 Planar curvature line condition and the analytic classification

We now calculate the condition the Lorentz conformal factor ρ must satisfy for a timelike minimal surface F to have planar curvature lines.

Lemma 3.6. *For a timelike minimal surface with no flat points, the following statements are equivalent:*

(1) x-curvature lines are planar.

(2) y-curvature lines are planar.

(3) $\rho_{xy} = 0$.

Proof. Since (x, y) are conformal curvature line coordinates, x-curvature lines are planar if and only if

$$\det(F_x, F_{xx}, F_{xxx}) = 0.$$

The Gauss-Weingarten equation (2.1) tells us that

$$F_{xxx} = -\frac{\rho_x}{\rho} N + AF_x + \frac{\rho_{xy}\rho + \rho_u \rho_v}{\rho^2} F_y$$

for some function A. Therefore, we have that

$$\det(F_x, F_{xx}, F_{xxx}) = \rho_{xy}\rho.$$

Since $\rho : \Sigma \to \mathbb{R}_+$, we have that x-curvature lines are planar if and only if $\rho_{xy} = 0$. Similarly, one can calculate that y-curvature lines are planar if and only if $\rho_{xy} = 0$. □

Therefore, by finding solutions to the following system of partial differential equations, we may find all timelike minimal surfaces of Bonnet-type:

$$\begin{cases} \rho \cdot \Box\rho - ({\rho_x}^2 - {\rho_y}^2) - 1 = 0 & \text{(timelike minimality condition)}, \quad (3.7a) \\ \rho_{xy} = 0 & \text{(planar curvature line condition)}. \quad (3.7b) \end{cases}$$

To solve the above system, we first reduce (3.7) to a system of ordinary differential equations as in [1, Theorem 2.1].

Lemma 3.7. *For a solution $\rho : \Sigma \to \mathbb{R}_+$ to (3.7), there exist real-valued functions $f(x)$ and $g(y)$ such that*

$$\begin{cases} \rho_x = f(x), & (3.8a) \\ \rho_y = g(y). & (3.8b) \end{cases}$$

Then, ρ can be written in terms of $f(x)$ and $g(y)$ as follows:

Case (1) *If $\Box\rho$ is nowhere zero on Σ, then*

$$\rho(x, y) = \frac{f(x)^2 - g(y)^2 + 1}{f_x(x) - g_y(y)}, \quad (3.9)$$

where $f(x)$ and $g(y)$ satisfy the following system of ordinary differential equations:

$$\begin{cases} (f_x(x))^2 = (c-d)f(x)^2 + c & \text{(3.10a)} \\ f_{xx}(x) = (c-d)f(x) & \text{(3.10b)} \\ (g_y(y))^2 = (c-d)g(y)^2 + d & \text{(3.10c)} \\ g_{yy}(y) = (c-d)g(y) & \text{(3.10d)} \end{cases}$$

for real constants c and d such that $c^2 + d^2 \neq 0$.

Case (2) *If $\Box\rho \equiv 0$ on Σ, i.e. $\Box\rho$ is identically zero on Σ, then*

$$\rho(x,y) = (\sinh\phi)\cdot x - (\cosh\phi)\cdot y \tag{3.11}$$

where $f(x) = \sinh\phi$ and $g(y) = -\cosh\phi$ for some constant $\phi \in \mathbb{R}$.

Proof. By integrating Equation (3.7b) with respect to v, we obtain

$$\rho_x = C_1(x)$$

for some integral constant $C_1(x)$. Similarly, we get $\rho_y = C_2(y)$ for some integral constant $C_2(y)$ by integrating (3.7b) with respect to u. Define $f(x) := C_1(x)$ and $g(y) := C_2(y)$ to get (3.8). Inputing (3.8) to (3.7a), we get

$$\rho(f_x - g_y) - (f^2 - g^2) - 1 = 0.$$

To prove the first case, first assume that $\Box\rho$ is not identically equal to zero. Then we can choose a point (u_0, v_0) such that $\Box(u_0, v_0) \neq 0$, implying that we can choose a neighborhood $\Sigma \subset \mathbb{R}^{1,1}$ of (u_0, v_0) such that $\Box\rho$ is nowhere zero on Σ. Since $\Box\rho = f_u - g_v \not\equiv 0$,

$$\rho(x,y) = \frac{f(x)^2 - g(y)^2 + 1}{f_x(x) - g_y(y)},$$

i.e. we have (3.9). Then from (3.8a), we have

$$f = \rho_x = \frac{2ff_x(f_x - g_y) - (f^2 - g^2 + 1)f_{xx}}{(f_x - g_y)^2}$$

or

$$\begin{aligned} 0 &= f(f_x - g_y)^2 - 2ff_x(f_x - g_y) + (f^2 - g^2 + 1)f_{xx} \\ &= ff_x^2 - 2ff_xg_y + fg_y^2 - 2ff_x^2 + 2ff_xg_y + (f^2 - g^2 + 1)f_{xx} \\ &= f(g_y^2 - f_x^2) + (f^2 - g^2 + 1)f_{xx}. \end{aligned} \tag{3.12}$$

After multiplying both sides by $\frac{2f_x}{(f^2-g^2+1)^2}$, we have that

$$0 = \frac{2f_xf_{xx}(f^2 - g^2 + 1) - (f_x^2 - g_y^2)\cdot 2ff_x}{(f^2 - g^2 + 1)^2} = \left(\frac{f_x^2 - g_y^2}{f^2 - g^2 + 1}\right)_x.$$

Integrating both sides with respect to x, we obtain that

$$\frac{f_x^2 - g_y^2}{f^2 - g^2 + 1} = k_3(y) \tag{3.13}$$

for some $k_3(y)$. Substituting $k_3(y)$ for (3.12), we have that

$$0 = -fk_3(y)(f^2 - g^2 + 1) + f_{xx}(f^2 - g^2 + 1) = (f^2 - g^2 + 1)(f_{xx} - fk_3(y)).$$

Since $f^2 - g^2 + 1 \neq 0$, we have that $f_{xx} = k_3(y)f$, implying that $k_3(y) = \hat{c} \in \mathbb{R}$ is a constant, i.e.

$$f_{xx} = \hat{c}f. \tag{3.14}$$

Multiplying both sides of (3.14) with $2f_x$ and integrating with respect to x gives us that

$$f_x^2 = \hat{c}f^2 + c$$

for some constant c.

On the other hand, from (3.8b), we have

$$g = \rho_y = \frac{-2gg_y(f_x - g_y) + (f^2 - g^2 + 1)g_{yy}}{(f_x - g_y)^2}$$

or

$$\begin{aligned} 0 &= g(f_x - g_y)^2 + 2gg_y(f_x - g_y) - (f^2 - g^2 + 1)g_{yy} \\ &= gf_x^2 - 2gf_xg_y + gg_y^2 + 2gf_xg_y - 2gg_y^2 - (f^2 - g^2 + 1)g_{yy} \\ &= g(f_x^2 - g_y^2) - (f^2 - g^2 + 1)g_{vv}. \end{aligned} \tag{3.15}$$

Substituting (3.13) with $k_3(y) = \hat{c}$ into (3.15), we get that

$$0 = \hat{c}g(f^2 - g^2 + 1) - (f^2 - g^2 + 1)g_{yy} = (f^2 + g^2 - 1)(-g_{yy} + \hat{c}g).$$

Again. since $f^2 - g^2 + 1 \neq 0$, we have that

$$g_{yy} = \hat{c}g. \tag{3.16}$$

Multiplying both sides of (3.16) with $2g_y$ and integrating with respect to y gives us that

$$g_y^2 = \hat{c}g^2 + d$$

for some constant d. Now, from (3.13),

$$\hat{c}(f^2 - g^2 + 1) = f_x^2 - g_y^2 = \hat{c}f^2 + c - \hat{c}g^2 - d = \hat{c}(f^2 - g^2 + 1) - \hat{c} + c - d,$$

implying that $\hat{c} = c - d$, giving us (3.10). Lastly, $c = d = 0$ implies $f(x)$ and $g(y)$ are both constants by (3.10), a contradiction since we assumed that $\Box\rho \not\equiv 0$.

Now assume that $\Box\rho$ is identically equal to zero on some simply-connected domain $\Sigma \subset \mathbb{R}^2$. Since $\Box\rho = f_x(x) - g_y(y) \equiv 0$, $g(y)^2 - f(x)^2 = 1$ for all x and y. This implies that both $f(x)$ and $g(y)$ are constant, and we can set $f := \sinh\phi$ and $g := \cosh\phi$ for some constant $\phi \in \mathbb{R}$. Solving (3.8), we obtain (3.11). □

We now solve (3.10) by first obtaining a general solution, and then finding an appropriate initial condition to get an explicit solution for $f(x)$ and $g(y)$. First, if $c = d$, then (3.10a) and (3.10c) imply that $c = d > 0$, and using (3.10b) and (3.10d), we may obtain the explicit solutions:

$$f(x) = \pm\sqrt{c}\,x + \tilde{C}_1 \quad \text{and} \quad g(y) = \pm\sqrt{d}\,y + \tilde{C}_2 \tag{3.17}$$

for some real constants of integration $\tilde{C}_1$ and $\tilde{C}_2$.

Now, assuming that $c \neq d$, we can explicitly solve for $f(x)$ and $g(y)$ to find that

$$\begin{aligned} f(x) &= C_1 e^{\sqrt{c-d}\,x} + C_2 e^{-\sqrt{c-d}\,x}, \quad 4(d-c)C_1C_2 = c, \\ g(y) &= C_3 e^{\sqrt{c-d}\,y} + C_4 e^{-\sqrt{c-d}\,y}, \quad 4(d-c)C_3C_4 = d, \end{aligned} \tag{3.18}$$

where $C_1, \ldots, C_4 \in \mathbb{C}$ are constants of integration. Furthermore, since $f(x)$ and $g(y)$ are real-valued functions, $C_1, \ldots, C_4$ must satisfy

$$\begin{cases} C_1, C_2, C_3, C_4 \in \mathbb{R}, & \text{if } c > d, \\ C_1 = \overline{C_2} \text{ and } C_3 = \overline{C_4}, & \text{if } d > c, \end{cases} \tag{3.19}$$

where $\bar{\cdot}$ denotes the usual complex conjugation.

In the following series of lemmata, we identify the correct initial conditions based on the values of c and d.

Lemma 3.8 (cf. Lemma 2.3 of [28])**.** *$f(x)$ (resp. $g(y)$) satisfying (3.10) has a zero if and only if either $c > 0$ or $f(x) \equiv 0$ (resp. $d > 0$ or $g(y) \equiv 0$).*

Lemma 3.9 (cf. Lemma 2.4 of [28])**.** *$f(x)$ (resp. $g(y)$) satisfying (3.10) has no zero if and only if either $c < 0$ or $f(x) = \pm e^{\sqrt{-d}x}$, where $d < 0$ (resp. $d < 0$ or $g(y) = \pm e^{\sqrt{c}y}$ where $c > 0$).*

Therefore, we can conclude the following about the nature of $f(x)$ and $g(y)$ depending on the values of c and d:

$$\begin{array}{l|l} c > 0 : f \text{ has a zero} & d > 0 : g \text{ has a zero} \\ c = 0 : \begin{cases} f \equiv 0 & (c = 0_0) \\ f = \pm e^{\sqrt{-d}\,x}, d < 0 & (c = 0_e) \end{cases} & d = 0 : \begin{cases} g \equiv 0 & (d = 0_0) \\ g = \pm e^{\sqrt{c}\,y}, c > 0 & (d = 0_e) \end{cases} \\ c < 0 : f \text{ has no zero} & d < 0 : g \text{ has no zero.} \end{array} \tag{3.20}$$

For the cases where f or g have no zero, we use the following lemmata to identify a possible initial condition.

Lemma 3.10. *Suppose that $g(y) \not\equiv 0$, i.e. $g(y)$ is not identically equal to 0. Then there is some y_0 such that $g(y_0)^2 = 1$ if and only if $c \geq 0$.*

	Initial condition	Applicable values of (c, d)
Sheet 1	$f(0) = 0$, $g(0) = 0$	$(+,+)$, $(+, 0_0)$, $(0_0, +)$
Sheet 2	$f(0) = 0$, $g(0) = \pm 1$	$(+, 0_e)$, $(+,-)$, $(0_0,-)$
Sheet 3	$f(0) = \pm 1$, $g(0) = \pm 1$	$(0_e,-)$
Sheet 4	$f_x(0) = 0$, $g_y(0) = 0$	$(-,-)$

Table 3.1: Choice of initial conditions and the corresponding applicable cases.

Proof. If $c = d$, then the statement is a direct result of (3.17); therefore, assume that $c \neq d$. To show one direction, assume that there is some y_0 such that $g(y_0)^2 = 1$. Then (3.10c) implies that $c \geq 0$.

Now assume that $c \geq 0$. If $c > d$, then for

$$y_0 := \frac{\log\left(\frac{\sqrt{c-d}+\sqrt{c}}{2|C_3|\sqrt{c-d}}\right)}{\sqrt{c-d}}.$$

we have that $g(y_0)^2 = 1$ via (3.18).

If $c < d$, then from (3.19), we have that $\overline{C_3}C_3 = \frac{d}{4(d-c)}$, implying that we may write $C_3 = \sqrt{\frac{d}{4(d-c)}}e^{i\Theta}$ and $C_4 = \sqrt{\frac{d}{4(d-c)}}e^{-i\Theta}$ for some $\Theta \in \mathbb{R}$. Therefore, by (3.18), we have that

$$g(y) = \sqrt{\tfrac{d}{d-c}}\cos\left(\sqrt{d-c}\,y + \Theta\right).$$

Since we have $d > c \geq 0$, we have that $\sqrt{\frac{d}{d-c}} > 1$; therefore, there is some y_0 such that $g(y_0)^2 = 1$. □

Lemma 3.11. *Suppose that $f(x) \not\equiv 0$. Then there is some x_0 such that $f(x_0)^2 = 1$ if and only if $2c \geq d$.*

Proof. The proof is similar to that of Lemma 3.10. □

Lemma 3.12. *If $c < 0$ and $d < 0$, then there is some x_0 (resp. y_0) such that $f_x(x_0) = 0$ (resp. $g_y(y_0) = 0$).*

Proof. From (3.10a) and $c < 0$, we deduce that $c - d > 0$. Therefore, if

$$x_0 := \frac{\log\left(\frac{-c}{4(c-d)C_1^2}\right)}{2\sqrt{c-d}},$$

then $f_x(x_0) = 0$ by (3.18). The statement for $g(y)$ is proven similarly. □

Therefore, of the possible 16 cases coming from (3.20), we only need to consider the 8 cases specified in Table 3.1 with their respective initial conditions. Note that we shift the parameters x and y to assume without loss of generality that $x_0 = y_0 = 0$.

By using these initial conditions to solve (3.10), we obtain the following set of explicit solutions for f and g.

Proposition 3.13. *For a non-planar generalized timelike minimal surface of Bonnet-type $F(x, y)$, the real-analytic solution $\rho : \mathbb{R}^2 \to \mathbb{R}$ of (3.7) is precisely given as follows:*

Case (1) *Let $\Box\rho \not\equiv 0$, i.e. $\Box\rho$ is not identically equal to zero. Then,*

$$\rho(x,y) = \frac{f(x)^2 - g(y)^2 + 1}{f_x(x) - g_y(y)},$$

where $f(x)$ and $g(y)$ are given as follows (see Table 3.1):

Sheet 1: For $c \geq 0$ and $d \geq 0$ such that $c^2 + d^2 \neq 0$,

$$f(x) = \begin{cases} \sqrt{\frac{c}{c-d}}\sinh(\sqrt{c-d}\,x), & \text{if } c \neq d, \\ \sqrt{c}\,x, & \text{if } c = d, \end{cases}$$

$$g(y) = \begin{cases} -\sqrt{\frac{d}{c-d}}\sinh(\sqrt{c-d}\,y), & \text{if } c \neq d, \\ -\sqrt{d}\,y, & \text{if } c = d. \end{cases}$$

Sheet 2: For $c \geq 0$ and $d \in \mathbb{R}$ such that $c^2 + d^2 \neq 0$,

$$\begin{aligned} f(x) &= \sqrt{\tfrac{c}{c-d}}\sinh(\sqrt{c-d}\,x), \\ g(y) &= -\cosh(\sqrt{c-d}\,y) - \sqrt{\tfrac{c}{c-d}}\sinh(\sqrt{c-d}\,y). \end{aligned}$$

Sheet 3: For $c \geq 0$ and $d < 2c$,

$$\begin{aligned} f(x) &= \cosh(\sqrt{c-d}\,y) + \sqrt{\tfrac{2c-d}{c-d}}\sinh(\sqrt{c-d}\,y), \\ g(y) &= -\cosh(\sqrt{c-d}\,y) - \sqrt{\tfrac{c}{c-d}}\sinh(\sqrt{c-d}\,y). \end{aligned}$$

Sheet 4: For $d < c < 0$,

$$\begin{aligned} f(x) &= \sqrt{\tfrac{c}{d-c}}\cosh(\sqrt{c-d}\,x), \\ g(y) &= -\sqrt{\tfrac{d}{d-c}}\cosh(\sqrt{c-d}\,y). \end{aligned}$$

Case (2) *If $\Box\rho \equiv 0$, then for some constant ϕ such that $\phi \in [0, 2\pi)$,*

$$\rho(x,y) = (\sinh\phi)\cdot x - (\cosh\phi)\cdot y.$$

Proof. The proof is essentially the same as that of [28, Proposition 2.1]. □

Remark 3.14. We make a few essential remarks about Proposition 3.13.

- We have now extended the domain globally under our setting. Therefore, we may deduce that non-planar timelike minimal surfaces of Bonnet-type do not have any flat points globally, and we may drop this condition from now. (In fact, we may also infer that these surfaces admit isothermic coordinates globally.)
- We now allow ρ to map into $\mathbb{R}$ as opposed to $\mathbb{R}_+$. By doing so, we now treat timelike minimal surfaces of Bonnet-type as generalized timelike minimal surfaces. (We can

show that these surfaces are actually *minfaces*, see Section 3.5.)

- In case (1), Sheet 1 through Sheet 3, we allow $c - d < 0$. Even in such case, we see that $f(x)$ and $g(y)$ are real-valued analytic functions via the identities

$$\cosh\left(\sqrt{c-d}\,x\right) = \cos\left(\sqrt{d-c}\,x\right), \quad \sinh\left(\sqrt{c-d}\,x\right) = \sqrt{-1}\sin\left(\sqrt{d-c}\,x\right).$$

  Furthermore, Sheet 2 and Sheet 3 also include the case when $c = d$. However, since the resulting solution is the same solution as that in case (1) up to shift of parameters x and y, we do not write these cases explicitly.

- For case (2), we note that this is a Lorentzian analogue of the Bonnet-Lie transformation (see, for example, [11, §394]), giving an associated family of the surface with solution $\rho(x, y) = -y$ up to coordinate change. To see this explicitly, we introduce a parameter λ and consider the following change of coordinates:

$$\begin{cases} \tilde{x} := \cosh\phi \cdot x - \sinh\phi \cdot y, & \tilde{y} := \sinh\phi \cdot x - \cosh\phi \cdot y, \\ \lambda := \mathsf{e}^{-j\phi}, & \tilde{\mathsf{q}} := -\frac{1}{2}\lambda^{-2} = \lambda^{-2}\mathsf{q}. \end{cases}$$

Summarizing, we obtain the following complete classification of non-planar timelike minimal surfaces of Bonnet-type.

Theorem 3.15. *Let $F(x, y)$ be a non-planar generalized timelike minimal surface in $\mathbb{R}^{2,1}$ with isothermic coordinates (x, y) such that the induced metric is $\mathrm{d}s^2 = \rho^2(\mathrm{d}x^2 - \mathrm{d}y^2)$. Then F has planar curvature lines if and only if $\rho(x, y)$ satisfies Proposition 3.13. Furthermore, for different values of (c, d) or λ as in Remark 3.14, the Lorentz conformal factor $\rho(x, y)$ or the surface $F(x, y)$ has the following properties, based on Figure 3.1:*

Case (1): *If $\Box\rho \not\equiv 0$, when (c, d) are on the region marked by*

- ① : *ρ is constant in the x-direction, but periodic in the y-direction,*
- ② : *ρ is periodic in both the x-direction and the y-direction,*
- ③, ④, ⑥, ⑦, ⑨, *or* ⑩ : *ρ is not periodic in both the x-direction and the y-direction,*
- ⑤ : *ρ is not periodic in the x-direction, but constant in the y-direction,*
- ⑧ : *ρ is constant in the x-direction, but not periodic in the y-direction.*

Case (2): *If $\Box\rho \equiv 0$, when λ is on the region marked by*

- ⑪ : *F is a surface of revolution,*
- ⑫ : *F is a surface in the associated family of* ⑪.

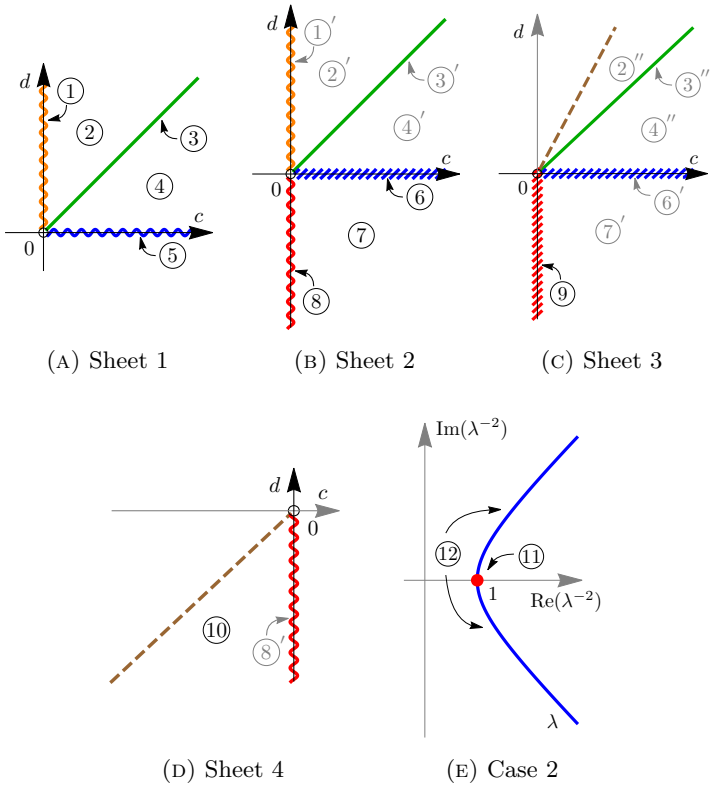

(A) Sheet 1 (B) Sheet 2 (C) Sheet 3

(D) Sheet 4 (E) Case 2

Figure 3.1: Bifurcation diagrams per choice of initial conditions as in Table 3.1.

3.1.4 Axial directions and the Weierstrass data

From the explicit solutions of the Lorentz conformal factor ρ, we now aim to recover the Weierstrass data. The Weierstrass data is not unique for a given timelike minimal surface; for example, applying any rigid motion to the surface will change its Weierstrass data. Therefore, to decide how the surface is aligned in the ambient space $\mathbb{R}^{2,1}$, we use the existence of *axial directions* as defined in [29, Proposition 2.2] (see also [112, Proposition 3.A]). After aligning axial directions according to its causality, we recover the unit normal vector, allowing us to calculate the Weierstrass data. First, we show the existence of axial directions.

Proposition 3.16. *If there exists x_1 (resp. y_1) such that $f(x_1) \neq 0$ (resp. $g(y_1) \neq 0$) in Proposition 3.13, then there exists a unique non-zero constant vector $\vec{v}_1$ (resp. $\vec{v}_2$) such that*

$$\langle m(x,y), \vec{v}_1 \rangle = \langle m_y(x,y), \vec{v}_1 \rangle = 0 \quad (\textit{resp. } \langle n(x,y), \vec{v}_2 \rangle = \langle n_x(x,y), \vec{v}_2 \rangle = 0),$$

where $m := \rho^{-2}(F_x \times F_{xx})$ (resp. $n := \rho^{-2}(F_y \times F_{yy})$) and

$$\vec{v}_1 := -\frac{\rho_x}{\rho} N - \frac{\rho_{xx}\rho - {\rho_x}^2}{\rho^2} F_x + \frac{\rho_x \rho_y}{\rho^2} F_y \quad (\textit{resp. } \vec{v}_2 := \frac{\rho_y}{\rho} N - \frac{\rho_x \rho_y}{\rho^2} F_x + \frac{\rho_{yy}\rho - {\rho_y}^2}{\rho^2} F_y). \tag{3.21}$$

Furthermore, if $\vec{v}_1$ and $\vec{v}_2$ both exist, then they are orthogonal to each other. We call $\vec{v}_1$ and $\vec{v}_2$ the axial directions *of $F(x,y)$.*

Proof. Similar to the proof of Proposition 2.12, using (3.6) and (3.7), we may calculate that

all the required property holds. □

We use (3.6), (3.7), (3.9), (3.10), and (3.21) to calculate that the causality of $\vec{v_1}$ and $\vec{v_2}$ depends on c and d, respectively; explicitly,

$$\langle \vec{v}_1, \vec{v}_1 \rangle = c \quad \text{and} \quad \langle \vec{v}_2, \vec{v}_2 \rangle = -d.$$

Hence, we remark that, by Table 3.1, at least one of $\vec{v}_1$ or $\vec{v}_2$ is always spacelike when they both exist. By aligning the axial directions in the ambient space $\mathbb{R}^{2,1}$ correctly, we now calculate the unit normal vector using the following lemma. Note that we define $\vec{e}_j$ as the unit vectors in the ξ_j direction for $j = 1, 2, 0$.

Lemma 3.17. *For the different alignments of $\vec{v}_1$ or $\vec{v}_2$, we can deduce the following regarding the unit normal vector $N(x, y) = (N_1(x, y), N_2(x, y), N_0(x, y))$:*

Alignment of axial direction	*Property of the unit normal vector*
$\vec{v}_1 \parallel \vec{e}_2$	$N_2 = \pm\frac{1}{\sqrt{c}}\frac{\rho_x}{\rho}$
$\vec{v}_1 \parallel \vec{e}_1 + \vec{e}_0$	$N_1 - N_0 = \pm\frac{\rho_x}{\rho}$
$\vec{v}_1 \parallel \vec{e}_0$	$N_0 = \pm\frac{1}{\sqrt{-c}}\frac{\rho_x}{\rho}$
$\vec{v}_2 \parallel a_1\vec{e}_1 + a_0\vec{e}_0$	$a_1N_1 - a_0N_0 = \pm\sqrt{\frac{a_0^2 - a_1^2}{d}}\frac{\rho_y}{\rho}$
$\vec{v}_2 \parallel a_1\vec{e}_1 + a_2\vec{e}_2$	$a_1N_1 + a_2N_2 = \pm\sqrt{\frac{a_1^2 + a_2^2}{-d}}\frac{\rho_y}{\rho}$

Here, a_1, a_2 and a_0 are any real constants.

Proof. We only prove the claim for assuming $\vec{v}_2 = a_1\vec{e}_1 + a_0\vec{e}_0$, since all the other cases can be proven similarly. We know that from Proposition 3.16,

$$\begin{aligned} 0 = \langle n, \vec{v}_2 \rangle &= \langle \rho^{-2}(F_y \times F_{yy}), a_1\vec{e}_1 + a_0\vec{e}_0 \rangle \\ &= \langle -\rho^{-1}\rho_x N - \rho^{-2}F_x, a_1\vec{e}_1 + a_0\vec{e}_0 \rangle \\ &= -\rho^{-1}\rho_x(a_1N_1 - a_0N_0) - \rho^{-2}(a_1(F_1)_x - a_0(F_0)_x) \\ &= -\rho^{-1}\rho_x(a_1N_1 - a_0N_0) - (a_1(N_1)_x - a_0(N_0)_x) \end{aligned}$$

using the Rodrigues equations, implying that

$$\frac{(a_1F_1 - a_0F_0)_x}{a_1N_1 - a_0N_0} = -\frac{\rho_x}{\rho}.$$

Integrating both sides with respect to x gives us that

$$a_1N_1 - a_0N_0 = k_4(y)\frac{1}{\rho} \tag{3.22}$$

for some function $k_4(y)$.

Now we also know that

$$\begin{aligned}0 &= \langle n_x, \vec{v}_2\rangle \\ &= \langle -\rho^{-2}(\rho_{yy}\rho - \rho_y^2)N - \rho^{-3}\rho_y F_y, a_1\vec{e}_1 + a_0\vec{e}_0\rangle \\ &= -\rho^{-2}(\rho_{yy}\rho - \rho_y^2)(a_1N_1 - a_0N_0) - \rho^{-3}\rho_y(a_1(F_1)_y - a_0(F_0)_y) \\ &= -\rho^{-2}(\rho_{yy}\rho - \rho_y^2)(a_1N_1 - a_0N_0) - \rho^{-1}\rho_y(a_1(N_1)_y - a_0(N_0)_y),\end{aligned}$$

telling us that

$$\frac{(a_1X_1 - a_0X_0)_y}{a_1N_1 - a_0N_0} = \left(\frac{\rho_y}{\rho}\right)_y\left(\frac{\rho_y}{\rho}\right)^{-1}.$$

Integrating both sides with respect to y and comparing with (3.22) tells us that

$$k_4(y)\frac{1}{\rho} = a_1N_1 - a_0N_0 = k_5(x)\frac{\rho_y}{\rho}$$

for some function $k_5(x)$; hence,

$$a_1N_1 - a_0N_0 = B_1\frac{\rho_y}{\rho}$$

for some constant B_1.

Finally, using the fact that $\langle v_2, v_2\rangle = -d$ gives us the desired conclusion. □

Using the fact that the meromorphic function h of the Weierstrass data is the unit normal vector function under the stereographic projection, and that $\mathtt{q} = -h_z\eta = -\frac{1}{2}$, we recover the Weierstrass data via

$$h(z) = h(x,y) = \frac{1}{1-N_1}(N_2 + jN_0) \quad \text{and} \quad \eta(z) = \frac{1}{2h_z},$$

where the signs of N_1, N_2, and N_0 are decided so that h satisfies the Cauchy-Riemann type conditions (3.1).

Sheet 1

Assume that $c > 0$ and $d > 0$. We have that $\vec{v}_1$ is spacelike, while $\vec{v}_2$ is timelike; therefore, we align the axial directions so that $\vec{v}_1 \parallel \vec{e}_2$ and $\vec{v}_2 \parallel \vec{e}_0$. Then by Lemma 3.17, we have that

$$N = \left(\pm\sqrt{1 - \frac{1}{c}\frac{\rho_x^2}{\rho^2} + \frac{1}{d}\frac{\rho_y^2}{\rho^2}}, \pm\frac{1}{\sqrt{c}}\frac{\rho_x}{\rho}, \pm\frac{1}{\sqrt{d}}\frac{\rho_y}{\rho}\right).$$

Since we know that a homothety in the (c,d)-plane amounts to a homothety in the (x,y)-plane, by Proposition 3.13, we can let $c = 4\cos^2 c_1$ and $d = 4\sin^2 c_1$ for $c_1 \in \left(0, \frac{\pi}{2}\right)$ without

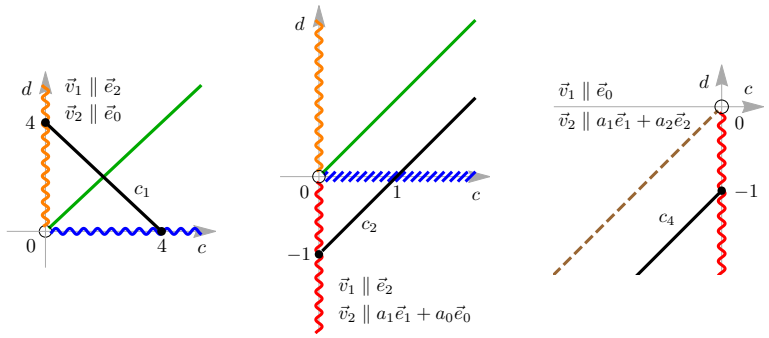

(A) Sheet 1 (B) Sheet 2 (C) Sheet 4

Figure 3.2: (c, d)-paths for different sheets.

loss of generality (see Figure 3.2(A)). Using the unit normal vector, we find that

$$h_1^{c_1}(z) = \begin{cases} \frac{\sqrt{\cos(2c_1)}}{\cos c_1 - \sin c_1} \operatorname{tanh}\left(\sqrt{\cos(2c_1)}\, z\right), & \text{if } c_1 \in (0, \frac{\pi}{4}), \\ \sqrt{2} z, & \text{if } c_1 = \frac{\pi}{4}, \\ -\frac{\sqrt{-\cos(2c_1)}}{\cos c_1 - \sin c_1} \tan\left(\sqrt{-\cos(2c_1)}\, z\right), & \text{if } c_1 \in (\frac{\pi}{4}, \frac{\pi}{2}), \end{cases}$$
$$\eta_1^{c_1}(z) = \begin{cases} \frac{1}{2(\cos c_1 + \sin c_1)} \operatorname{cosh}^2\left(\sqrt{\cos(2c_1)}\, z\right), & \text{if } c_1 \in (0, \frac{\pi}{4}), \\ \frac{1}{2\sqrt{2}}, & \text{if } c_1 = \frac{\pi}{4}, \\ \frac{1}{2(\cos c_1 + \sin c_1)} \cos^2\left(\sqrt{-\cos(2c_1)}\, z\right), & \text{if } c_1 \in (\frac{\pi}{4}, \frac{\pi}{2}). \end{cases} \tag{3.23}$$

Note that $h_1^{c_1}(z)$ and $\eta_1^{c_1}(z)$ is also well-defined when $c_1 = 0, \frac{\pi}{2}$ by considering the directional limits.

Remark 3.18. The Weierstrass data given in (3.23) show that surfaces in Sheet 1 form a one-parameter family of surfaces. However, by considering these surfaces separately, one can get different, and perhaps simpler, Weierstrass data.

- For surfaces (1) and (2), by using $c = 4\sinh^2(\log \tilde{c}_1)$ and $d = 4\cosh^2(\log \tilde{c}_1)$ for $\tilde{c}_1 \geq 1$, we obtain
$$h_1^{\tilde{c}_1}(z) = \tilde{c}_1 \tan z, \quad \eta_1^{\tilde{c}_1}(z) = \frac{1}{2\tilde{c}_1} \cos^2 z.$$
- For the surface (5), by letting $\vec{v}_1 \parallel \vec{e}_1$ and $\vec{v}_2 \parallel \vec{e}_0$, we obtain that
$$\tilde{h}_1^{c_1}(z)\big|_{c_1=\frac{\pi}{2}} = \mathrm{e}^z, \quad \tilde{\eta}_1^{c_1}(z)\big|_{c_1=\frac{\pi}{2}} = \frac{1}{2}\mathrm{e}^{-z}.$$

Sheet 2

Assume that $c \geq 0$ but $d \in \mathbb{R}$, implying that now $\vec{v}_2$ changes its causal character. Therefore, we align the axial directions so that $\vec{v}_1 \parallel \vec{e}_2$ and $\vec{v}_2 \parallel a_1\vec{e}_1 + a_0\vec{e}_0$. Since we only need to find the unit normal vector of surfaces (6), (7), and (8), we let $c = c_2^2$ and $d = c_2^2 - 1$ for $c_2 \geq 0$, and further assume that $a_1 = 1$ and $a_0 = c_2$ (see Figure 3.2(B)). Then we have that the unit

normal vector is

$$N = \left(c_2 N_0 \pm \frac{\rho_y}{\rho},\, \pm\frac{1}{c_2}\frac{\rho_x}{\rho},\, N_0 \right),$$

where N_0 can be found from the fact that $\langle N, N\rangle = 1$. From the unit normal vector, after applying a shift of parameter $y \mapsto y - \log(1 + c_2)$, we calculate that

$$h_2^{c_2}(z) = j\mathsf{e}^{jz} - jc_2, \quad \eta_2^{c_2}(z) = \frac{1}{2}\mathsf{e}^{-jz}. \tag{3.24}$$

Similar to the preceding case, note that $h_2^{c_2}(z)$ and $\eta_2^{c_2}(z)$ is also well-defined when $c_2 = 0$ by considering the directional limits.

Remark 3.19. Note that if $c_2 > 1$, then (3.24) describes Weierstrass data for the surface ④, aligned differently in the ambient space $\mathbb{R}^{2,1}$ to the one given by (3.23) for $c_1 \in \left(\frac{\pi}{4}, \frac{\pi}{2}\right)$.

Sheet 3

We only need to find the data for the surface ⑨ here, so assume that $c = 0$ and $d = -1$. We align the axial directions so that $\vec{v}_1 \parallel \vec{e}_1 + \vec{e}_0$ and $\vec{v}_2 \parallel \vec{e}_2$, implying that the unit normal vector is

$$N = \left(N_0 \pm \frac{\rho_x}{\rho},\, \pm\frac{1}{\sqrt{-d}}\frac{\rho_y}{\rho},\, N_0 \right),$$

where N_0 can be found from the fact that N has unit length. After making the parameter shift $x \mapsto x - \log 2$, we calculate the Weierstrass data as

$$h_3(z) = \mathsf{e}^z + j, \quad \eta_3 = \frac{1}{2}\mathsf{e}^{-z}. \tag{3.25}$$

Sheet 4

Here, we have that $d < c \leq 0$. Align the axial directions so that $\vec{v}_1 \parallel \vec{e}_0$ and $\vec{v}_2 \parallel a_1\vec{e}_1 + a_2\vec{e}_2$. In this case, we let $c = -c_4^2$ and $d = -c_4^2 - 1$ for $c_4 \geq 0$, and let $a_1 = 1$ and $a_2 = c_4$ (see Figure 3.2(C)). Then, the unit normal vector is

$$N = \left(-c_4 N_2 \pm \frac{\rho_y}{\rho}, N_2, \pm\frac{1}{c_4}\frac{\rho_x}{\rho} \right).$$

Using this, after a shift of parameter $y \mapsto y - \log(\sqrt{1 + c_4^2})$, we obtain that

$$h_4^{c_4}(z) = j\mathsf{e}^{jz} + c_4, \quad \eta_4^{c_4} = \frac{1}{2}\mathsf{e}^{-jz}. \tag{3.26}$$

Case 2

Finally, we assume that $\Box\rho \equiv 0$, and by Remark 3.14, we only consider the case $\rho(x, y) = -y$. We assume that the axial direction is $\vec{v}_2 = \vec{e}_1 + \vec{e}_0$. Then similar to Lemma 3.17, we can calculate that

$$N_1 - N_0 = \frac{\rho_y}{\rho}.$$

Since $\rho_x \equiv 0$, we have that $N(x, y)$ has the form $N(x, y) = (N_1(y),\, 0,\, N_0(y)) \cdot T(x)$ for an isometry transform $T(x) \in \mathrm{SO}(2, 1)$ keeping the lightlike axis $\vec{v}_2$. Hence, we obtain the

following lemma.

Lemma 3.20. *If $\rho(x,y)=y$, then the unit normal vector N is given by*

$$N(x,y)=\left(\frac{y^2+1}{2y},0,\frac{y^2-1}{2y}\right)\cdot\begin{pmatrix}1-\frac{x^2}{2} & x & -\frac{x^2}{2}\\ -x & 1 & -x\\ \frac{x^2}{2} & -x & 1+\frac{x^2}{2}\end{pmatrix}$$
$$=\left(\frac{1-x^2+y^2}{2y},\frac{x}{y},-\frac{1+x^2-y^2}{2y}\right).$$

Therefore, we recover the Weierstrass data as follows:

$$h_5(z)=\frac{z+j}{1-jz},\quad \eta_5(z)=\frac{1}{4}(jz-1)^2. \tag{3.27}$$

Finally, by considering $(h_5,\eta_5\,\mathrm{d}z)\mapsto(h_5,\lambda^{-2}\eta_5\,\mathrm{d}z)$ for λ as in Remark 3.14, we obtain the Weierstrass data for surfaces (11) and (12).

In summary, we obtain the following complete classification of timelike minimal surfaces of Bonnet-type.

Theorem 3.21. *A generalized timelike minimal surface of Bonnet-type in Minkowski 3-space must be a piece of one, and only one, of*

- *plane* (P) $(0,\mathrm{d}z)$,

(1) *timelike catenoid with timelike axis* ($\mathrm{C_T}$) $\left(\tan z,\frac{1}{2}\cos^2 z\,\mathrm{d}z\right)$,

(2) *doubly periodic timelike minimal Bonnet-type surface (with timelike axial direction)* ($\mathrm{B_{Tper}}$)
$$\left\{\left(\tilde{c}_1\tan z,\tfrac{1}{2\tilde{c}_1}\cos^2 z\,\mathrm{d}z\right):\tilde{c}_1>1\right\},$$

(3) *timelike Enneper-type surface* (E) $\left(\sqrt{2}z,\frac{1}{2\sqrt{2}}\,\mathrm{d}z\right)$,

(4) *timelike minimal Bonnet-type surface with timelike axial direction of first kind* ($\mathrm{B_{T1}}$),
$$\left\{\left(j\mathrm{e}^{jz}-jc_2,\tfrac{1}{2}\mathrm{e}^{-jz}\,\mathrm{d}z\right):c_2>1\right\},$$

(5) *immersed timelike catenoid with spacelike axis* ($\mathrm{C_{S1}}$) $\left(\mathrm{e}^z,\frac{1}{2}\mathrm{e}^{-z}\,\mathrm{d}z\right)$,

(6) *timelike minimal Bonnet-type surface with lightlike axial direction of first kind* ($\mathrm{B_{L1}}$)
$$\left(j\mathrm{e}^{jz}-j,\tfrac{1}{2}\mathrm{e}^{-jz}\,\mathrm{d}z\right),$$

(7) *timelike minimal Bonnet-type surface with spacelike axial direction* ($\mathrm{B_S}$),
$$\left\{\left(j\mathrm{e}^{jz}-jc_2,\tfrac{1}{2}\mathrm{e}^{-jz}\,\mathrm{d}z\right):0<c_2<1\right\},$$

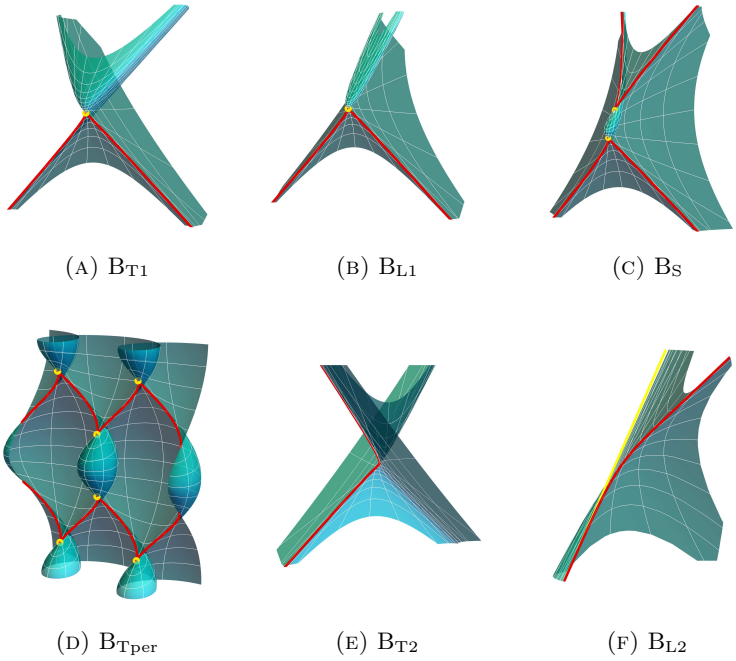

(A) B_{T1} (B) B_{L1} (C) B_{S}

(D) $\mathrm{B}_{\mathrm{Tper}}$ (E) B_{T2} (F) B_{L2}

Figure 3.3: Timelike minimal Bonnet-type surfaces. As in Remark 3.14, we treat these as generalized timelike minimal surfaces, admitting singularities, and we highlighted the singularities on these surfaces.

⑧ *non-immersed timelike catenoid with spacelike axis* (C_{S2}) $\left(j\mathsf{e}^{jz}, \frac{1}{2}\mathsf{e}^{-jz}\,\mathrm{d}z\right)$,

⑨ *timelike minimal Bonnet-type surface with lightlike axial direction of second kind* (B_{L2}) $(\mathsf{e}^{z}+j, \frac{1}{2}\mathsf{e}^{-z}\,\mathrm{d}z)$,

⑩ *timelike minimal Bonnet-type surface with timelike axial direction of second kind* (B_{T2})

$$\left\{\left(j\mathsf{e}^{jz}+c_4, \tfrac{1}{2}\mathsf{e}^{-jz}\,\mathrm{d}z\right) : c_4 > 0\right\},$$

⑪ *timelike catenoid with lightlike axis* (C_{L}) $\left(\frac{z+j}{1-jz}, \frac{1}{4}(jz-1)^2\,\mathrm{d}z\right)$, *or one member of its associated family* ⑫,

given with their respective Weierstrass data.

3.2 Null curves of timelike minimal surfaces of Bonnet-type

In this section, we consider timelike minimal surfaces of Bonnet-type in terms of their generating null curves (see Fact 3.3). First, we introduce the theory of null curves in $\mathbb{R}^{2,1}$. For an in-depth discussion of the theory of null curves, we refer the readers to works such as [21, 44, 61, 79, 92, 111].

3.2.1 Frenet-Serre type formula for non-degenerate null curves

A regular curve $\gamma = \gamma(t)\colon I \to \mathbb{R}^{2,1}$ is called a *null curve* if

$$\langle \gamma', \gamma' \rangle = 0,$$

and γ is said to be *non-degenerate* if γ' and γ'' are linearly independent at each point on I. (Here, $'$ denotes $\frac{\mathrm{d}}{\mathrm{d}t}$.) For a non-degenerate null curve $\gamma(t)$, we can normalize (see [92, Section 2], for example) the parameter so that

$$\langle \ddot{\gamma}(s), \ddot{\gamma}(s) \rangle = 1, \tag{3.28}$$

where $\dot{}$ denotes $\frac{\mathrm{d}}{\mathrm{d}s}$. A parameter s satisfying (3.28) is called a *pseudo-arclength parameter*, introduced in [21]. From now on, let s denote a pseudo-arclength parameter. If we take the vector fields

$$\boldsymbol{\sigma}(s) := \dot{\gamma}(s), \quad \boldsymbol{e}(s) := \ddot{\gamma}(s),$$

and then there is a unique null vector field $\boldsymbol{n}$ such that

$$\langle \boldsymbol{n}, \boldsymbol{\sigma} \rangle = -2, \quad \langle \boldsymbol{n}, \boldsymbol{e} \rangle = 0.$$

If we set the *lightlike curvature* (see [61, p.47]) of γ to be

$$\kappa_\gamma(s) := -\left\langle \dot{\boldsymbol{n}}(s), \boldsymbol{e}(s) \right\rangle, \tag{3.29}$$

we get

$$-\dot{\boldsymbol{n}} = \kappa_\gamma \boldsymbol{e}, \qquad \dot{\boldsymbol{e}} = -\frac{\kappa_\gamma}{2}\boldsymbol{\sigma} + \frac{1}{2}\boldsymbol{n}.$$

Therefore, we obtain the following Frenet-Serre type formula for non-degenerate null curves.

Proposition 3.22 (cf. [61, 79])**.** *For a non-degenerate null curve γ parametrized by pseudo-arclength parameter, the null frame $\mathcal{F} := \{\boldsymbol{\sigma}, \boldsymbol{e}, \boldsymbol{n}\}$ satisfies*

$$\mathcal{F}' = \mathcal{F} \begin{pmatrix} 0 & -\kappa_\gamma/2 & 0 \\ 1 & 0 & -\kappa_\gamma \\ 0 & 1/2 & 0 \end{pmatrix}.$$

Moreover, the lightlike curvature κ_γ of γ is written as

$$\kappa_\gamma = \langle \dddot{\gamma}, \dddot{\gamma} \rangle. \tag{3.30}$$

Example 3.23. A non-degenerate null curve parametrized by pseudo-arclength with constant lightlike curvature κ_γ is called a *null helix* in [44, 61], and such curves have been studied by

many authors. Any null helix γ is congruent to one of the following:

$$\begin{cases} \gamma(s) = \frac{1}{\kappa_\gamma}\left(\cos(cs), \sin(cs), cs\right), & \text{when } \kappa_\gamma = c^2 > 0, \\ \gamma(s) = \left(\frac{s^2}{2}, -\frac{s^3}{6} + \frac{s}{2}, \frac{s^3}{6} + \frac{s}{2}\right), & \text{when } \kappa_\gamma = 0, \\ \gamma(s) = \frac{1}{\kappa_\gamma}\left(cs, \cosh(cs), \sinh(cs)\right), & \text{when } \kappa_\gamma = -c^2 < 0. \end{cases}$$

3.2.2 Characterization of timelike minimal surfaces of Bonnet-type

Using the theory of null curves, we now characterize timelike minimal surfaces of Bonnet-type in terms of its generating null curves. We first remark on the relationship between the generating null curves and the normalization of the Hopf differential factor.

Lemma 3.24 (cf. p. 347 of [62])**.** *The normalization of the Hopf differential factor* $\mathfrak{q} = -\frac{1}{2}$ *of a timelike minimal surface* F *implies that the generating null curves are parametrized by pseudo-arclength.*

Proof. Let F be represented via two generating null curves $\alpha(u)$ and $\beta(v)$ as in (3.5). By the Gauss-Weingarten equations, we have

$$\alpha_{uu}(= 2F_{uu}) = 2\frac{\rho_u}{\rho}\alpha_u - N, \quad \beta_{vv}(= 2F_{vv}) = 2\frac{\rho_v}{\rho}\beta_v - N,$$

where ρ is the Lorentz conformal factor of the first fundamental form and N is the unit normal of F. Therefore, we can check that

$$\langle \alpha_{uu}, \alpha_{uu} \rangle = \langle \beta_{vv}, \beta_{vv} \rangle = \langle N, N \rangle = 1,$$

i.e. u and v are pseudo-arclength parameters of $\alpha(u)$ and $\beta(v)$, respectively. □

Now we state and prove the theorem relating the lightlike curvatures of the generating null curves and the planar curvature line condition (3.7b).

Theorem 3.25. *Away from flat points and singular points, a timelike minimal surface* F *has planar curvature lines if and only if it has negative Gaussian curvature, and its generating null curves have the same constant lightlike curvature.*

Proof. We consider a timelike minimal surface F written as in (3.5), with its first fundamental form as in (3.3). For $z = x + jy = (u+v)/2 + j(u-v)/2$, the planar curvature line condition (3.7b) can be expressed as

$$\rho_{uu} - \rho_{vv} = 0. \tag{3.31}$$

Let us take the null frames $\mathcal{F}_\alpha := \{\boldsymbol{\sigma}_\alpha, \boldsymbol{e}_\alpha, \boldsymbol{n}_\alpha\}$ for α and $\mathcal{F}_\beta := \{\boldsymbol{\sigma}_\beta, \boldsymbol{e}_\beta, \boldsymbol{n}_\beta\}$ for β as in Section 3.2.1. By using the frame of the surface F, we can check that $\boldsymbol{n}_\alpha$ and $\boldsymbol{n}_\beta$ are written as

$$\boldsymbol{n}_\alpha = \left(\frac{2\rho_u}{\rho}\right)^2 \alpha_u - \frac{1}{\rho^2}\beta_v - 4\frac{\rho_u}{\rho}N, \quad \boldsymbol{n}_\beta = -\frac{1}{\rho^2}\alpha_u + \left(\frac{2\rho_v}{\rho}\right)^2 \beta_v - 4\frac{\rho_v}{\rho}N. \tag{3.32}$$

Since we normalized the Hopf differential factor as $\mathtt{q} = -\frac{1}{2}$, we have that u and v are pseudo-arclength parameters of α and β by Lemma 3.24; hence, we can take

$$\boldsymbol{e}_\alpha = \alpha_{uu} \quad \text{and} \quad \boldsymbol{e}_\beta = \beta_{vv}.$$

By the Gauss-Weingarten equations, $(\boldsymbol{e}_\alpha)_u$ and $(\boldsymbol{e}_\beta)_v$ can be expressed as

$$\begin{aligned}(\boldsymbol{e}_\alpha)_u &= 2\frac{\rho_{uu}\rho + {\rho_u}^2}{\rho^2}\alpha_u - \frac{1}{2\rho^2}\beta_v - 2\frac{\rho_u}{\rho}N \\ (\boldsymbol{e}_\beta)_v &= -\frac{1}{2\rho^2}\alpha_u + 2\frac{\rho_{vv}\rho + {\rho_v}^2}{\rho^2}\beta_v - 2\frac{\rho_v}{\rho}N.\end{aligned} \tag{3.33}$$

By (3.29), (3.32) and (3.33), the lightlike curvatures κ_α and κ_β of the generating null curves α and β can be calculated as

$$\kappa_\alpha = \langle \boldsymbol{n}_\alpha, (\boldsymbol{e}_\alpha)_u \rangle = -4\frac{\rho_{uu}}{\rho}, \quad \kappa_\beta = \langle \boldsymbol{n}_\beta, (\boldsymbol{e}_\beta)_v \rangle = -4\frac{\rho_{vv}}{\rho}, \tag{3.34}$$

and hence

$$\kappa_\alpha(u) - \kappa_\beta(v) = -4\frac{\rho_{uu} - \rho_{vv}}{\rho}.$$

Therefore, we conclude that κ_α are κ_β are the same constant if and only if the Lorentz conformal factor ρ satisfies the planar curvature line condition (3.31). □

3.2.3 Deformations of null curves with constant lightlike curvature

We now consider continuous deformations of null curves preserving their pseudo-arclength parametrization and constantness of lightlike curvatures. As in [28, 29], we consider a deformation to be "continuous" with respect to a parameter if the deformation dependent on the parameter converges uniformly over compact subdomains component-wise. First, we introduce how the lightlike curvatures of generating null curves are determined for a timelike minimal surface of Bonnet-type.

Proposition 3.26. *The lightlike curvatures κ_α and κ_β of the generating null curves of a timelike minimal surface of Bonnet-type is given by the constants c and d in* (3.10) *via*

$$\kappa_\alpha = \kappa_\beta = d - c. \tag{3.35}$$

Proof. By (3.34), we have

$$\kappa_\alpha = \kappa_\beta = -2\frac{\rho_{uu} + \rho_{vv}}{\rho} = -\frac{\rho_{xx} + \rho_{yy}}{\rho}.$$

Using (3.10a) and (3.10c), we prove the desired relation. □

A deformation of a timelike minimal surface of Bonnet-type corresponds to a deformation of its generating null curves, which have constant lightlike curvatures. Therefore, by using the relation (3.35), we can deform null curves with constant curvature preserving the pseudo-arclength parametrization and the constantness of lightlike curvature (each of null curves

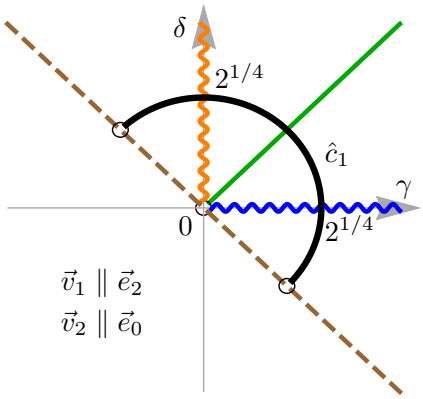

Figure 3.4: Modified version of a path in Sheet 1 to include the timelike plane in the deformation.

may have different constant lightlike curvature).

As an example, we give a deformation of null curves coming from the surfaces in Sheet 1. To do this, we first consider a slightly modified method of the one we used to obtain the Weierstrass data (3.23) in Section 3.1.4. Since $c \geq 0$ and $d \geq 0$, we define γ and δ so that $\gamma^2 = c$ and $\delta^2 = d$. Let $\gamma = 2^{1/4} \cos \hat{c}_1$ and $\delta = 2^{1/4} \sin \hat{c}_1$ for $\hat{c}_1 \in \left(-\frac{\pi}{4}, \frac{3\pi}{4}\right)$ (see Figure 3.4).

Then we can calculate similarly as before to obtain that

$$
\begin{aligned}
h_{\mathrm{P}}^{\hat{c}_1}(z) &= \begin{cases} \frac{\sqrt{\cos(2\hat{c}_1)}}{\cos\hat{c}_1 - \sin\hat{c}_1} \, \mathtt{tanh}\left(\frac{\sqrt{\cos(2\hat{c}_1)}}{2^{3/4}} z\right), & \text{if } \hat{c}_1 \in (-\frac{\pi}{4}, \frac{\pi}{4}), \\ \frac{1}{2^{1/4}} z, & \text{if } \hat{c}_1 = \frac{\pi}{4}, \\ -\frac{\sqrt{-\cos(2\hat{c}_1)}}{\cos\hat{c}_1 - \sin\hat{c}_1} \, \mathtt{tan}\left(\frac{\sqrt{-\cos(2\hat{c}_1)}}{2^{3/4}} z\right), & \text{if } \hat{c}_1 \in (\frac{\pi}{4}, \frac{3\pi}{4}), \end{cases} \\
\eta_{\mathrm{P}}^{\hat{c}_1}(z) &= \begin{cases} \frac{1}{2^{1/4}(\cos\hat{c}_1 + \sin\hat{c}_1)} \, \mathtt{cosh}^2\left(\frac{\sqrt{\cos(2\hat{c}_1)}}{2^{3/4}} z\right), & \text{if } \hat{c}_1 \in (-\frac{\pi}{4}, \frac{\pi}{4}), \\ \frac{1}{2^{3/4}}, & \text{if } \hat{c}_1 = \frac{\pi}{4}, \\ \frac{1}{2^{1/4}(\cos\hat{c}_1 + \sin\hat{c}_1)} \, \mathtt{cos}^2\left(\frac{\sqrt{-\cos(2\hat{c}_1)}}{2^{3/4}} z\right), & \text{if } \hat{c}_1 \in (\frac{\pi}{4}, \frac{3\pi}{4}). \end{cases}
\end{aligned}
\tag{3.36}
$$

Remark 3.27. By noticing that $\gamma^2 = 2^{-3/2}(4\cos^2\hat{c}_1)$ and $\delta^2 = 2^{-3/2}(4\sin^2\hat{c}_1)$, and the fact that a homothety in the (c, d)-plane amounts to a homothety in the (x, y)-plane, one can also get the parameromorphic data $h_{\mathrm{P}}^{\hat{c}_1}(z)$ of (3.36) from that of (3.23) by applying a homothety change in the domain $z \mapsto 2^{-3/4} z$.

Now to get the parametrization, let $F_{\mathrm{P}}^{\hat{c}_1}(x, y)$ be defined from $(h_{\mathrm{P}}^{\hat{c}_1}, \eta_{\mathrm{P}}^{\hat{c}_1} \, \mathrm{d}z)$ via the Weierstrass-type representation in Fact 3.2. We define

$$
\hat{F}_{\mathrm{P}}^{\hat{c}_1}(x, y) = R^{\hat{c}_1} \left(F_{\mathrm{P}}^{\hat{c}_1}(x, y) - F_{\mathrm{P}}^{\hat{c}_1}(0, 0) \right), \tag{3.37}
$$

where

$$
R^{\hat{c}_1} = \left(1 - \sin\left(\hat{c}_1 + \tfrac{\pi}{4}\right)\right) |\cos 2\hat{c}_1| + \sin\left(\hat{c}_1 + \tfrac{\pi}{4}\right). \tag{3.38}
$$

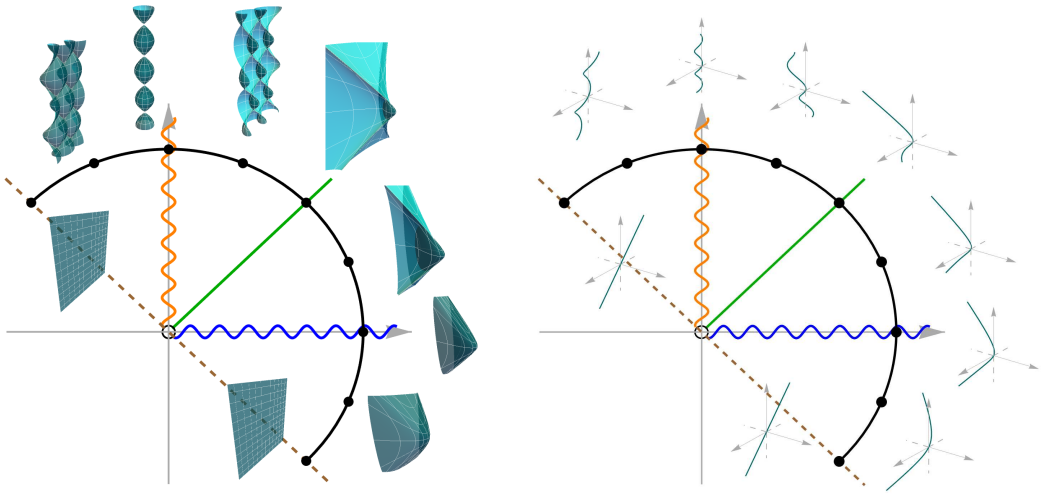

Figure 3.5: Deformation of null curves with constant lightlike curvature, with their respective surfaces.

A straightforward calculation then shows that

$$\lim_{\hat{c}_1\to\frac{\pi}{4}} \hat{F}_{\mathrm{P}}^{\hat{c}_1}(2^{1/4}x, 2^{1/4}y) = \tfrac{1}{\sqrt{2}}\left(x^2+y^2,\, x-xy^2-\tfrac{1}{3}x^3,\, -y-x^2y-\tfrac{1}{3}y^3\right),$$

$$\lim_{\hat{c}_1\searrow-\frac{\pi}{4}} \hat{F}_{\mathrm{P}}^{\hat{c}_1}(x,y) = \left(0,\, \tfrac{3}{2^{3/4}}x, -\tfrac{3}{2^{3/4}}y\right) = \lim_{\hat{c}_1\nearrow\frac{3\pi}{4}} \hat{F}_{\mathrm{P}}^{\hat{c}_1}(x,y),$$

implying that $\hat{F}_{\mathrm{P}}^{\hat{c}_1}(x,y)$ for $\hat{c}_1 \in \left[-\frac{\pi}{4}, \frac{3\pi}{4}\right]$ gives a continuous deformation consisting of every surface in Sheet 1, including the timelike minimal Enneper-type surface and the timelike plane.

To obtain a deformation of null curves from the surface, let us now take $A_1 = \sqrt{\cos 2\hat{c}_1}$. After applying a suitable homothety to the domain, the generating null curves of the surfaces in the Sheet 1 discussed in (3.37) are written as

$$\alpha^{\hat{c}_1}(s) = \left(\tfrac{\sinh^2(A_1 s)}{2A_1^2}, \tfrac{2\cos\hat{c}_1 A_1 s - \sin\hat{c}_1 \sinh(2A_1 s)}{4A_1^3}, \tfrac{2\sin\hat{c}_1 A_1 s - \cos\hat{c}_1 \sinh(2A_1 s)}{4A_1^3}\right),$$
$$\beta^{\hat{c}_1}(s) = \alpha^{\hat{c}_1}(s)\cdot \begin{pmatrix} 1 & 0 & 0 \\ 0 & 1 & 0 \\ 0 & 0 & -1 \end{pmatrix},$$

i.e.

$$\tfrac{1}{2}(\alpha^{\hat{c}_1}(u) + \beta^{\hat{c}_1}(v)) = \tfrac{1}{2^{3/2}R^{\hat{c}_1}} \hat{F}_{\mathrm{P}}^{\hat{c}_1}\left(\tfrac{2^{3/4}}{2}(u+v), \tfrac{2^{3/4}}{2}(u-v)\right).$$

Note that although A_1 is zero at $\hat{c}_1 = \frac{\pi}{4}$ and may have complex values, $\alpha^{\hat{c}_1}$ are well-defined non-degenerate null curves for all $\hat{c}_1 \in \left(-\frac{\pi}{4}, \frac{3\pi}{4}\right)$. By Lemma 3.24, s is a pseudo-arclength parameter for each $\alpha^{\hat{c}_1}$, and the curves have constant curvature $-4\cos(2\hat{c}_1)$. Moreover, if we apply the scaling factor of the ambient space $R^{\hat{c}_1}$, then we can deform $\alpha^{\hat{c}_1}$ to a lightlike line by considering the directional limit as $\hat{c}_1$ tends to $-\frac{\pi}{4}$ or $\frac{3\pi}{4}$, see Figure 3.5.

3.3 Characterization of timelike Thomsen surfaces via null curves

Thomsen showed in [109] that the two classes minimal surfaces, those with planar curvature lines, and those that are also affine minimal, called *Thomsen surfaces*, have a striking relationship; namely, they are conjugate minimal surfaces of each other. Manhart showed in [82] that the analogous result holds for maximal surfaces in $\mathbb{R}^{2,1}$. In this section, we investigate the relationship between the two classes of timelike minimal surfaces, those with planar curvature lines and those that are also affine minimal.

3.3.1 The affine minimal condition – revisited

A timelike minimal surface which is also affine minimal is called a *timelike Thomsen surface*, defined by Magid in [81], who proved the following by applying a result by Manhart [83].

Fact 3.28 ([81], cf. [83])**.** *Away from flat points, a timelike minimal surface F is affine minimal if and only if on the null coordinates (u, v), there exist functions $\theta = \theta(u)$ and $\vartheta = \vartheta(v)$ such that*

$$F_u = (\cos\theta, \sin\theta, 1), \quad F_v = (\cos\vartheta, \sin\vartheta, 1),$$

and $\mathrm{d}\theta/\mathrm{d}u$, $\mathrm{d}\vartheta/\mathrm{d}v$ are both solutions to the equation

$$2\omega^4 + 2\omega\omega'' - \frac{7}{2}\omega'^2 - k\omega^3 = 0 \quad \textit{for some fixed } k \in \mathbb{R}, \tag{3.39}$$

where $'$ now denotes $\frac{\mathrm{d}}{\mathrm{d}u}$ or $\frac{\mathrm{d}}{\mathrm{d}v}$.

Magid also solved the above equation explicitly.

Remark 3.29. Milnor [85] called the "angle" functions θ and ϑ the *Weierstrass functions*, and determined the sign of the Gaussian curvature of timelike minimal surfaces using the functions.

In this subsection, we give a geometric interpretation of Fact 3.28 by using the notion of lightlike curvature of non-degenerate null curves. Let $\alpha(u)$ and $\beta(v)$ be the generating null curves of a timelike minimal surface F where

$$\alpha(u) = \int_{u_0}^{u} \big(\cos\theta(\tau), \sin\theta(\tau), 1\big)\,\mathrm{d}\tau + \alpha(u_0), \quad \beta(v) = \int_{v_0}^{v} \big(\cos\vartheta(\tau), \sin\vartheta(\tau), 1\big)\,\mathrm{d}\tau + \beta(v_0)$$

for some real constants u_0 and v_0. Here, we remark that the parameters u and v are not pseudo-arclength parameters.

In the next proposition, we show that the constant k in the affine minimal equation (3.39) represents the lightlike curvature of generating null curves, giving a geometric characterization of timelike Thomsen surfaces.

Proposition 3.30. *A timelike minimal surface F satisfies the affine minimal equation* (3.39) *if and only if the generating null curves α and β of F have the same constant lightlike curvature.*

Proof. We show that the generating null curves α and β must have lightlike curvature k. By the similarity of the argument, it is enough to consider the claim for $\alpha(u)$.

Since $\langle \alpha', \alpha' \rangle = \theta'^2$, we may assume that $\theta' > 0$, and we can take the pseudo-arclength

$$s = \int_{u_0}^{u} \big(\theta'(\tau)\big)^{1/4} \, \mathrm{d}\tau.$$

By (3.30), we obtain

$$\kappa_\alpha(s) = \dot{u}^6 \left\langle \alpha''', \alpha''' \right\rangle + 9\dot{u}^2\ddot{u}^2\langle \alpha'', \alpha'' \rangle + 6\dot{u}^4\ddot{u}\langle \alpha''', \alpha'' \rangle + 2\dot{u}^3\dddot{u}\langle \alpha''', \alpha' \rangle. \tag{3.40}$$

After straightforward calculations, we get

$$\langle \alpha'', \alpha'' \rangle = \theta'^2, \quad \langle \alpha''', \alpha'' \rangle = \theta'\theta'', \quad \langle \alpha''', \alpha' \rangle = -\theta'^2, \quad \langle \alpha''', \alpha''' \rangle = \theta''^2 + \theta'^4,$$
$$\dot{u} = \big(\theta'\big)^{-1/2}, \quad \ddot{u} = -\frac{\theta''}{2\theta'^2}, \quad \dddot{u} = \frac{2\theta''^2 - \theta'\theta'''}{2\theta'^{7/2}}.$$

Substituting these to (3.40), we obtain

$$2\theta'^3\kappa_\alpha = 2\theta'^4 - \frac{7}{2}\theta''^2 + 2\theta'\theta'''.$$

Hence, the lightlike curvature κ_α is constant if and only if $\omega = \theta'$ satisfies the affine minimal equation (3.39). □

In conjunction with the non-degenerate null curves with constant lightlike curvature in Example 3.23, Proposition 3.30 gives another proof of the classification result of timelike Thomsen surface given in [81]. Furthermore, Theorem 3.25 and Proposition 3.30 give us the next theorem relating the two classes of timelike minimal surfaces, a result different from the cases of minimal surfaces in $\mathbb{R}^3$ and maximal surfaces in $\mathbb{R}^{2,1}$.

Theorem 3.31. *Let T denote the set of timelike Thomsen surfaces, B the set of timelike minimal surfaces of Bonnet-type, and B^* the conjugates of surfaces in B. Then,*

$$T = B \cup B^*, \quad B \cap B^* = \{\textit{timelike planes}\}. \tag{3.41}$$

Remark 3.32. Note that for the minimal surface case, the relation between minimal surfaces of Bonnet-type and Thomsen surfaces can be expressed using analogous notations $\tilde{T}$, $\tilde{B}$ and $\tilde{B}^*$, denoting the set of Thomsen surfaces, the set of minimal surfaces of Bonnet-type, and the conjugates of surfaces in $\tilde{B}$, respectively, as:

$$\tilde{T} = \tilde{B}^*, \quad \tilde{B} \cap \tilde{B}^* = \{\text{planes, Enneper surface}\}.$$

Similarly, by letting $\hat{T}$, $\hat{B}$ and $\hat{B}^*$ denote the analogous sets for maximal surfaces, respectively, we have that

$$\hat{T} = \hat{B}^*, \quad \hat{B} \cap \hat{B}^* = \left\{ \begin{matrix} \text{spacelike planes, maximal Enneper-type surface,} \\ \text{associated family of spacelike catenoid with lightlike axis} \end{matrix} \right\}.$$

3.3.2 Characterization of the associated family of timelike Thomsen surfaces

Finally, as a corollary of Theorem 3.25 and Proposition 3.30, we can also characterize timelike minimal surfaces whose generating null curves have different constant lightlike curvature with the same sign.

Corollary 3.33. *Away from flat points, a timelike minimal surface $\tilde{F}$ whose generating null curves α and β have constant lightlike curvatures κ_α and κ_β with the same sign is contained in the associated family of a timelike Thomsen surface F. In particular, F is either*

- *a timelike minimal surface of Bonnet-type if $K < 0$, or*
- *the conjugate of a timelike minimal surface of Bonnet-type if $K > 0$.*

Moreover, such a timelike Thomsen surface F is unique if neither lightlike curvatures of null curves is zero.

Proof. As in Remark 3.4, the generating null curves of F^μ are

$$\alpha^\mu = \mu\alpha, \quad \beta^\mu = \beta/\mu.$$

They have the lightlike curvatures $\kappa_{\mu\alpha} = \kappa_\alpha/\mu$ and $\kappa_{\beta/\mu} = \mu\kappa_\beta$, respectively. Hence, we can take the unique solution $\mu = \sqrt{\kappa_\alpha/\kappa_\beta}$ to the equation

$$\kappa_{\mu\alpha} = \kappa_{\beta/\mu}, \quad \mu > 0,$$

for which F^μ is a timelike Thomsen surface. The surface F^μ is either in B or B^* depending on the sign of the Gaussian curvature K. □

Remark 3.34. Similarly, one can consider the geometric characterization of timelike minimal surfaces whose generating null curves have constant curvatures with different signs. By (3.34), such a surface can be constructed via the equation

$$\kappa_\alpha + \kappa_\beta = -4\frac{\rho_{uu} + \rho_{vv}}{\rho} = 0.$$

We do know that such surface is not in the set T as in (3.41). However, the geometric qualities of such surfaces are unknown.

3.4 Deformation of timelike Thomsen surfaces

In this section, we show that there exists a continuous deformation consisting exactly of all timelike Thomsen surfaces. We do this by first showing that there exists a continuous deformation consisting exactly of all timelike minimal surfaces of Bonnet-type, and then applying the result that relates these surfaces to timelike Thomsen surfaces.

We have already shown in Section 3.2.3 that every surface in Sheet 1, including the timelike minimal Enneper-type surface, and the timelike plane are conjoined by a continuous deformation given by $\hat{F}_{\mathrm{P}}^{\hat{c}_1}(x, y)$ in (3.37).

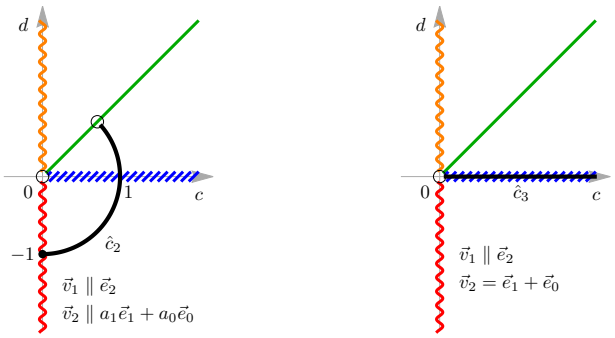

(A) Sheet 2 to Sheet 1 (B) Sheet 2 to C_L

Figure 3.6: (c, d)-paths for deformations.

3.4.1 Deformation to Sheet 2

We now show that there is a continuous deformation of all the surfaces in Sheet 2, and hence, all the surfaces in Sheet 1 and Sheet 2 are connected via the timelike minimal Enneper-type surface. We first normalize the axial directions as in Section 3.1.4, and let $c = \cos\hat{c}_2$ and $d = \sin\hat{c}_2$, while $a_1 = \sqrt{\cos\hat{c}_2 - \sin\hat{c}_2}$ and $a_0 = \sqrt{\cos\hat{c}_2}$ for $\hat{c}_2 \in \left[-\frac{\pi}{2}, \frac{\pi}{4}\right]$ (see Figure 3.6(A)). After calculating the normal vector, we find that

$$\begin{aligned} h^{\hat{c}_2}_{\mathrm{S2}}(z) &= \begin{cases} j\left(\left(\frac{a_0}{a_1}+1\right)\mathsf{e}^{a_1 jz} - \frac{a_0}{a_1}\right), & \text{if } \hat{c}_2 \neq \frac{\pi}{4}, \\ \frac{1}{2^{1/4}}z + j, & \text{if } \hat{c}_2 = \frac{\pi}{4}, \end{cases} \\ \eta^{\hat{c}_2}_{\mathrm{S2}}(z) &= \begin{cases} \frac{1}{2(a_1+a_0)}\mathsf{e}^{-a_1 jz}, & \text{if } \hat{c}_2 \neq \frac{\pi}{4}, \\ \frac{1}{2^{3/4}}, & \text{if } \hat{c}_2 \neq \frac{\pi}{4}. \end{cases} \end{aligned} \tag{3.42}$$

Remark 3.35. Note that the Weierstrass data $\left\{\left(h^{\hat{c}_2}_{\mathrm{S2}}, \eta^{\hat{c}_2}_{\mathrm{S2}}\,\mathrm{d}z\right) : \hat{c}_2 \in \left[-\frac{\pi}{2}, \frac{\pi}{4}\right)\right\}$ describes the same set of surfaces as $\left\{\left(h^{c_2}_2, \eta^{c_2}_2\,\mathrm{d}z\right) : c_2 \in [0,\infty)\right\}$ as in (3.24), up to homothety and translation in the domain, the (x, y)-plane. Explicitly,

$$h^{\hat{c}_2}_{\mathrm{S2}}\left(\tfrac{1}{a_1}\left(z - j\log\left(1+\tfrac{a_0}{a_1}\right)\right)\right) = j\mathsf{e}^{jz} - j\tfrac{a_0}{a_1} = h^{c_2}_2(z)\Big|_{c_2=\frac{a_0}{a_1}}.$$

To get the parametrization, let $F^{\hat{c}_2}_{\mathrm{S2}}(x, y)$ be defined from the Weierstrass data

$$\left(h^{\hat{c}_2}_{\mathrm{S2}}, \eta^{\hat{c}_2}_{\mathrm{S2}}\,\mathrm{d}z\right)$$

via the Weierstrass-type representation in Fact 3.2, and consider

$$\hat{F}^{\hat{c}_2}_{\mathrm{S2}}(x, y) = F^{\hat{c}_2}_{\mathrm{S2}}(x, y) - F^{\hat{c}_2}_{\mathrm{S2}}(0, 0).$$

Then we have that

$$\lim_{\hat{c}_2 \nearrow \frac{\pi}{4}} \hat{F}^{\hat{c}_2}_{\mathrm{S2}}\left(x, y - 2^{1/4}\right) + \left(\tfrac{1}{\sqrt{2}},\, 0,\, -\tfrac{2\sqrt{2}}{3}\right) = \lim_{\hat{c}_1 \to \frac{\pi}{4}} \hat{F}^{\hat{c}_1}_{\mathrm{P}}(x, y),$$

implying that there is a deformation joining surfaces in Sheet 1 and Sheet 2.

3.4.2 Deformation to the timelike catenoid with lightlike axis

Now we show that there exists a deformation to the timelike catenoid with lightlike axis. Consider Sheet 2, where $c = {\hat{c}_3}^2$ and $d = 0$ for ${\hat{c}_3}^2 \in (0, \infty)$, and normalize the axial directions so that $\vec{v}_1 \parallel \vec{e}_2$ and $\vec{v}_2 = \vec{e}_1 + \vec{e}_0$ (see Figure 3.6(B)). Calculating the Weierstrass data gives

$$h^{\hat{c}_3}_{\mathrm{C_L}}(z) = \frac{j\left((\hat{c}_3+1)\mathsf{e}^{j\hat{c}_3 z} - 1\right)}{(\hat{c}_3 - 1)\mathsf{e}^{j\hat{c}_3 z} + 1}, \quad \eta^{\hat{c}_3}_{\mathrm{C_L}}(z) = \tfrac{1}{4{\hat{c}_3}^2}\mathsf{e}^{-j\hat{c}_3 z}\left((\hat{c}_3 - 1)\mathsf{e}^{j\hat{c}_3 z} + 1\right)^2. \tag{3.43}$$

Then note that

$$h^{\hat{c}_3}_{\mathrm{C_L}}(z)\Big|_{\hat{c}_3=1} = 2j\mathsf{e}^{jz} - j = h^{\hat{c}_2}_{\mathrm{S2}}(x, y)\Big|_{\hat{c}_2=0}, \quad \lim_{\hat{c}_3 \searrow 0} h^{\hat{c}_3}_{\mathrm{C_L}}(z) = \frac{z + j}{1 - jz} = h_5(z).$$

Therefore, by calculating $F^{\hat{c}_3}_{\mathrm{C_L}}(x, y)$ from $(h^{\hat{c}_3}_{\mathrm{C_L}}(z), h^{\hat{c}_3}_{\mathrm{C_L}}(z)\,\mathrm{d}z)$ via Fact 3.2 and defining

$$\hat{F}^{\hat{c}_3}_{\mathrm{C_L}}(x, y) = F^{\hat{c}_3}_{\mathrm{C_L}}(x, y) - F^{\hat{c}_3}_{\mathrm{C_L}}(0, 0),$$

we see that

$$\hat{F}^{\hat{c}_3}_{\mathrm{C_L}}(x, y)\Big|_{\hat{c}_3=1} = \hat{F}^{\hat{c}_2}_{\mathrm{S2}}(x, y)\Big|_{\hat{c}_2=0},$$
$$\lim_{\hat{c}_3 \searrow 0} \hat{F}^{\hat{c}_3}_{\mathrm{C_L}}(x, y) = \tfrac{1}{2}\left(y - x^2 y - \tfrac{1}{3}y^3,\, -2xy,\, -y - x^2 y - \tfrac{1}{3}y^3\right),$$

implying that $\hat{F}^{\hat{c}_3}_{\mathrm{C_L}}(x, y)$ gives a deformation between timelike minimal Bonnet-type surface with lightlike axis of first kind and timelike catenoid with lightlike axis.

3.4.3 Deformation to Sheet 4

Since we have that

$$h^{c_4}_4(z)\Big|_{c_4=0} = j\mathsf{e}^{jz} = h^{\hat{c}_2}_{\mathrm{S2}}(z)\Big|_{\hat{c}_2=-\frac{\pi}{2}}$$

where $h^{c_4}_4$ is as in (3.26), we define $F^{c_4}_{S4}$ using the Weierstrass data $(h^{c_4}_4, \eta^{c_4}_4\,\mathrm{d}z)$. Then for

$$\hat{F}^{c_4}_{S4}(x, y) = F^{c_4}_{S4}(x, y) - F^{c_4}_{S4}(0, 0),$$

we can directly check that

$$\hat{F}^{c_4}_{S4}(x, y)\Big|_{c_4=0} = \hat{F}^{\hat{c}_2}_{\mathrm{S2}}(x, y)\Big|_{\hat{c}_2=-\frac{\pi}{2}},$$

implying that there is a deformation joining surfaces in Sheet 2 and Sheet 4.

3.4.4 Deformation to the timelike minimal Bonnet-type surface with lightlike axial direction of second kind

Finally, we show that the timelike minimal Bonnet-type surface with lightlike axial direction of second kind is also connected via a deformation to the immersed timelike catenoid with spacelike axis. To do this, instead of recalculating the Weierstrass data from the normal vector function, we take advantage of their respective Weierstrass data in Theorem 3.21, and consider

$$h^{\hat{c}_5}_{\mathrm{B_{L2}}}(z) = \mathsf{e}^{2^{1/4}z} + j\hat{c}_5, \quad \eta^{\hat{c}_5}_{\mathrm{B_{L2}}}(z) = \tfrac{1}{2^{5/4}}\mathsf{e}^{-2^{1/4}z} \tag{3.44}$$

for $\hat{c}_5 \in [0,1]$. Then it is easy to see that letting $\hat{c}_5 = 0$ gives the Weierstrass data for immersed timelike catenoid with spacelike axis, while letting $\hat{c}_5 = 1$ gives the Weierstrass data for timelike minimal Bonnet-type surface with lightlike axial direction of second kind.

Now we would like to see that the surfaces defined by $\hat{c}_5 \in (0,1)$ are also timelike minimal surfaces of Bonnet-type. To do this, recall that the choice of the paraholomorphic 1-form from the parameromorphic function decides the Hopf differential; therefore, a timelike minimal surface is uniquely determined by its Lorentz conformal factor up to isometries of the ambient space. Hence, by calculating the Lorentz conformal factor from $\left(h^{\hat{c}_5}_{\mathrm{B_{L2}}}, \eta^{\hat{c}_5}_{\mathrm{B_{L2}}}\,\mathrm{d}z\right)$ via (3.4), we find that the surfaces obtained for $\hat{c}_5 \in (0,1)$ are timelike minimal Bonnet-type surfaces with spacelike axial direction.

Using Remark 3.18 (or by directly calculating), for $F^{\hat{c}_5}_{\mathrm{B_{L2}}}(x,y)$ coming from Fact 3.2 using the Weierstrass data $\left(h^{\hat{c}_5}_{\mathrm{B_{L2}}}(z), \eta^{\hat{c}_5}_{\mathrm{B_{L2}}}(z)\,\mathrm{d}z\right)$, if we define

$$\hat{F}^{\hat{c}_5}_{\mathrm{B_{L2}}}(x,y) = F^{\hat{c}_5}_{\mathrm{B_{L2}}}(x,y).\begin{pmatrix} 0 & 1 & 0 \\ -1 & 0 & 0 \\ 0 & 0 & 1 \end{pmatrix} - \left(\frac{1}{\sqrt{2}}, 0, 0\right),$$

then we have

$$\hat{F}^{\hat{c}_5}_{\mathrm{B_{L2}}}(x,y)\Big|_{\hat{c}_5=0} = \hat{F}^{\hat{c}_1}_{\mathrm{P}}(x,y)\Big|_{\hat{c}_1=0}.$$

Summarizing, we arrive at the following result:

Theorem 3.36. *There exists a continuous deformation consisting exactly of all timelike minimal surfaces of Bonnet-type (see Figure 3.7 and 3.8).*

Corollary 3.37 (Corollary to Theorem 3.31 and Theorem 3.36)**.** *There exists a continuous deformation consisting exactly of all timelike Thomsen surfaces.*

3.5 Singularities of timelike Thomsen surfaces

By Remark 3.14, we understand that timelike minimal surfaces of Bonnet-type admit singularities, belonging to a class of surfaces called generalized timelike minimal surfaces. However, since we have obtained the paraholomorphic 1-form $\eta\,\mathrm{d}z$ for all generalized timelike minimal

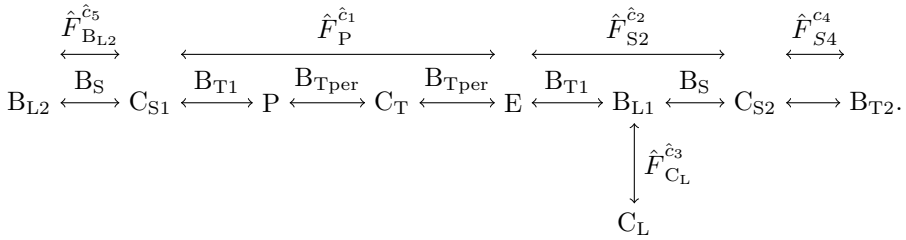

Figure 3.7: Diagram of deformations connecting timelike minimal surfaces of Bonnet-type.

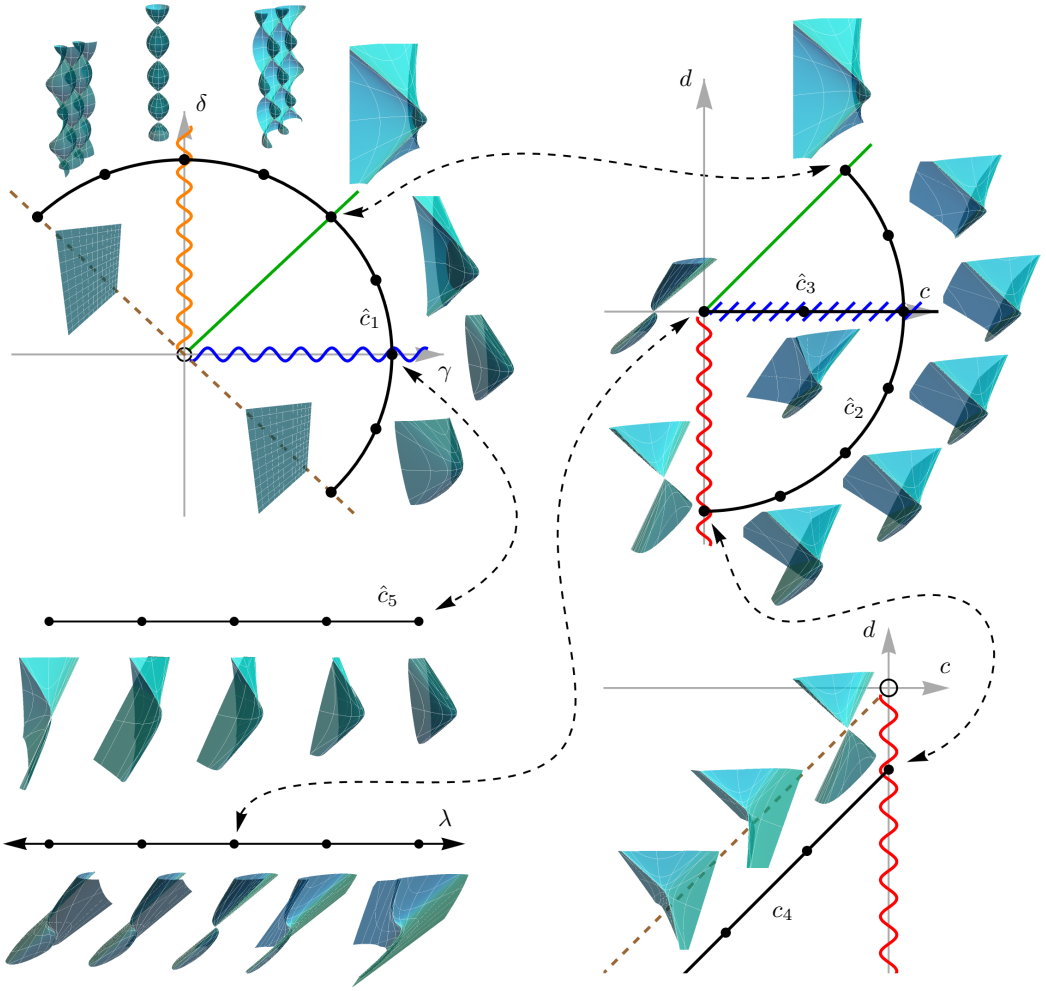

Figure 3.8: Continuous deformation of timelike minimal surfaces of Bonnet-type.

surfaces of Bonnet-type in Theorem 3.21, we can calculate that these surfaces are actually *minfaces*, using [108, Proposition 2.7] (see also [3, Fact A.7]).

We now aim to investigate the types of singularities appearing on these surfaces. Since the types of singularities of timelike catenoids and timelike Enneper-type surfaces have been investigated in [68, Lemma 2.12] and [108] (see also [3, Example 4.5]), we focus on recognizing the types of singularities on timelike minimal Bonnet-type surfaces.

Let $S(F) := \{(x,y) \in \mathbb{R}^2 : \rho(x,y) = 0\} = \{(x,y) \in \mathbb{R}^2 : |h(x,y)|^2 = -1\}$ be the singular set. Then using the explicit solution of the metric function in Proposition 3.13 or the explicit form of the function h of the Weierstrass data in Theorem 3.21, we understand that the singular set becomes 1-dimensional. To recognize the types of singularities of timelike minimal Bonnet-type surfaces, we refer to the following results from [108] (see also [120, Theorem 3] and [3, Fact 4.1]), analogous results of [110] and [47].

Fact 3.38. *Let $F(x,y) : \Sigma \to \mathbb{R}^{2,1}$ be a minface with Weierstrass data $(h, \eta\, \mathrm{d}z)$. Then, a point $p \in \Sigma$ is a singular point if and only if $|h(p)|^2 = -1$. Furthermore, for*

$$\psi := \frac{h_z}{h^2\eta}, \quad \Psi := \frac{h}{h_z}\psi_z,$$

the image of F around a singular point p is locally diffeomorphic to

- *a cuspidal edge if and only if $\operatorname{Re}\psi \neq 0$ and $\Im\psi \neq 0$ at p, or*
- *a swallowtail if and only if $\psi \in \mathbb{R} \setminus \{0\}$ and $\operatorname{Re}\Psi \neq 0$ at p.*

Using the Weierstrass data $(h, \eta\, \mathrm{d}z)$ of timelike minimal Bonnet-type surfaces from Theorem 3.21, we directly calculate ψ and Ψ. Then using Fact 3.38, we arrive at the following result.

Theorem 3.39. *Let $F(x,y)$ be a timelike minimal Bonnet-type surface with the Weierstrass data given in Theorem 3.21. Then, the image of F around a singular point $p = (x,y)$ is locally diffeomorphic to swallowtails (SW) only at the following points.*

Surface	*Points of SW*
$\mathrm{B}_{\mathrm{Tper}}$	$\left(\cos^{-1}(\pm 1), \cos^{-1}\left(\pm\frac{\tilde{c}_1}{\sqrt{\tilde{c}_1^2+1}}\right)\right), \left(\cos^{-1}(0), \cos^{-1}\left(\pm\frac{1}{\sqrt{\tilde{c}_1^2+1}}\right)\right)$
B_{T1}	$\big(0, \log(c_2+1)\big)$
B_{L1}	$(0, \log 2)$
B_{S}	$\big(0, \log(c_2 \pm 1)\big)$
B_{T2}	*None*
B_{L2}	*None*

Moreover, the images of F around singular points are locally diffeomorphic to cuspidal edges everywhere else (see Figure 3.3).

Combined with the result in [3, 68, 108], we obtain the following corollary.

Corollary 3.40. *Let $F(x, y)$ be a minface of Bonnet-type. If p is a singular point of $F(x, y)$, then the image of F around the singular point p must be locally diffeomorphic to one of the following: cuspidal edge, swallowtail or conelike (or shrinking) singularity.*

Using the duality for singularities on timelike minimal surfaces and their conjugate surfaces, proved in [68] and [108] (cf. [3, Fact A.12]), we finally obtain the following result:

Corollary 3.41 (Corollary to Theorem 3.31 and Corollary 3.40)**.** *Any singular point on a timelike Thomsen surface is locally diffeomorphic to one of the following: cuspidal edge, swallowtail, cuspidal cross cap, conelike (or shrinking) singularity or fold singularity.*

Remark 3.42. Note that in Figure 3.3(F), the surface $\mathrm{B}_{\mathrm{L}2}$ defined over the domain $\mathbb{C}'$ is drawn; in fact, this surface can be extended to a lightlike line (drawn as a yellow line in Figure 3.3(F)) as in the cases of catenoids with spacelike and lightlike axes ([45, 46]).

To see this explicitly, first note that the surface (9) in Theorem 3.21 is parametrized as

$$F(x, y) = \left(x + e^{-x}\sinh y, -y - \tfrac{e^x}{2}\cosh y, -x - (e^{-x} + \tfrac{e^x}{2})\sinh y\right).$$

Putting $\varrho(x) = -x - \tilde{y}$ for $\tilde{y} \in \mathbb{R}$, we note that

$$\lim_{x\to-\infty} F(x, \sinh^{-1}(e^x\varrho(x))) = (-\tilde{y}, 0, \tilde{y}).$$

Chapter 4

Discrete minimal surfaces with symmetries

In the case of smooth minimal surfaces in Euclidean 3-space $\mathbb{R}^3$, the Schwarz reflection principle has been used to good effect to extend minimal surfaces and study their global behavior. The Schwarz reflection principle for minimal surfaces comes in two forms. One states that if the minimal surface lies to one side of a plane and has a curvature-line boundary lying in that plane and meeting it perpendicularly, then the surface extends smoothly by reflection to the other side of the plane. The other states that if the minimal surface contains a boundary line segment, then it can be smoothly extended across the line by including the 180 degree rotation of the surface about that line. When one of these two situations holds on a minimal surface, the other one holds on the conjugate minimal surface.

By the nature of the Schwarz reflection principle, we expect that the surfaces constructed will have relatively high degrees of symmetry. Such symmetry has been seen in numerous works, see, for example, [32, 55, 56, 65–67, 97, 98, 106].

Such symmetry has also been exploited in the discrete case as well: for discrete S-isothermic minimal nets, see, for example, [15, 22, 23]; for discrete isothermic constant mean curvature nets, see, for example, [57].

In this chapter, we investigate how a similar reflection principle will work in the case of discrete isothermic minimal nets and discrete asymptotic minimal nets. The benefit of this is that it provides us a further tool for extending discrete minimal surfaces described locally (which has been well investigated) to surfaces considered at a more global level (which has not received as much attention yet). For example, we will construct the central part of a discrete minimal trinoid, which can then be regarded as existing on a global level, since it is not a simply connected surface, as it is topologically equivalent to the sphere minus three disks. Like in the smooth case, we expect to see relatively high degrees of symmetry in the surfaces we construct in this way.

4.1 Preliminaries

Let our domain be a $\mathbb{Z}^2$ lattice with $(m,n) \in \mathbb{Z}^2$, and let $(ijkl)$ denote the vertices of an elementary quadrilateral $((m,n),(m+1,n),(m+1,n+1),(m,n+1))$. For simplicity, we have chosen our domain to be $\mathbb{Z}^2$; however, the theory will hold true for subdomains of $\mathbb{Z}^2$. If F is a discrete net $F : \mathbb{Z}^2 \to \mathbb{R}^3$, then we write $F(m,n) = F_{m,n} = F_i$ over any elementary quadrilateral, and let

$$\mathrm{d}F_{ij} := F_j - F_i.$$

A discrete net F is called a *circular net* if F_i, F_j, F_k, and F_l are concircular, representing a discrete notion of curvature line coordinates [90].

4.1.1 Discrete isothermic nets

First we recall from [17, Definition 4] how the cross ratio of four points in $\mathbb{R}^3$ are defined.

Definition 4.1. Let $x_1, \dots, x_4 \in \mathbb{R}^3$, and let $\mathbb{R}^3$ be identified with the set of quaternions $\mathbb{H}$ under the usual identification $\mathbb{R}^3 \ni x_i \sim X_i \in \mathbb{H}$. The pair of eigenvalues $\{q, \bar{q}\}$ of the quaternion

$$(X_1 - X_2)(X_2 - X_3)^{-1}(X_3 - X_4)(X_4 - X_1)^{-1}$$

is called the *cross ratio of* $x_1, \dots, x_4$. In the case where $x_1, \dots, x_4$ are concircular, $q = \bar{q} \in \mathbb{R}$, and we write

$$\mathrm{cr}(x_1, x_2, x_3, x_4) = q.$$

Remark 4.2. It was further proved in [17, Lemma 1] that this cross ratio is invariant under Möbius transformations.

Using this definition of cross ratios, discrete isothermic nets are defined as follows in [17, Definition 6]:

Definition 4.3. A circular net F is called a *discrete isothermic net* if on every elementary quadrilateral $(ijkl)$,

$$\mathrm{cr}(F_i, F_j, F_k, F_l) = \frac{a_{ij}}{a_{il}} \in \mathbb{R}_{<0},$$

where a_{ij} (resp. a_{il}) are edge-labeling scalar functions defined on unoriented edges; that is,

$$a_{ij} = a_{lk} \quad \text{and} \quad a_{il} = a_{jk} \tag{4.1}$$

on every elementary quadrilateral $(ijkl)$. We call a_{ij} and a_{il} the *cross ratio factorizing functions*.

It is shown in [17, Theorem 6] that, for any discrete net F, the discrete isothermicity of F is equivalent to the existence of another discrete net F^* such that

$$\mathrm{d}F^*_{ij} = \frac{a_{ij}}{\|\,\mathrm{d}F_{ij}\|^2}\,\mathrm{d}F_{ij}, \quad \mathrm{d}F^*_{il} = \frac{a_{il}}{\|\,\mathrm{d}F_{il}\|^2}\,\mathrm{d}F_{il}.$$

If such an F^* exists, F^* is called a *Christoffel transformation* of F, and $(F^*)^* = F$ up to scaling and translation in $\mathbb{R}^3$.

4.1.2 Discrete Gaussian and mean curvatures

For any two parallel circular nets F and G, i.e. F and G are both circular nets with parallel corresponding edges, the mixed area of F and G is defined on every elementary quadrilateral as

$$A(F,G)_{ijkl} := \frac{1}{4}(\delta F_{ik} \wedge \delta G_{jl} + \delta G_{ik} \wedge \delta F_{jl})$$

where $\delta F_{ik} := F_k - F_i$ and the exterior algebra $\wedge^2\mathbb{R}^3 (\ni u \wedge v)$ is identified with the Lie algebra o(3), i.e. for any $u, v, w \in \mathbb{R}^3$,

$$(u \wedge v)\, w = (u \cdot w)v - (v \cdot w)u$$

for the usual inner product of $x, y \in \mathbb{R}^3$ expressed as $x \cdot y$. Note that $A(F)_{ijkl} := A(F,F)_{ijkl}$ gives the area of the quadrilateral spanned by the image of F over an elementary quadrilateral $(ijkl)$.

It is known through [74] that any circular net F has a parallel circular net $N : \mathbb{Z}^2 \to S^2 \subset \mathbb{R}^3$ taking values in the unit sphere. Such an N is called a *discrete Gauss map* of F.

Remark 4.4. If a discrete line bundle $L : \mathbb{Z}^2 \to \{\text{lines in } \mathbb{R}^3\}$ is the normal bundle of F, i.e. $F_i, F_i + N_i \in L_i$, then L constitutes a discrete line congruence in the sense of [36, Definition 2.1], as any two neighboring lines intersect. One can see that after a choice of one normal direction at one vertex of F (an initial condition), the line congruence condition and the parallel mesh condition uniquely determine the normal bundle L over all vertices in the domain, since any two neighboring normal lines must intersect at equal distance from the vertices on the surface.

Furthermore, it is not difficult to see that the parallel net F^t defined as $F^t := F + tN$ for some constant t is also a circular net parallel to F. This allows us to consider the mixed area of F and F^t, and recover the discrete version of the Steiner's formula based on mixed areas (see [95, 105]):

$$\begin{aligned} A(F^t)_{ijkl} &= A(F)_{ijkl} + 2tA(F,N)_{ijkl} + t^2 A(N)_{ijkl} \\ &= (1 - 2tH_{ijkl} + t^2 K_{ijkl})A(F)_{ijkl} \end{aligned}$$

where H_{ijkl} and K_{ijkl} are defined on each elementary quadrilateral as:

Definition 4.5. We call

$$H_{ijkl} = -\frac{A(F,N)_{ijkl}}{A(F)_{ijkl}}, \quad K_{ijkl} = \frac{A(N)_{ijkl}}{A(F)_{ijkl}}$$

the mean and Gaussian curvatures of a circular net F with Gauss map N.

With the notion of mean curvature on any elementary quadrilateral $(ijkl)$ available, discrete isothermic minimal nets and discrete isothermic constant mean curvature (cmc) nets can be defined as:

Definition 4.6. A circular net F is called a discrete isothermic minimal (resp. cmc) net if $H \equiv 0$ (resp. $H \equiv c \neq 0$ for some non-zero constant c) on every elementary quadrilateral.

4.1.3 Planar reflection principle for discrete isothermic minimal and cmc nets

Since circular nets are a discrete analogue of curvature line coordinates, the following notion is natural.

Definition 4.7. Let $F : \mathbb{Z}^2 \to \mathbb{R}^3$ be a circular net. A discrete space curve F_{m,n_0} (resp. $F_{m_0,n}$) depending on m (resp. n) for each $n_0 \in \mathbb{Z}$ (resp. $m_0 \in \mathbb{Z}$) is called a *discrete curvature line*.

Without loss of generality, let $n_0 \in \mathbb{Z}$, and let F be a discrete isothermic minimal or cmc net, defined on the domain $D := \{(m,n) \in \mathbb{Z}^2 : n \leq n_0\}$ with corresponding Gauss map N. Suppose that the discrete curvature line F_{m,n_0} is contained in a plane $\mathcal{P}$, and further suppose that the unit normal at each vertex (m,n_0) is contained in the plane containing the discrete curvature line, i.e. $F_{m,n_0} + N_{m,n_0} \in \mathcal{P}$.

If we extend F to the domain $\tilde{D} := \{(m,n) \in \mathbb{Z}^2 : n > n_0\}$ by reflecting the vertices across the plane $\mathcal{P}$, then as mentioned in Remark 4.4, the unit normal N also gets uniquely determined on the extended domain. The uniqueness of the unit normal and the symmetry of the discrete net then forces the unit normal to be symmetric with respect to $\mathcal{P}$ as well, giving us the following reflective property of minimal and cmc nets:

Proposition 4.8. *Let $F : D \to \mathbb{R}^3$ be a discrete isothermic minimal (resp. cmc) net with corresponding Gauss map N. Suppose that the discrete curvature line F_{m,n_0} and the normal line congruence L_{m,n_0} along this discrete curve lie in a plane $\mathcal{P}$. Extending F to $\mathbb{Z}^2 = D \cup \tilde{D}$ so that the extension is symmetric with respect to $\mathcal{P}$ results in a discrete minimal (resp. cmc) net on $\mathbb{Z}^2$.*

4.2 Reflection properties of discrete minimal nets

In this section, we take a closer look at the reflection properties of discrete minimal nets.

4.2.1 Discrete isothermic minimal nets

Exploiting the relationship between holomorphic functions on the complex plane and conformality, a definition of discrete holomorphic functions was given in [17, Definition 8] as:

Definition 4.9. A map $g : \mathbb{Z}^2 \to \mathbb{R}^2 \cong \mathbb{C}$ is called a *discrete holomorphic function* if

$$\mathrm{cr}(g_i, g_j, g_k, g_l) = \frac{a_{ij}}{a_{il}} \in \mathbb{R}_{<0}$$

for some edge-labeling scalar functions a_{ij} and a_{il}, i.e. satisfying the condition (4.1).

Using the facts that

- cross ratios are invariant under Möbius transformations,
- a discrete isothermic net on the unit sphere corresponds to a discrete holomorphic function on the complex plane via stereographic projection,

- the Christoffel transform of a discrete minimal net is its own Gauss map, and
- the Christoffel transformation is involutive,

a Weierstrass representation for a discrete minimal net was given in [17, Theorem 9] as follows:

Fact 4.10. *For a discrete holomorphic function g with cross ratio factorizing functions a_{ij} and a_{il}, a discrete isothermic net F defined via*

$$\begin{cases} \mathrm{d}F_{ij} = a_{ij}\,\mathrm{Re}\left((1-g_ig_j, \sqrt{-1}(1+g_ig_j), g_i+g_j)\dfrac{1}{\mathrm{d}g_{ij}}\right) \\ \mathrm{d}F_{il} = a_{il}\,\mathrm{Re}\left((1-g_ig_l, \sqrt{-1}(1+g_ig_l), g_i+g_l)\dfrac{1}{\mathrm{d}g_{il}}\right) \end{cases}$$

becomes a discrete isothermic minimal net. Furthermore, any discrete isothermic minimal net can be obtained via some discrete holomorphic function g.

4.2.2 Discrete asympotic minimal nets

In this section, we make use of shift notations:

$$F = F_{m,n},\ F_1 = F_{m+1,n},\ F_{\bar{1}} = F_{m-1,n},\ F_2 = F_{m,n+1},\ F_{\bar{2}} = F_{m,n-1}.$$

Discrete asymptotic nets were defined as follows in several different contexts (see, for example [19, 102, 103, 118]):

Definition 4.11. A discrete net $\tilde{F} : \mathbb{Z}^2 \to \mathbb{R}^3$ is a *discrete asymptotic net* if each vertex and its neighboring four vertices are coplanar, i.e. $\tilde{F}, \tilde{F}_1, \tilde{F}_{\bar{1}}, \tilde{F}_2, \tilde{F}_{\bar{2}} \in \mathcal{P}_{m,n}$ for some plane $\mathcal{P}_{m,n}$ for each (m,n).

Following [19], we assume that the discrete asymptotic nets here are non-degenerate, i.e. $\tilde{F}_i$, $\tilde{F}_j$, $\tilde{F}_k$, $\tilde{F}_l$ are non-planar.

For a discrete asymptotic net $\tilde{F}$, the Gauss map N is defined as the unit normal to the tangent plane $\mathcal{P}_{m,n}$. Similar to discrete curvature lines, discrete asymptotic lines can be defined as follows:

Definition 4.12. Let $\tilde{F} : \mathbb{Z}^2 \to \mathbb{R}^3$ be a discrete asymptotic net. A discrete space curve $\tilde{F}_{m,n_0}$ (resp. $\tilde{F}_{m_0,n}$) depending on m (resp. n) for each $n_0 \in \mathbb{Z}$ (resp. $m_0 \in \mathbb{Z}$) is called a *discrete asymptotic line*.

Recently, a representation of discrete asymptotic minimal net, where the minimality comes via the edge-constraint condition, was given in [59, Definition 3.1, Theorem 3.14, Lemma 3.17]:

Fact 4.13. *For a discrete holomorphic function g with cross ratio factorizing functions a_{ij}*

and a_{il}, a discrete asymptotic net $\tilde{F}$ defined via

$$\begin{cases} \mathrm{d}\tilde{F}_{ij} = a_{ij}\,\mathrm{Re}\left((1-g_ig_j, \sqrt{-1}(1+g_ig_j), g_i+g_j)\dfrac{\sqrt{-1}}{\mathrm{d}g_{ij}}\right) \\ \mathrm{d}\tilde{F}_{il} = a_{il}\,\mathrm{Re}\left((1-g_ig_l, \sqrt{-1}(1+g_ig_l), g_i+g_l)\dfrac{\sqrt{-1}}{\mathrm{d}g_{il}}\right) \end{cases}$$

becomes a discrete asymptotic minimal net, in the sense of the discrete minimal edge-constraint nets.

Remark 4.14. It was further shown in [59, Lemma 3.17] that $\tilde{F}$ defined from a discrete holomorphic function g via Fact 4.13 shares the same unit normal as the discrete isothermic minimal net F defined from the same g via Fact 4.10. In such case, $\tilde{F}$ is called the conjugate discrete minimal net of F.

4.2.3 Reflection properties of discrete minimal nets

To consider planar discrete space curves, it will be advantageous to use the following notation to denote three consecutive edges:

$$\mathrm{d}F := F_{m+1,n} - F_{m,n}, \quad \mathrm{d}F_1 := F_{m+2,n} - F_{m+1,n}, \quad \mathrm{d}F_{\bar{1}} := F_{m,n} - F_{m-1,n}.$$

We first focus on circular nets: let F be a circular net. Then we have the following lemma, characterizing planar discrete curvature lines in terms of the Gauss map.

Lemma 4.15. *A discrete curvature line on a circular net F is planar if and only if the image of the Gauss map N along the curvature line is contained in a circle.*

Proof. Without loss of generality, the planarity of a discrete curvature line is equivalent to the condition

$$\det(\mathrm{d}F_{\bar{1}}, \mathrm{d}F, \mathrm{d}F_1) = 0$$

on any three consecutive edges. However, since F and N are parallel meshes, the above condition is equivalent to

$$\det(\mathrm{d}N_{\bar{1}}, \mathrm{d}N, \mathrm{d}N_1) = 0.$$

Therefore, a discrete curvature line is planar if and only if the image of the Gauss map along the curvature line is planar, i.e. contained in a circle. □ □

Hence, by further requiring that the normal line congruence, i.e. the linear span of unit normals placed on the vertices, along the planar curvature line is also included in the same plane, we obtain the following corollary, also mentioned briefly in [22].

Corollary 4.16. *The normal line congruence along a planar discrete curvature line is contained in the same plane if and only if the image of the Gauss map along the curvature line is contained in a great circle.*

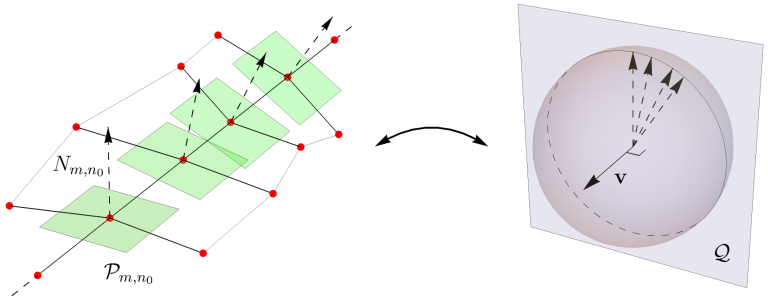

Figure 4.1: A discrete asymptotic net containing a straight line and its Gauss map.

Switching our focus to discrete asymptotic nets, now let $\tilde{F}$ be a discrete asymptotic net. Then we can prove the following lemma characterizing a discrete asymptotic line that is a straight line (see also [22]).

Lemma 4.17. *A discrete asymptotic line on a discrete asymptotic net $\tilde{F}$ is a straight line if and only if the image of the Gauss map N along the discrete asymptotic line is contained in a great circle.*

Proof. To show one direction, suppose that a discrete asymptotic line $\tilde{F}_{m,n_0}$ is a straight line. Then the tangent planes $\mathcal{P}_{m,n_0}$ at each vertex along $\tilde{F}_{m,n_0}$ must include this straight line. Therefore, N_{m,n_0} must be contained in the plane perpendicular to the straight line, i.e. the image of the Gauss map along the discrete asymptotic line is contained in a great circle.

To show the other direction, now suppose that N_{m,n_0} is contained in a great circle, and let $\mathcal{Q}$ denote the plane containing the great circle with a normal vector $\vec{v}$. Then all the tangent planes $\mathcal{P}_{m,n_0}$ must be perpendicular to $\mathcal{Q}$. Hence, from the non-degeneracy condition, any two consecutive tangent planes $\mathcal{P}$ and $\mathcal{P}_1$ must intersect along a line parallel to the normal vector $\vec{v}$. However, $\mathcal{P}$ and $\mathcal{P}_1$ intersect along the edge $\mathrm{d}\tilde{F}$, i.e. $\mathrm{d}\tilde{F} \parallel \vec{v}$, and it follows that $\tilde{F}_{m,n_0}$ must be a straight line in the direction of $\vec{v}$. (See Figure 4.1.) □ □

The fact that a discrete isothermic minimal net F and its conjugate discrete asymptotic minimal net $\tilde{F}$ share the same Gauss map N, as mentioned in Remark 4.14, immediately yields the following corollary.

Corollary 4.18. *The normal line congruence along a planar discrete curvature line on a discrete isothermic minimal net F is contained in the same plane if and only if the corresponding discrete asymptotic line on the conjugate discrete asymptotic minimal net $\tilde{F}$ is a straight line.*

Now we prove a reflection principle for discrete asymptotic minimal nets. Recall that for some $n_0 \in \mathbb{Z}^2$, D and $\tilde{D}$ were defined as $D := \{(m,n) \in \mathbb{Z}^2 : n \leq n_0\}$ and $\tilde{D} := \{(m,n) \in \mathbb{Z}^2 : n > n_0\}$, respectively.

Theorem 4.19. *Let $n_0 \in \mathbb{Z}^2$, and $\tilde{F} : D \subset \mathbb{Z}^2 \to \mathbb{R}^3$ be a discrete asymptotic minimal net with corresponding Gauss map N. Suppose that the discrete asymptotic line $\tilde{F}_{m,n_0}$ is a straight line ℓ. Extending $\tilde{F}$ to the domain $\mathbb{Z}^2 = D \cup \tilde{D}$ so that the extension is symmetric with respect to the line ℓ, the extension is a discrete asymptotic minimal net on $\mathbb{Z}^2$.*

Proof. Let $F : D \to \mathbb{R}^3$ be the conjugate discrete isothermic minimal net. Then by Corollary 4.18, we have that the discrete curvature line F_{m,n_0} and the normal line congruence along the curvature line are contained in the same plane $\mathcal{Q}_1$. Therefore, we may invoke Proposition 4.8 to reflect F across $\mathcal{Q}_1$ so that F and N are now defined on $\mathbb{Z}^2$. Now, let $\tilde{F}$ be the conjugate discrete asymptotic minimal net of the extended discrete isothermic minimal net F, where $\tilde{F}\Big|_D$ agrees with the original $\tilde{F}$. We now show that $\tilde{F}$ is symmetric with respect to ℓ.

Let $\mathcal{Q}_2$ be the plane such that $N_{m,n_0} \in \mathcal{Q}_2$ for any $m \in \mathbb{Z}$; it follows that ℓ is perpendicular to $\mathcal{Q}_2$. By construction, N is symmetric with respect to the plane $\mathcal{Q}_2$.

Now, let $T \in \mathrm{SO}(3)$ be a rotation around ℓ by 180 degrees, and consider $\hat{F} := T\tilde{F}$. By the definition of Gauss maps of discrete asymptotic nets, it must follow that one choice of the Gauss map $\hat{N}$ of $\hat{F}$ be $\hat{N} = -TN$. The fact that ℓ is perpendicular to $\mathcal{Q}_2$ implies that $\hat{N}_{m,n}$ is symmetric to $N_{m,n}$ with respect to the plane $\mathcal{Q}_2$. However, because N is symmetric with respect to $\mathcal{Q}_2$, it follows that $N_{m,n_0+k} = \hat{N}_{m,n_0-k}$. Since, $\tilde{F}$ and $\hat{F}$ share the same initial condition along ℓ, we have $\tilde{F}_{m,n_0+k} = \hat{F}_{m,n_0-k}$ by Fact 4.13. □ □

4.3 Examples of discrete minimal nets with symmetry

Let $F : \mathbb{Z}^2 \to \mathbb{R}^3$ be a discrete isothermic minimal surface with Gauss map N, and choose a point $(m_0, n_0) \in \mathbb{Z}^2$. Suppose that the discrete curves F_{m,n_0} and $F_{m_0,n}$, and also the normal line congruences along these curves, are contained in the planes $\mathcal{P}_1$ and $\mathcal{P}_2$, respectively. Denote the quadrilateral $(m_0, n_0), (m_0+1, n_0), (m_0+1, n_0+1), (m_0, n_0+1)$ by $(ijkl)$, and the image of this quadrilateral under F by F_{ijkl}.

Lemma 4.20. *The angle between F_{ij} and F_{il} and the angle between N_{ij} and N_{il} are supplementary angles.*

Proof. Let $\mathcal{Q}_1$ and $\mathcal{Q}_2$ be the planes cutting S^2 containing the discrete curves N_{m,n_0} and $N_{m_0,n}$, respectively. Since F and N are parallel meshes, the angle between $\mathcal{P}_1$ and $\mathcal{P}_2$ equals that between $\mathcal{Q}_1$ and $\mathcal{Q}_2$. However, since by Christoffel duality, or the Weierstrass representation, the orientations of F and N are opposite, giving us the desired conclusion. □ □

Remark 4.21. Since stereographic projection is a Möbius transformation, it preserves angles. Therefore, to determine the angle between N_{ij} and N_{il}, one only needs to look at the angle between the circles containing g_{m,n_0} and $g_{m_0,n}$.

Before looking at the examples, we comment on how to change the Weierstrass data of a given smooth minimal surface so that it is parametrized with isothermic coordinates (see, for example, [16, Section 2.3]). Let a (smooth) minimal surface $X : \Sigma \subset \mathbb{R}^2 \cong \mathbb{C} \to \mathbb{R}^3$ be represented by

$$X(z) = \mathrm{Re} \int (1 - g(z)^2, \sqrt{-1}(1 + g(z)^2), 2g(z)) f(z)\, \mathrm{d}z$$

over a simply-connected domain Σ on which g is meromorphic, while f and fg^2 are holo-

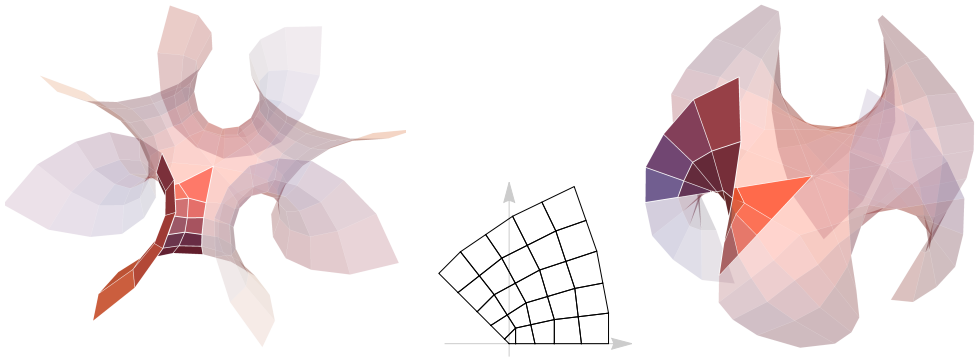

Figure 4.2: A discrete higher order Enneper surface from a discrete power function and its conjugate. The left-hand side is a discrete isothermic minimal net having planar symmetry; the right-hand side is a discrete asymptotic minimal net having line symmetry. This figure was drawn with $k = 3$. (See also [99].)

morphic. Then the coordinate w satisfying

$$(w_z)^2 = fg_z \quad (\text{resp. } (w_z)^2 = -\sqrt{-1}fg_z), \tag{4.2}$$

for $w_z = \frac{\partial w}{\partial z}$, becomes an isothermic (resp. conformal asymptotic) coordinate of X, and X can be represented as

$$X(w) = \operatorname{Re} \int (1 - g(w)^2, \sqrt{-1}(1 + g(w)^2), 2g(w)) \frac{1}{g_w(w)} \, \mathrm{d}w$$
$$(\text{resp. } X(w) = \operatorname{Re} \int (1 - g(w)^2, \sqrt{-1}(1 + g(w)^2), 2g(w)) \frac{\sqrt{-1}}{g_w(w)} \, \mathrm{d}w).$$

Example 4.22. Recall that the well-known Enneper surface and higher order Enneper surfaces can be represented via the Weierstrass data $g(z) = z^k$ and $f(z) = 1$ for $k \in \mathbb{N}$. Taking the coordinate change as in (4.2) (and applying a suitable homothety on the domain depending on k), we obtain new Weierstrass data $g(w) = w^{\frac{2k}{k+1}}$.

Therefore, from the discrete power function z^γ defined in [2] (see also [6, 58]), let g be the discrete power function with $\gamma = \frac{2k}{k+1}$. Then, $g_{m,0} \in \mathbb{R}_{\geq 0}$ while $g_{0,n}$ is on the line $z = re^{\sqrt{-1}\frac{k\pi}{k+1}}$ for $r \in \mathbb{R}_{\geq 0}$. Hence, $F_{m,0}$ and $F_{0,n}$ are on planes meeting at an angle $\frac{\pi}{k+1}$. Reflecting the surface iteratively with respect to these planes give us the discrete isothermic analogue of higher order Enneper surfaces, and by considering its conjugate via Fact 4.13, we obtain a discrete asymptotic net with line symmetries (see Figure 4.2).

Example 4.23. Planar Enneper surfaces (see, for example [64]) are examples of minimal surfaces with planar ends. In particular, the planar Enneper surface with 2-fold symmetry is given by the Weierstrass data $g(z) = z^3$ and $f(z) = \frac{1}{g_z(z)}$; hence, z is an isothermic coordinate.

The discrete power function z^3 following [2, 6, 58] becomes immersed on the domain $D := \{(m, n) \in \mathbb{Z}^2 : m \geq 0, n \geq 0\} \setminus \{(0, 0)\}$, and $g_{m,0} \in \mathbb{R}$ while $g_{0,n}$ is on the line $z = -r\sqrt{-1}$ for $r \in \mathbb{R}_{>0}$. Therefore, $F_{m,0}$ and $F_{0,n}$ are on planes meeting at an angle $\frac{\pi}{2}$, and the resulting surface has 2-fold symmetry, and by considering its conjugate via Fact 4.13, we

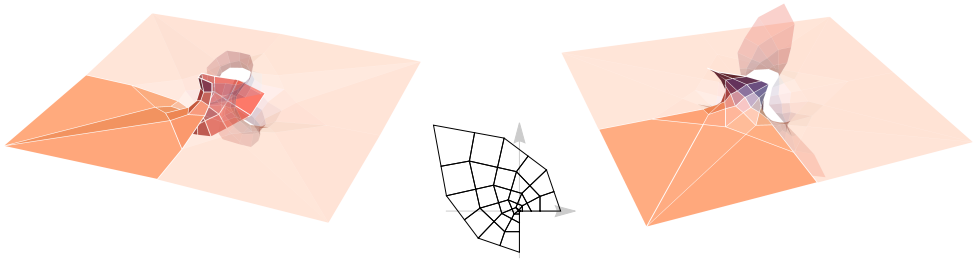

Figure 4.3: Discrete planar Enneper surface with 2-fold symmetry from discrete power function z^3 and its conjugate. The left-hand side is a discrete isothermic minimal net having planar symmetry; the right-hand side is a discrete asymptotic minimal net having line symmetry.

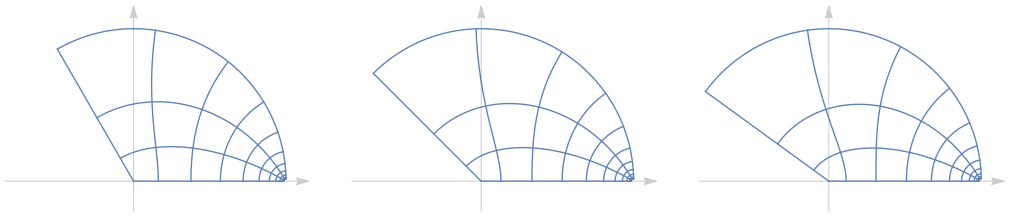

Figure 4.4: Images of smooth $g(w)$ giving fundamental pieces of the minimal k-noids, drawn for $k = 3, 4, 5$.

obtain an example of a discrete asymptotic net with line symmetries (see Figure 4.3).

Example 4.24. The minimal k-noids (for $k \in \mathbb{N}$, $k \geq 3$) of Jorge-Meeks in [63] are minimal surfaces that are topologically equivalent to the sphere minus k disks with k catenoidal ends, given by the Weierstrass data $g(z) = z^{k-1}$ and $f(z) = \frac{1}{(z^k-1)^2}$. Changing coordinates as in (4.2) (and applying a suitable homothety on the domain depending on k), we obtain new Weierstrass data $g(w) = (\tanh w)^{\frac{2k-2}{k}}$ with isothermic coordinate w. Under such settings, a fundamental piece of the minimal k-noid can be drawn over the region $w \in [0, \infty] \times \left[0, \frac{\pi}{4}\right] \subset \mathbb{R}^2 \cong \mathbb{C}$ over which $g(w)$ has values

$$g(w) \in D_k := \left\{ z = re^{\sqrt{-1}\theta} : 0 \leq r \leq 1, 0 \leq \theta \leq \tfrac{(k-1)\pi}{k} \right\} \setminus \{1\}.$$

In fact, as also demonstrated in Figure 4.4,

$$g(w) = \begin{cases} r(w), & \text{if } w \in [0, \infty] \times \{0\} \\ r(w)e^{\sqrt{-1}\frac{(k-1)\pi}{k}}, & \text{if } w \in \{0\} \times \left[0, \frac{\pi}{4}\right] \\ e^{\sqrt{-1}\theta(w)}, & \text{if } w \in [0, \infty] \times \{\frac{\pi}{4}\}. \end{cases}$$

To discretize g (numerically) over the domain $\{(m, n) \in \mathbb{Z}^2 : m \geq 0, 0 \leq n \leq n_{\max}\}$, we require that

- $g_{0,0} = 0$ and $g_{0,n_{\max}} = e^{\sqrt{-1}\frac{(k-1)\pi}{k}}$,
- $g_{m,0} \in [0, 1)$ is a strictly increasing sequence,

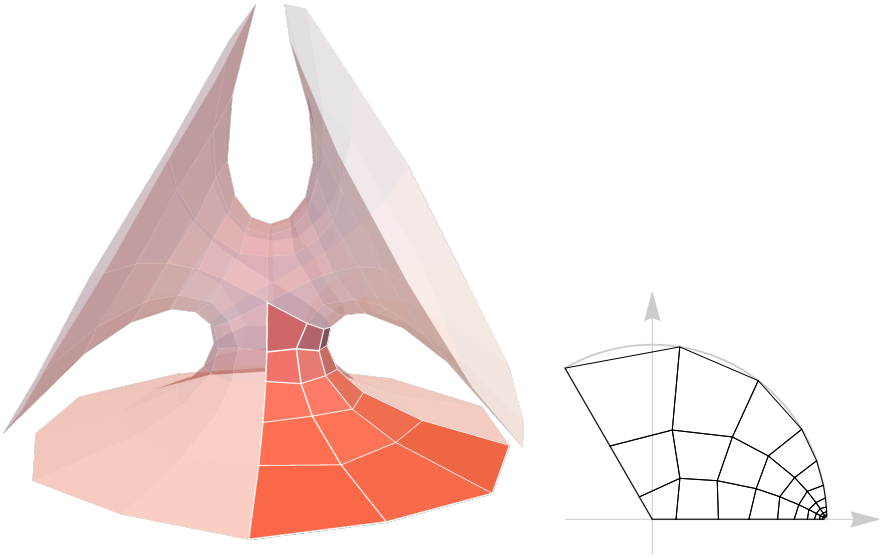

Figure 4.5: Numerical solution of discrete trinoid ($k = 3$) given with its discrete holomorphic function satisfying the boundary conditions (with $n_{\max} = 3$).

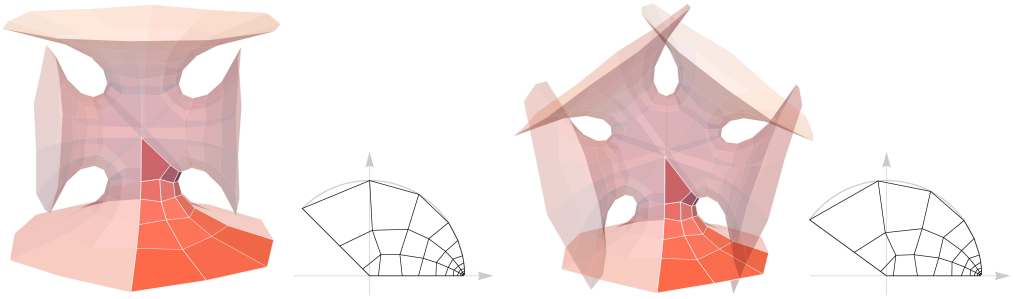

Figure 4.6: Numerical solutions of discrete 4-noid and 5-noid given with their discrete holomorphic functions satisfying the boundary conditions (with $n_{\max} = 3$).

- $g_{0,n} = r_n e^{\sqrt{-1}\frac{(k-1)\pi}{k}}$ where $r_n \in [0, 1]$ is a strictly increasing finite sequence,
- $g_{m,n_{\max}} = e^{\sqrt{-1}\theta_m}$ where $\theta_m \in \left(0, \frac{(k-1)\pi}{k}\right]$ is a strictly decreasing sequence,
- the cross ratio of g over any elementary quadrilateral is equal to -1, and
- $g_{m,n} \in D_k$ for all (m, n) in the domain.

By the definition of g, we know that

- the planes containing $F_{m,0}$ and $F_{0,n}$ meet at an angle $\frac{\pi}{k}$, and
- the planes containing $F_{n,0}$ and $F_{m,n_{\max}}$ meet at an angle $\frac{\pi}{2}$,

giving us a discrete analogue of minimal k-noids of Jorge-Meeks (see Figures 4.5 and 4.6).

Example 4.25. By expanding on the idea of using the symmetry of k-noids as boundary conditions for the holomorphic data, we can create other discrete minimal nets with symmetries. In this example, we create discrete minimal nets with symmetry groups of the Platonic

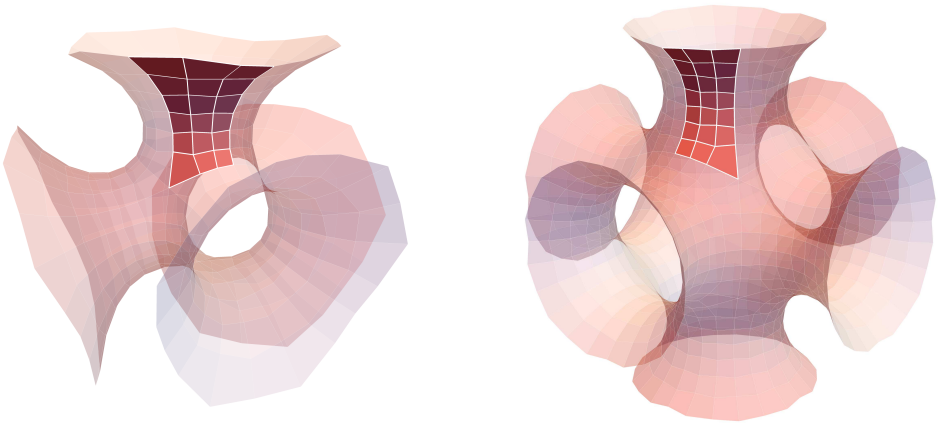

Figure 4.7: Numerical solutions of discrete minimal nets with tetrahedral symmetry on the left, and octahedral symmetry on the right.

solids [119]. As in the k-noids examples, we can ascertain the boundary conditions from the symmetries of the discrete minimal net by calculating the angles at which the great circles meet (see, for example, [10]). Then, by finding discrete holomorphic functions satisfying the given boundary conditions, we can obtain discrete minimal nets with symmetry groups of the Platonic solids. Here, we show two numerical examples of discrete minimal nets with such symmetries in Figure 4.7.

Remark 4.26. One may notice that while most of the vertices on the examples have degree 4, i.e. 4 edges meet at the vertex, there are vertices with degree higher than 4. While this may indicate the existence of a branch point on the Gauss map, we have avoided this issue by assigning these vertices to be one of the "corner" points of the fundamental piece, and treating the Gauss map as coming from a holomorphic function on a simply-connected domain in the complex plane. In fact, on these vertices, the definition of discrete minimality as in [17, Definition 7] might not be directly applicable; however, the definition via Steiner's formula (as in Definition 4.5 and Definition 4.6) allows us to consider mean curvatures on the faces around such points, and determine minimality at these points as well.

Chapter 5

Spheres in Lorentz-Möbius geometry

In this chapter, we introduce the basics of Lorentz-Möbius geometry, analogous to Möbius geometry for 3-dimensional Riemannian spaceforms. The specific theory of Lorentz-Möbius geometry has been explored in [37, 38, 107, 113], where the spacelike surface and timelike surface cases have been discussed separately. However, the work [24] suggests that one can view isothermic surface theory in Lorentz-Möbius geometry uniformly regardless of the signature of the metric induced on a surface. Lorentz-Möbius geometry is an especially good candidate for this, not only because it is an example of a symmetric R-space, but also because one can treat both spacelike surfaces and timelike surfaces in this setting. This chapter gives the preparatory materials to achieve this, and shows how both spacelike surfaces and timelike surfaces can be treated as maps into the projective lightcone of 5-dimensional pseudo-Riemannian space with signature $(-++++-)$. Most of the content in this chapter is a Lorentzian analogue of the work done in excellent works such as [26, 52, 100], and the arguments are modeled after [27, 96].

5.1 Pentaspherical coordinates for Lorentzian spaceforms

In this chapter, let $\mathbb{R}^{3,2}$ denote the 5-dimensional pseudo-Riemannian space with signature $(-++++-)$ and inner product $\langle\!\langle \cdot, \cdot \rangle\!\rangle$, i.e. for $X, Y \in \mathbb{R}^{3,2}$,

$$(X, Y) = \left\langle\!\!\left\langle (x_0, x_1, x_2, x_3, x_4)^t, (y_0, y_1, y_2, y_3, y_4)^t \right\rangle\!\!\right\rangle = -x_0y_0 + x_1y_1 + x_2y_2 + x_3y_3 - x_4y_4,$$

and let $\mathcal{L}$ denote the lightcone of $\mathbb{R}^{3,2}$, i.e.

$$\mathcal{L} = \{X \in \mathbb{R}^{3,2} : \langle\!\langle x, x \rangle\!\rangle = 0\}.$$

For some $\mathfrak{q}_\kappa \in \mathcal{L}$, such that $\langle\!\langle \mathfrak{q}_\kappa, \mathfrak{q}_\kappa \rangle\!\rangle = -\kappa$, define

$$M_\kappa = \{X \in \mathbb{L} : \langle\!\langle x, \mathfrak{q}_\kappa \rangle\!\rangle = -1\}.$$

Applying a suitable transformation $A \in \mathrm{SO}(3,2)$, we may assume without loss of generality that

$$\mathfrak{q}_\kappa = \left(0, 0, 0, \frac{1}{2}(\kappa - 1), \frac{1}{2}(\kappa + 1)\right)^t. \tag{5.1}$$

Denoting $\mathcal{R} = \mathbb{R}^{2,1} \cup \{\infty\}$, and for $x, y \in \mathbb{R}^{2,1}$, setting

$$x \cdot y = (x_0, x_1, x_2) \cdot (y_0, y_1, y_2) = -x_0 y_0 + x_1 y_1 + x_2 y_2,$$

we have the following lemma.

Lemma 5.1. *The map $\psi : \mathcal{R} \to M_\kappa$ defined by*

$$\psi(x) = \frac{1}{1 + \kappa(x \cdot x)} \begin{pmatrix} 2x^t \\ 1 - x \cdot x \\ 1 + x \cdot x \end{pmatrix}$$

is a bijection for any choice of κ.

Proof. To see that $\psi(x) \in M_\kappa$, we note that for $x \in \mathbb{R}^{2,1}$,

$$\begin{aligned} \langle\!\langle \psi(x), \psi(x) \rangle\!\rangle &= \left(\frac{1}{1 + \kappa(x \cdot x)}\right)^2 \left(4x \cdot x + (1 - x \cdot x)^2 - (1 + x \cdot x)^2\right) \\ &= \left(\frac{1}{1 + \kappa(x \cdot x)}\right)^2 \left(4x \cdot x + 1 - 2x \cdot x + x \cdot x^2 - 1 - 2x \cdot x - x \cdot x^2\right) \\ &= 0, \end{aligned}$$

while

$$\begin{aligned} \langle\!\langle \psi(x), \mathfrak{q}_\kappa \rangle\!\rangle &= \frac{1}{2}(\kappa - 1)(1 - x \cdot x) - \frac{1}{2}(\kappa + 1)(1 + x \cdot x) \\ &= \frac{1}{2(1 + \kappa(x \cdot x))}(\kappa - \kappa(x \cdot x) - 1 + x \cdot x - \kappa - \kappa(x \cdot x) - 1 - x \cdot x) \\ &= \frac{1}{1 + \kappa(x \cdot x)}(-\kappa(x \cdot x) - 1) \\ &= -1. \end{aligned}$$

Note that for $x = \infty$, we can take the appropriate limit to see that

$$\psi(\infty) = \begin{pmatrix} 0 \\ -\frac{1}{\kappa} \\ \frac{1}{\kappa} \end{pmatrix},$$

and hence $\psi(\infty) \in M_\kappa$.

To see that ψ is a bijection, we define $\phi : M_\kappa \to \mathcal{R}$ by

$$\phi(X) = \phi((y^t, y_3, y_4)^t) = \frac{y}{y_4 + y_3},$$

where $y = (y_0, y_1, y_2)$. Since $\langle\langle X, X \rangle\rangle = 0$, we have

$$y \cdot y = y_4^2 - y_3^2,$$

while since $\langle\langle X, \mathfrak{q}_\kappa \rangle\rangle = -1$,

$$y_3 + y_4 + \kappa(y_4 - y_3) = 2.$$

Using these relations, we calculate that

$$\begin{aligned}
\psi \circ \phi(X) &= \psi\left(\frac{y}{y_4 + y_3}\right) \\
&= \frac{1}{1 + \kappa\left(\frac{y}{y_4+y_3} \cdot \frac{y}{y_4+y_3}\right)} \begin{pmatrix} 2\frac{y^t}{y_4+y_3} \\ 1 - \left(\frac{y}{y_4+y_3} \cdot \frac{y}{y_4+y_3}\right) \\ 1 + \left(\frac{y}{y_4+y_3} \cdot \frac{y}{y_4+y_3}\right) \end{pmatrix} \\
&= \frac{(y_4+y_3)^2}{(y_4+y_3)^2 + \kappa(y \cdot y)} \begin{pmatrix} 2\frac{y^t}{y_4+y_3} \\ \frac{(y_4+y_3)^2 - y \cdot y}{(y_4+y_3)^2} \\ \frac{(y_4+y_3)^2 + y \cdot y}{(y_4+y_3)^2} \end{pmatrix} \\
&= \frac{1}{(y_4+y_3)^2 + \kappa(y \cdot y)} \begin{pmatrix} 2(y_4+y_3)y^t \\ (y_4+y_3)^2 - y \cdot y \\ (y_4+y_3)^2 + y \cdot y \end{pmatrix} \\
&= \frac{1}{(y_4+y_3)(y_4+y_3+\kappa(y_4-y_3))} \begin{pmatrix} 2(y_4+y_3)y^t \\ (y_4+y_3)(y_4+y_3-(y_4-y_3)) \\ (y_4+y_3)(y_4+y_3+(y_4-y_3)) \end{pmatrix} \\
&= \frac{1}{2}\begin{pmatrix} 2y^t \\ 2y_3 \\ 2y_4 \end{pmatrix} = \begin{pmatrix} y^t \\ y_3 \\ y_4 \end{pmatrix} = X.
\end{aligned}$$

On the other hand,

$$\begin{aligned}
\phi \circ \psi(x) &= \phi\left(\frac{1}{1 + \kappa(x \cdot x)} \begin{pmatrix} 2x^t \\ 1 - x \cdot x \\ 1 + x \cdot x \end{pmatrix}\right) \\
&= \frac{\frac{2x}{1+\kappa(x\cdot x)}}{\frac{1-x\cdot x}{1+\kappa(x\cdot x)} + \frac{1+x\cdot x}{1+\kappa(x\cdot x)}} \\
&= \frac{2x}{2} = x.
\end{aligned}$$

Hence, $\psi^{-1} = \phi$. □

This model of M_κ gives us two observations, which we explore in the following sections.

5.1.1 3-dimensional Lorentzian spaceforms

Let $\mathbb{S}^{2,1}$ denote the de Sitter 3-space (with constant sectional curvature 1), i.e. for the Minkowski 4-space $\mathbb{R}^{3,1}$ with signature $(-+++)$ and inner product $\langle\!\langle , \rangle\!\rangle_{3,1}$,

$$\mathbb{S}^{2,1} = \{x \in \mathbb{R}^{3,1} : \langle\!\langle x, x \rangle\!\rangle_{3,1} = 1\}.$$

Writing $x = (x_0, x_1, x_2, x_3) \in \mathbb{R}^{3,1}$, we have that $x \in \mathbb{S}^{2,1}$ if and only if

$$-x_0^2 + x_1^2 + x_2^2 + x_3^2 = 1.$$

Therefore, we have that for $X = (x_0, x_1, x_2, x_3, 1)^t \in \mathbb{R}^{3,2}$,

$$\langle\!\langle X, X \rangle\!\rangle = -x_0^2 + x_1^2 + x_2^2 + x_3^2 - 1 = 0,$$

and

$$\langle\!\langle X, \mathfrak{q}_1 \rangle\!\rangle = \left\langle\!\!\left\langle (x_0, x_1, x_2, x_3, 1)^t, (0, 0, 0, 0, 1)^t \right\rangle\!\!\right\rangle = -1,$$

implying that $X \in M_1$. Therefore, there is a natural bijection between $\mathbb{S}^{2,1}$ and M_1.

On the other hand, let $\mathbb{H}^{2,1}$ be the anti-de Sitter 3-space (with constant sectional curvature -1), i.e. for a 4-dimensional pseudo-Euclidean space $\mathbb{R}^{2,2}$ with signature $(--++)$ and inner product $\langle\!\langle , \rangle\!\rangle_{2,2}$,

$$\mathbb{S}^{2,1} = \{x \in \mathbb{R}^{2,2} : \langle\!\langle x, x \rangle\!\rangle_{2,2} = -1\}.$$

Again, writing $x = (x_0, x_1, x_2, x_3) \in \mathbb{R}^{2,2}$, we have that $x \in \mathbb{H}^{2,1}$ if and only if

$$-x_0^2 + x_1^2 + x_2^2 - x_3^2 = -1.$$

Hence, for $X = (x_0, x_1, x_2, 1, x_3) \in \mathbb{R}^{3,2}$,

$$\langle\!\langle X, X \rangle\!\rangle = -x_0^2 + x_1^2 + x_2^2 + 1 - x_3^2 = 0,$$

while

$$\langle\!\langle X, \mathfrak{q}_{-1} \rangle\!\rangle = \left\langle\!\!\left\langle (x_0, x_1, x_2, 1, x_3)^t, (0, 0, 0, -1, 0)^t \right\rangle\!\!\right\rangle = -1.$$

Therefore, we now have that $X \in M_{-1}$, and similarly, we have a natural bijection between $\mathbb{H}^{2,1}$ and M_{-1}.

For the Minkowski 3-space $\mathbb{R}^{2,1}$ (with constant sectional curvature 0), choosing

$$\mathfrak{o} = (0, 0, 0, 1, 1)^t,$$

then we have a bijection between $\mathbb{R}^{2,1}$ and M_0 via

$$\psi_0(x) = 2x + \mathfrak{o} + \frac{1}{2}(2x \cdot 2x)\mathfrak{q}_0$$

and

$$\phi_0(X) = \psi_0^{-1}(X) = \frac{1}{2}\left(X - \mathfrak{o} + \langle\!\langle X, \mathfrak{o} \rangle\!\rangle\, \mathfrak{q}_0\right).$$

5.1.2 Stereographic projection

Recall that for the de Sitter 3-space $\mathbb{S}^{2,1}$, one can define the following inverse stereographic projection σ_1 from $\mathcal{R}$ via

$$\sigma_1 : \mathcal{R} \to \mathbb{S}^{2,1} \subset \mathbb{R}^{3,1},$$

where

$$\sigma_1(x) = \frac{1}{1 + x \cdot x}(2x, 1 - x \cdot x).$$

Similarly, for the anti-de Sitter 3-space $\mathbb{H}^{2,1}$, we have the inverse stereographic projection

$$\sigma_{-1} : \mathcal{R} \to \mathbb{H}^{2,1} \subset \mathbb{R}^{2,2}$$

defined by

$$\sigma_{-1}(x) = \frac{1}{1 - x \cdot x}(2x, 1 + x \cdot x).$$

Define $\phi_1 : \mathbb{R}^{3,1} \to \mathbb{R}^{3,2}$ by

$$\phi_1((x_0, x_1, x_2, x_3)) = (x_0, x_1, x_2, x_3, 1)^t,$$

and $\phi_{-1} : \mathbb{R}^{2,2} \to \mathbb{R}^{3,2}$ by

$$\phi_{-1}((x_0, x_1, x_2, x_3)) = (x_0, x_1, x_2, 1, x_3)^t.$$

Then we have $\phi_1 \circ \sigma_1 : \mathbb{R}^3 \to \mathbb{R}^{3,2}$ where

$$\phi_1 \circ \sigma_1(x) = \frac{1}{1 + x \cdot x} \begin{pmatrix} 2x^t \\ 1 - x \cdot x \\ 1 + x \cdot x \end{pmatrix},$$

while

$$\phi_{-1} \circ \sigma_{-1}(x) = \frac{1}{1 - x \cdot x} \begin{pmatrix} 2x^t \\ 1 - x \cdot x \\ 1 + x \cdot x \end{pmatrix}.$$

Now, to calculate the metric induced on M_κ, we let $X(t) : (-\epsilon, \epsilon) \to M_\kappa$ such that

$$X(t) = \psi(x(t)) = \frac{1}{1 + \kappa(x(t) \cdot x(t))} \begin{pmatrix} 2x(t)^t \\ 1 - x(t) \cdot x(t) \\ 1 + x(t) \cdot x(t) \end{pmatrix}.$$

Then we can calculate that

$$\frac{\mathrm{d}}{\mathrm{d}t} X(t) = \dot{X} = \frac{1}{(1 + \kappa(x \cdot x))^2} \begin{pmatrix} \dot{x}^t + \kappa(x \cdot x)\dot{x}^t - 2\kappa(x \cdot \dot{x})x^t \\ -(\kappa + 1)(x \cdot \dot{x}) \\ -(\kappa - 1)(x \cdot \dot{x}) \end{pmatrix}.$$

Therefore, the tangent space of M_κ at X has the form

$$T_X M_\kappa = \left\{ \mathcal{T}_a = \begin{pmatrix} a^t + \kappa(x\cdot x)a^t - 2\kappa(x\cdot a)x^t \\ -(\kappa+1)(x\cdot a) \\ -(\kappa-1)(x\cdot a) \end{pmatrix} : a \in \mathcal{R} \right\},$$

and we can calculate that

$$\langle\!\langle \mathcal{T}_a, \mathcal{T}_b \rangle\!\rangle = \frac{4}{1+\kappa(x\cdot x)}\, a\cdot b. \tag{5.2}$$

Therefore, the M_κ are the stereographic projections of Lorentzian 3-spaceforms with non-zero sectional curvature, allowing us to see the following proposition.

Proposition 5.2 (cf. [96, Lemma 2.5])**.** *M_κ has constant sectional curvature κ.*

Furthermore, all the variants of M_κ obtained for different values of κ are all conformally equivalent. Therefore, instead of viewing $\mathbb{R}^{2,1}$, $\mathbb{S}^{2,1}$, and $\mathbb{H}^{2,1}$ separately, we can projectivize the lightcone and view the Lorentzian 3-spaceforms with constant sectional curvatures uniformly.

Remark 5.3. Note that (5.2) says that when $\kappa = 0$, then the metric on M_κ is four times the usual metric in $\mathbb{R}^{2,1}$. The different metric is a result of our choice of normalization for $\mathfrak{q}_\kappa$. This does not pose a problem, as the sectional curvature of $\mathbb{R}^{2,1}$ does not change under similarity transformations.

However, to remedy this, from now on, we assume without loss of generality that $\mathfrak{q}_0 = (0,0,0,-1,1)$. Then

$$M_0 = \left\{ \begin{pmatrix} x \\ \frac{1}{2}(1-x\cdot x) \\ \frac{1}{2}(1+x\cdot x) \end{pmatrix} : x \in \mathbb{R}^{2,1} \right\}.$$

Then for $\mathfrak{o} = \frac{1}{2}(0,0,0,1,1)$,

$$\psi_0(x) = x + \mathfrak{o} + \frac{1}{2}(x\cdot x)\mathfrak{q}$$

defines a bijection between $\mathbb{R}^{2,1} \subset \mathbb{R}^{3,2}$ with inverse

$$\phi_0(X) = X - \mathfrak{o} + \langle\!\langle X, \mathfrak{o} \rangle\!\rangle\, \mathfrak{q}.$$

Note that such a particular choice of $\mathfrak{o}$ and $\mathfrak{q}_0$ allows one to see the bijection more clearly, as follows: We have that

$$\langle \mathfrak{o}, \mathfrak{q}_0 \rangle = \{X \in \mathbb{R}^{3,2} : X = (0,0,0,a,b) \text{ for some } a,b \in \mathbb{R}\},$$

and hence

$$\langle \mathfrak{o}, \mathfrak{q}_0 \rangle^\perp = \{X \in \mathbb{R}^{3,2} : X = (a,b,c,0,0) \text{ for some } a,b,c \in \mathbb{R}\}.$$

Therefore, it is easy to see that $\psi_0 : \langle \mathfrak{o}, \mathfrak{q}_0 \rangle^\perp \cong \mathbb{R}^{2,1} \to M_0$.

However, one does not need to choose $\mathfrak{o}$ and $\mathfrak{q}_0$ as given: Choosing any $\mathfrak{o}, \mathfrak{q}_0 \in \mathcal{L}$ such that $\langle\!\langle \mathfrak{o}, \mathfrak{q}_0 \rangle\!\rangle = -1$, we note that

$$\langle \mathfrak{o}, \mathfrak{q}_0 \rangle \cong \mathbb{R}^{1,1},$$

implying that

$$\langle \mathfrak{o}, \mathfrak{q}_0 \rangle^\perp \cong \mathbb{R}^{2,1}.$$

Then the ψ_0 defined as above gives a bijection between $\langle \mathfrak{o}, \mathfrak{q} \rangle^\perp \cong \mathbb{R}^{2,1}$ and M_0.

Now, for $\langle \mathfrak{q}_0 \rangle \in \mathbb{P}(\mathcal{L})$, there is no $\alpha \in \mathbb{R}$ such that $\alpha \mathfrak{q}_0 \in M_0 \cong \mathbb{R}^{2,1}$, since $\mathfrak{q}_0 \in \mathcal{L}$. (Recall that $X \in M_0$ if and only if $X \in \mathcal{L}$ and $\langle\!\langle X, \mathfrak{q}_0 \rangle\!\rangle = -1$.) This can also be seen from the fact that for $\kappa = 0$,

$$\psi(\infty) = (0, 0, 0, -1, 1)^t = \mathfrak{q}_0.$$

Hence, the choice of $\mathfrak{q}_0$ determines which point in the projective light cone $\mathbb{P}(\mathcal{L})$ corresponds to the point at infinity for $\mathbb{R}^{2,1}$. Similarly, for $\kappa = 0$, we see that

$$\psi((0, 0, 0)) = \frac{1}{2}(0, 0, 0, 1, 1) = \mathfrak{o},$$

implying that the choice of $\mathfrak{o}$ determines the point of origin for $\mathbb{R}^{2,1}$.

5.2 Spheres in Lorentzian spaceforms

So far, we have seen that the points in Lorentzian spaceforms correspond to $\mathbb{P}(\mathcal{L})$. In this section, we see how the spheres in Lorentzian spaceforms are represented in $\mathbb{R}^{3,2}$.

5.2.1 Set of spheres

Let

$$\mathcal{S} = (z, z_3, z_4)^t \in \mathbb{R}^{3,2} \setminus \{0\}$$

for some $z \in \mathbb{R}^{2,1}$, and consider

$$\tilde{\mathcal{S}} := \{Y \in M_\kappa : \langle\!\langle \mathcal{S}, Y \rangle\!\rangle = 0\}. \tag{5.3}$$

Let $Y \in \tilde{\mathcal{S}}$, and for now, assume that $\kappa = 0$, i.e. there is some $y \in \mathbb{R}^{2,1}$ such that

$$Y = \frac{1}{2}(2y, 1 - y \cdot y, 1 + y \cdot y)^t.$$

Then we have that

$$\begin{aligned} 0 = 2\langle\!\langle \mathcal{S}, Y \rangle\!\rangle &= \langle\!\langle (z, z_3, z_4)^t, (2y, 1 - y \cdot y, 1 + y \cdot y)^t \rangle\!\rangle \\ &= 2y \cdot z + z_3(1 - y \cdot y) - z_4(1 + y \cdot y) \\ &= 2y \cdot z - y \cdot y(z_3 + z_4) + z_3 - z_4. \end{aligned}$$

Dividing both sides by $z_3 + z_4$ and rearranging the terms gives

$$y \cdot y - \frac{2y \cdot z}{z_3 + z_4} + \frac{z \cdot z}{(z_3 + z_4)^2} = \frac{z \cdot z + z_3^2 - z_4^2}{(z_3 + z_4)^2},$$

or

$$\left(y - \frac{z}{z_3 + z_4}\right) \cdot \left(y - \frac{z}{z_3 + z_4}\right) = \frac{\langle\!\langle \mathcal{S}, \mathcal{S} \rangle\!\rangle}{(z_3 + z_4)^2}.$$

Therefore, $\tilde{\mathcal{S}}$ is the set of points on the sphere in $\mathbb{R}^{2,1}$ with center c and radius r, where

$$c = \frac{z}{z_3 + z_4} \quad \text{and} \quad r = \frac{\sqrt{\langle\!\langle \mathcal{S}, \mathcal{S} \rangle\!\rangle}}{z_3 + z_4} \in \mathbb{R} \cup i\mathbb{R}. \tag{5.4}$$

Since we have seen that the different M_κ are all conformally equivalent, which preserves spheres, we see that the $\tilde{\mathcal{S}}$ are the spheres in 3-dimensional Lorentzian spaceforms.

Now note that

$$\frac{1}{2}(1 - c \cdot c + r^2) = \frac{1}{2}\left(1 - \frac{z \cdot z}{(z_3 + z_4)^2} + \frac{z \cdot z + z_3^2 - z_4^2}{(z_3 + z_4)^2}\right) = \frac{z_3}{z_3 + z_4},$$

while

$$\frac{1}{2}(1 + c \cdot c - r^2) = \frac{1}{2}\left(1 + \frac{z \cdot z}{(z_3 + z_4)^2} - \frac{z \cdot z + z_3^2 - z_4^2}{(z_3 + z_4)^2}\right) = \frac{z_4}{z_3 + z_4}.$$

Since $\mathcal{S}$ has a scaling freedom, we may write

$$\mathcal{S} = \begin{pmatrix} z^t \\ z_3 \\ z_4 \end{pmatrix} = \begin{pmatrix} c^t \\ \frac{1}{2}(1 - c \cdot c + r^2) \\ \frac{1}{2}(1 + c \cdot c - r^2) \end{pmatrix}, \tag{5.5}$$

and identify the set of such $\mathcal{S}$ as the set of spheres.

5.2.2 Types of spheres

Note that in (5.4), the radius is $r \in \mathbb{R} \cup i\mathbb{R}$. When $r \in \mathbb{R}$ (resp. $r \in i\mathbb{R}$), then for a point y on the sphere, we have

$$(y - c) \cdot (y - c) = \alpha^2 \quad (\text{resp. } (y - c) \cdot (y - c) = -\alpha^2)$$

for some $c \in \mathbb{R}^{2,1}$ and $\alpha \in \mathbb{R}$. However, since

$$r^2 = \frac{\langle\!\langle \mathcal{S}, \mathcal{S} \rangle\!\rangle}{(z_3 + z_4)^2},$$

one can deduce that the causality of $\mathcal{S}$ determines the type of spheres we obtain, as follows:

- if $\mathcal{S}$ is timelike ($\langle\!\langle \mathcal{S}, \mathcal{S} \rangle\!\rangle < 0$), then $\tilde{\mathcal{S}}$ is a spacelike sphere,
- if $\mathcal{S}$ is spacelike ($\langle\!\langle \mathcal{S}, \mathcal{S} \rangle\!\rangle > 0$), then $\tilde{\mathcal{S}}$ is a timelike sphere, and
- if $\mathcal{S}$ is lightlike ($\langle\!\langle \mathcal{S}, \mathcal{S} \rangle\!\rangle = 0$), then $\tilde{\mathcal{S}}$ is a lightlike sphere.

To see this more precisely, consider the curve $Y(t)$ on the sphere defined by $\mathcal{S}$, i.e.

$$Y(t) : (-\epsilon, \epsilon) \to \tilde{\mathcal{S}}.$$

Since we have $\langle\!\langle Y, Y \rangle\!\rangle = 0$, we have that $\left\langle\!\left\langle \dot{Y}, Y \right\rangle\!\right\rangle = 0$, and hence

$$\dot{Y}/Y \in \langle Y \rangle^{\perp}/\langle Y \rangle \cong \mathbb{R}^{2,1}.$$

However, from the fact that $Y \in \tilde{\mathcal{S}}$, we also have that $\langle\!\langle Y, \mathcal{S} \rangle\!\rangle = 0$, implying that $\left\langle\!\left\langle \dot{Y}, \mathcal{S} \right\rangle\!\right\rangle = 0$. Therefore,

$$\dot{Y}/Y \in \langle Y, \mathcal{S} \rangle^{\perp}/\langle Y \rangle.$$

Finally, $\langle\!\langle Y, S \rangle\!\rangle = 0$ implies that

- if $\mathcal{S}$ is timelike, then $\dot{Y}/Y \in \langle Y, \mathcal{S} \rangle^{\perp}/\langle Y \rangle \cong \mathbb{R}^2$,
- if $\mathcal{S}$ is spacelike, then $\dot{Y}/Y \in \langle Y, \mathcal{S} \rangle^{\perp}/\langle Y \rangle \cong \mathbb{R}^{1,1}$, and
- if $\mathcal{S}$ is lightike, then $\dot{Y}/Y \in \langle Y, \mathcal{S} \rangle^{\perp}/\langle Y \rangle \cong \mathbb{R}^{1,0}$.

In summary, we have the following proposition:

Proposition 5.4. *Let $\mathcal{S} \in \mathbb{R}^{3,2}$ be a non-zero vector, and let $\tilde{\mathcal{S}}$ be the sphere determined by $\mathcal{S}$ via* (5.3)*. Then the causality of $\mathcal{S}$ determines the type of metric induced on the sphere $\tilde{\mathcal{S}}$. Precisely,*

- *if $\mathcal{S}$ is timelike, then $\tilde{\mathcal{S}}$ is a spacelike sphere,*
- *if $\mathcal{S}$ is spacelike, then $\tilde{\mathcal{S}}$ is a timelike sphere, and*
- *if $\mathcal{S}$ is lightlike, then $\tilde{\mathcal{S}}$ is a lightlike sphere.*

5.2.3 Planes in Minkowski 3-space in Lorentz-Möbius geometry

One way of viewing planes is to consider them as spheres of infinite radius. To do this, let $\mathcal{S} \in \mathbb{R}^{3,2}$ determine a sphere with center $c = p + \rho n$ and non-zero radius r, where $\rho \in \mathbb{R}$ such that $r^2 = \sigma\rho^2$ for an appropriate choice of $\sigma \in \{\pm 1\}$. Therefore, the point $p \in \mathbb{R}^{2,1}$ is on the sphere, and n is the vector (of squared norm ± 1) pointing from p towards the center c, i.e. n is perpendicular to the tangent plane of the sphere at p. Under this setting, Proposition 5.4 tells us that $n \cdot n = \sigma$. Remembering that $\mathcal{S}$ can have a freedom of scaling factor, we write $\mathcal{S}$ as

$$\mathcal{S} = \frac{1}{2\rho} \begin{pmatrix} 2(p+\rho n)^t \\ 1 - (p+\rho n) \cdot (p+\rho n) + \sigma\rho^2 \\ 1 + (p+\rho n) \cdot (p+\rho n) - \sigma\rho^2 \end{pmatrix}.$$

Then,

$$\begin{aligned}\lim_{\rho\to\infty}\mathcal{S} &= \lim_{\rho\to\infty}\frac{1}{2\rho}\begin{pmatrix} 2(p+\rho n)^t \\ 1-p\cdot p-2\rho p\cdot n-\rho^2 n\cdot n+\sigma\rho^2 \\ 1+p\cdot p+2\rho p\cdot n+\rho^2 n\cdot n-\sigma\rho^2\end{pmatrix} \\ &= \lim_{\rho\to\infty}\frac{1}{2\rho}\begin{pmatrix} 2(p+\rho n)^t \\ 1-p\cdot p-2\rho p\cdot n \\ 1+p\cdot p+2\rho p\cdot n\end{pmatrix} \\ &= \begin{pmatrix} n^t \\ -p\cdot n \\ p\cdot n\end{pmatrix} := \mathcal{P}_{p,n}.\end{aligned}$$

Therefore, $\mathcal{P}_{p,n}$ determines a plane through the point p with normal n in Minkowski 3-space.

Another way to consider planes comes from the observation that planes are a notion that is unique to 3-dimensional Lorentzian spaceform with vanishing sectional curvature. Therefore, by choosing a point at infinity $\mathfrak{q}_0$ of M_0, one can view planes as spheres containing the point at infinity. Let $\mathcal{S}$ determine a sphere $\tilde{\mathcal{S}}$ for which $\mathfrak{q}_0 \in \tilde{\mathcal{S}}$, telling us that

$$0 = \langle\!\langle \mathcal{S}, \mathfrak{q}_0 \rangle\!\rangle = \left\langle\!\!\left\langle (n, n_3, n_4)^t, \left(0, 0, 0, -\tfrac{1}{2}, \tfrac{1}{2}\right) \right\rangle\!\!\right\rangle = -\tfrac{1}{2}n_3 - \tfrac{1}{2}n_4,$$

so we have $n_3 = n_4$. Then $Y \in \tilde{\mathcal{S}}$ if and only if

$$0 = \langle\!\langle \mathcal{S}, Y \rangle\!\rangle = \left\langle\!\!\left\langle (n, n_3, n_4)^t, (p, \tfrac{1}{2}(1-p\cdot p), \tfrac{1}{2}(1+p\cdot p))^t \right\rangle\!\!\right\rangle = n\cdot p - n_3.$$

Hence, $\tilde{\mathcal{S}}$ is a plane through the point p with normal n, and we can write

$$\mathcal{S} = (n, -n\cdot p, n\cdot p)^t = \mathcal{P}_{p,n}.$$

Finally, since

$$\left\langle\!\!\left\langle \mathcal{P}_{p,n}, \mathcal{P}_{p,n} \right\rangle\!\!\right\rangle = n\cdot n,$$

we see that Proposition 5.4 still applies to planes; that is, the causality of $\mathcal{P}_{p,n}$ determines the type of metric induced on the plane.

Since the type of metric induced on the tangent plane of a surface x depends on the causality of the Gauss map n, it is natural to consider the causality of $\mathcal{P}_{x,n}$ at each point. Let $x(u,v)$ be a surface in some 3-dimensional Lorentzian spaceform with constant sectional curvature κ. Then one can lift $x(u,v)$ into $X(u,v) \in M_\kappa$, i.e.

$$X = \psi(x) = \frac{1}{1+\kappa(x\cdot x)}\begin{pmatrix} 2x^t \\ 1-x\cdot x \\ 1+x\cdot x\end{pmatrix}.$$

Then (5.2) implies that

$$\langle\!\langle \mathrm{d}X, \mathrm{d}X \rangle\!\rangle = \langle\!\langle \mathcal{T}_{\mathrm{d}x}, \mathcal{T}_{\mathrm{d}x} \rangle\!\rangle = \frac{4}{1 + \kappa(x \cdot x)} \, \mathrm{d}x \cdot \mathrm{d}x,$$

telling us that the metric induced on X is conformally equivalent to the metric induced on x in the spaceform.

Bibliography

[1] U. Abresch. Constant mean curvature tori in terms of elliptic functions. *J. Reine Angew. Math.* **374**: 169–192, 1987. DOI: 10.1515/crll.1987.374.169.

[2] S. I. Agafonov and A. I. Bobenko. Discrete Z^γ and Painlevé equations. *Internat. Math. Res. Notices* **2000**(4): 165–193, 2000. DOI: 10.1155/S1073792800000118.

[3] S. Akamine. Behavior of the Gaussian curvature of timelike minimal surfaces with singularities. *Hokkaido Math. J.* to appear. arXiv: 1701.00238.

[4] S. Akamine, J. Cho, and Y. Ogata. Analysis of timelike Thomsen surfaces. *J. Geom. Anal.* To appear. DOI: 10.1007/s12220-019-00166-7.

[5] S. Akamine, J. Cho, and Y. Ogata. Analysis of timelike Thomsen surfaces–with deformations and singularities, preprint. arXiv: 1808.09641.

[6] H. Ando, M. Hay, K. Kajiwara, and T. Masuda. An explicit formula for the discrete power function associated with circle patterns of Schramm type. *Funkcial. Ekvac.* **57**(1): 1–41, 2014. DOI: 10.1619/fesi.57.1.

[7] V. I. Arnol'd. *Singularities of caustics and wave fronts.* Vol. 62. Mathematics and its Applications (Soviet Series). Dordrecht: Kluwer Academic Publishers Group, 1990. DOI: 10.1007/978-94-011-3330-2.

[8] V. I. Arnol'd, S. M. Guseĭn-Zade, and A. N. Varchenko. *Singularities of differentiable maps. Vol. I.* Vol. 82. Monographs in Mathematics. Boston, MA: Birkhäuser Boston, Inc., 1985. DOI: 10.1007/978-1-4612-5154-5.

[9] W. Barthel, R. Volkmer, and I. Haubitz. Thomsensche Minimalflächen–analytisch und anschaulich. German. *Resultate Math.* **3**(2): 129–154, 1980. DOI: 10.1007/BF03323354.

[10] J. Berglund and W. Rossman. Minimal surfaces with catenoid ends. *Pacific J. Math.* **171**(2): 353–371, 1995. DOI: 10.2140/pjm.1995.171.353.

[11] L. Bianchi. *Lezioni di Geometria Differenziale, Volume II.* Italian. Seconda edizione. Pisa: Enrico Spoerri, 1903.

[12] W. Blaschke. *Vorlesungen über Differentialgeometrie und geometrische Grundlagen von Einsteins Relativitätstheorie II: Affine Differentialgeometrie.* German. Berlin: Springer, 1923.

[13] A. I. Bobenko. Integrable surfaces. *Funktsional. Anal. i Prilozhen.* **24**(3): 68–69, 1990. DOI: 10.1007/BF01077966.

[14] A. I. Bobenko. Surfaces of constant mean curvature and integrable equations. *Russian Math. Surveys* **46**(4): 1–45, 1991. DOI: 10.1070/RM1991v046n04ABEH002826.

[15] A. I. Bobenko, U. Bücking, and S. Sechelmann. Discrete minimal surfaces of Koebe type. In: *Modern approaches to discrete curvature*. L. Najman and P. Romon (Eds.). Vol. 2184. Lecture Notes in Math. Cham: Springer, 2017, 259–291. DOI: 10.1007/978-3-319-58002-9_8.

[16] A. I. Bobenko and U. Eitner. *Painlevé equations in the differential geometry of surfaces*. Vol. 1753. Lecture Notes in Math. Berlin: Springer-Verlag, 2000. DOI: 10.1007/b76883.

[17] A. I. Bobenko and U. Pinkall. Discrete isothermic surfaces. *J. Reine Angew. Math.* **475**: 187–208, 1996. DOI: 10.1515/crll.1996.475.187.

[18] A. I. Bobenko, H. Pottmann, and J. Wallner. A curvature theory for discrete surfaces based on mesh parallelity. *Math. Ann.* **348**(1): 1–24, 2010. DOI: 10.1007/s00208-009-0467-9.

[19] A. I. Bobenko and Y. B. Suris. *Discrete differential geometry*. Graduate Studies in Mathematics 98. Providence, RI: American Mathematical Society, 2008.

[20] O. Bonnet. Observations sur les surfaces minima. French. *C. R. Acad. Sci. Paris* **41**: 1057–1058, 1855.

[21] W. B. Bonnor. Null curves in a Minkowski space-time. *Tensor (N.S.)* **20**: 229–242, 1969.

[22] U. Bücking. Approximation of conformal mappings by circle patterns and discrete minimal surfaces. Ph.D. Thesis. Technische Universität Berlin, 2007.

[23] U. Bücking. Minimal surfaces from circle patterns: boundary value problems, examples. In: *Discrete differential geometry*. A. I. Bobenko, P. Schröder, J. M. Sullivan, and G. M. Ziegler (Eds.). Vol. 38. Oberwolfach Semin. Basel: Birkhäuser, 2008, 37–56. DOI: 10.1007/978-3-7643-8621-4_2.

[24] F. E. Burstall, N. M. Donaldson, F. Pedit, and U. Pinkall. Isothermic submanifolds of symmetric R-spaces. *J. Reine Angew. Math.* **660**: 191–243, 2011. DOI: 10.1515/crelle.2011.075.

[25] F. E. Burstall, U. Hertrich-Jeromin, and W. Rossman. Discrete linear Weingarten surfaces. *Nagoya Math. J.* **231**: 55–88, 2018. DOI: 10.1017/nmj.2017.11.

[26] F. E. Burstall and S. D. Santos. Special isothermic surfaces of type d. *J. Lond. Math. Soc. (2)* **85**(2): 571–591, 2012. DOI: 10.1112/jlms/jdr050.

[27] J. Cho, K. Naokawa, Y. Ogata, M. Pember, W. Rossman, and M. Yasumoto. *Discretization of isothermic surfaces in Lie sphere geometry*. submitted.

[28] J. Cho and Y. Ogata. Deformation and singularities of maximal surfaces with planar curvature lines. *Beitr. Algebra Geom.* **59**(3): 465–489, 2018. DOI: 10.1007/s13366-018-0399-1.

[29] J. Cho and Y. Ogata. Deformation of minimal surfaces with planar curvature lines. *J. Geom.* **108**(2): 463–479, 2017. DOI: 10.1007/s00022-016-0352-0.

[30] E. B. Christoffel. Ueber einige allgemeine Eigenschaften der Minimumsflächen. *J. Reine Angew. Math.* **67**: 218–228, 1867. DOI: 10.1515/crll.1867.67.218.

[31] J. N. Clelland. Totally quasi-umbilic timelike surfaces in $\mathbb{R}^{1,2}$. *Asian J. Math.* **16**(2): 189–208, 2012. DOI: 10.4310/AJM.2012.v16.n2.a2.

[32] C. J. Costa. Example of a complete minimal immersion in $\mathbf{R^3}$ of genus one and three embedded ends. *Bol. Soc. Brasil. Mat.* **15**(1-2): 47–54, 1984. DOI: 10.1007/BF02584707.

[33] G. Darboux. *Leçons sur la théorie générale des surfaces et les applications géométriques du calcul infinitéstimal, Première partie.* Paris: Gauthier-Villars, 1887.

[34] H. Dobriner. Die flächen constanter krümmung mit einem system sphärischer krümmungslinien dargestellt mit hilfe von thetafunctionen zweier variabeln. *Acta Math.* **9**(1): 73–104, 1887. DOI: 10.1007/BF02406731.

[35] H. Dobriner. Die Minimalflächen mit einem System sphärischer Krümmungslinien. *Acta Math.* **10**(1): 145–152, 1887. DOI: 10.1007/BF02393699.

[36] A. Doliwa, P. M. Santini, and M. Mañas. Transformations of quadrilateral lattices. *J. Math. Phys.* **41**(2): 944–990, 2000. DOI: 10.1063/1.533175.

[37] M. P. Dussan and M. A. Magid. Time-like isothermic surfaces associated to Grassmannian systems. *Doc. Math.* **10**: 527–549, 2005.

[38] M. P. Dussan. Space-like isothermic surfaces and Grassmannian systems. *Tsukuba J. Math.* **30**(1): 81–102, 2006. DOI: 10.21099/tkbjm/1496165030.

[39] L. P. Eisenhart. *A treatise on the differential geometry of curves and surfaces.* Boston: Ginn and Company, 1909.

[40] N. Ejiri, S. Fujimori, and T. Shoda. A remark on limits of triply periodic minimal surfaces of genus 3. *Topology Appl.* **196**(part B): 880–903, 2015. DOI: 10.1016/j.topol.2015.05.014.

[41] A. Enneper. Analytisch-geometrische Untersuchungen. *Z. Math. Phys.* **9**: 96–125, 1864.

[42] A. Enneper. Untersuchungen über die Flächen mit planen und sphärischen Krümmungslinien. German. *Abh. Königl. Ges. Wissensch. Göttingen* **23**: 1–96, 1878.

[43] I. Fernández, F. J. López, and R. Souam. The space of complete embedded maximal surfaces with isolated singularities in the 3-dimensional Lorentz-Minkowski space. *Math. Ann.* **332**(3): 605–643, 2005. DOI: 10.1007/s00208-005-0642-6.

[44] A. Ferrández, A. Giménez, and P. Lucas. Null helices in Lorentzian space forms. *Internat. J. Modern Phys. A* **16**(30): 4845–4863, 2001. DOI: 10.1142/S0217751X01005821.

[45] S. Fujimori, Y. W. Kim, S.-E. Koh, W. Rossman, H. Shin, H. Takahashi, M. Umehara, K. Yamada, and S.-D. Yang. Zero mean curvature surfaces in $\mathbf{L^3}$ containing a light-like line. *C. R. Math. Acad. Sci. Paris* **350**(21-22): 975–978, 2012. DOI: 10.1016/j.crma.2012.10.024.

[46] S. Fujimori, Y. W. Kim, S.-E. Koh, W. Rossman, H. Shin, M. Umehara, K. Yamada, and S.-D. Yang. Zero mean curvature surfaces in Lorentz-Minkowski 3-space and 2-dimensional fluid mechanics. *Math. J. Okayama Univ.* **57**: 173–200, 2015.

[47] S. Fujimori, K. Saji, M. Umehara, and K. Yamada. Singularities of maximal surfaces. *Math. Z.* **259**(4): 827–848, 2008. DOI: 10.1007/s00209-007-0250-0.

[48] A. Fujioka and J. Inoguchi. Timelike Bonnet surfaces in Lorentzian space forms. *Differential Geom. Appl.* **18**(1): 103–111, 2003. DOI: 10.1016/S0926-2245(02)00141-9.

[49] A. Fujioka and J. Inoguchi. Timelike surfaces with harmonic inverse mean curvature. In: *Surveys on geometry and integrable systems.* M. A. Guest, R. Miyaoka, and Y. Ohnita (Eds.). Vol. 51. Adv. Stud. Pure Math. Tokyo: Math. Soc. Japan, 2008, 113–141.

[50] E. Goursat. Sur un mode de transformation des surfaces minima. *Acta Math.* **11**(1-4): 257–264, 1887. DOI: 10.1007/BF02418050.

[51] E. Goursat. Sur un mode de transformation des surfaces minima. *Acta Math.* **11**(1-4): 135–186, 1887. DOI: 10.1007/BF02418047.

[52] U. Hertrich-Jeromin. *Introduction to Möbius differential geometry.* Vol. 300. London Mathematical Society Lecture Note Series. Cambridge: Cambridge University Press, 2003.

[53] U. Hertrich-Jeromin. Supplement on curved flats in the space of point pairs and isothermic surfaces: a quaternionic calculus. *Doc. Math.* **2**: 335–350, 1997.

[54] U. Hertrich-Jeromin, E. Musso, and L. Nicolodi. Möbius geometry of surfaces of constant mean curvature 1 in hyperbolic space. *Ann. Global Anal. Geom.* **19**(2): 185–205, 2001. DOI: 10.1023/A:1010738712475.

[55] D. A. Hoffman and W. H. Meeks III. A complete embedded minimal surface in $\mathbf{R^3}$ with genus one and three ends. *J. Differential Geom.* **21**(1): 109–127, 1985. DOI: 10.4310/jdg/1214439467.

[56] D. A. Hoffman and W. H. Meeks III. Embedded minimal surfaces of finite topology. *Ann. of Math. (2)* **131**(1): 1–34, 1990. DOI: 10.2307/1971506.

[57] T. Hoffmann. Discrete curves and surfaces. Ph.D. Thesis. Technische Universität Berlin, 2000.

[58] T. Hoffmann, W. Rossman, T. Sasaki, and M. Yoshida. Discrete flat surfaces and linear Weingarten surfaces in hyperbolic 3-space. *Trans. Amer. Math. Soc.* **364**(11): 5605–5644, 2012. DOI: 10.1090/S0002-9947-2012-05698-4.

[59] T. Hoffmann, A. O. Sageman-Furnas, and M. Wardetzky. A discrete parametrized surface theory in $\mathbb{R}^3$. *Int. Math. Res. Not. IMRN* **2017**(14): 4217–4258, 2017. DOI: 10.1093/imrn/rnw015.

[60] J. Inoguchi. Timelike surfaces of constant mean curvature in Minkowski 3-space. *Tokyo J. Math.* **21**(1): 141–152, 1998. DOI: 10.3836/tjm/1270041992.

[61] J. Inoguchi and S. Lee. Null curves in Minkowski 3-space. *Int. Electron. J. Geom.* **1**(2): 40–83, 2008.

[62] J. Inoguchi and M. Toda. Timelike minimal surfaces via loop groups. *Acta Appl. Math.* **83**(3): 313–355, 2004. DOI: 10.1023/B:ACAP.0000039015.45368.f6.

[63] L. P. Jorge and W. H. Meeks III. The topology of complete minimal surfaces of finite total Gaussian curvature. *Topology* **22**(2): 203–221, 1983. DOI: 10.1016/0040-9383(83)90032-0.

[64] H. Karcher. Construction of minimal surfaces. *Preprint No. 12, SFB 256, Universität Bonn*, 1989.

[65] H. Karcher. Embedded minimal surfaces derived from Scherk's examples. *Manuscripta Math.* **62**(1): 83–114, 1988. DOI: 10.1007/BF01258269.

[66] H. Karcher. The triply periodic minimal surfaces of Alan Schoen and their constant mean curvature companions. *Manuscripta Math.* **64**(3): 291–357, 1989. DOI: 10.1007/BF01165824.

[67] H. Karcher and K. Polthier. Construction of triply periodic minimal surfaces. *Philos. Trans. Roy. Soc. London Ser. A* **354**(1715): 2077–2104, 1996. DOI: 10.1098/rsta.1996.0093.

[68] Y. W. Kim, S.-E. Koh, H. Shin, and S.-D. Yang. Spacelike maximal surfaces, timelike minimal surfaces, and Björling representation formulae. *J. Korean Math. Soc.* **48**(5): 1083–1100, 2011. DOI: 10.4134/JKMS.2011.48.5.1083.

[69] Y. W. Kim and S.-D. Yang. Prescribing singularities of maximal surfaces via a singular Björling representation formula. *J. Geom. Phys.* **57**(11): 2167–2177, 2007. DOI: 10.1016/j.geomphys.2007.04.006.

[70] O. Kobayashi. Maximal surfaces in the 3-dimensional Minkowski space $\mathbf{L^3}$. *Tokyo J. Math.* **6**(2): 297–309, 1983. DOI: 10.3836/tjm/1270213872.

[71] O. Kobayashi. Maximal surfaces with conelike singularities. *J. Math. Soc. Japan* **36**(4): 609–617, 1984. DOI: 10.2969/jmsj/03640609.

[72] E. Koch and W. Fischer. On 3-periodic minimal surfaces with noncubic symmetry. *Z. Krist.* **183**(1-4): 129–152, 1988. DOI: 10.1524/zkri.1988.183.14.129.

[73] J. J. Konderak. A Weierstrass representation theorem for Lorentz surfaces. *Complex Var. Theory Appl.* **50**(5): 319–332, 2005. DOI: 10.1080/02781070500032895.

[74] B. G. Konopelchenko and W. K. Schief. Three-dimensional integrable lattices in Euclidean spaces: conjugacy and orthogonality. *R. Soc. Lond. Proc. Ser. A Math. Phys. Eng. Sci.* **454**(1980): 3075–3104, 1998. DOI: 10.1098/rspa.1998.0292.

[75] W. Kreft. Beiträge zur Goursat'schen Transformation der Minimalflächen. PhD thesis. Westf. Wilhelms-Univ., 1908.

[76] M. L. Leite. Surfaces with planar lines of curvature and orthogonal systems of cycles. *J. Math. Anal. Appl.* **421**(2): 1254–1273, 2015. DOI: 10.1016/j.jmaa.2014.07.047.

[77] K. Leschke and K. Moriya. Simple factor dressing and the López–Ros deformation of minimal surfaces in Euclidean 3-space. *Math. Z.* **291**(3-4): 1015–1058, 2019. DOI: 10.1007/s00209-018-2217-8.

[78] F. J. López and A. Ros. On embedded complete minimal surfaces of genus zero. *J. Differential Geom.* **33**(1): 293–300, 1991.

[79] R. López. Differential geometry of curves and surfaces in Lorentz-Minkowski space. *Int. Electron. J. Geom.* **7**(1): 44–107, 2014.

[80] M. A. Magid. Lorentzian isothermic surfaces in R^n_j. *Rocky Mountain J. Math.* **35**(2): 627–640, 2005. DOI: 10.1216/rmjm/1181069750.

[81] M. A. Magid. Timelike Thomsen surfaces. *Results Math.* **20**(3-4): 691–697, 1991. DOI: 10.1007/BF03323205.

[82] F. Manhart. Bonnet-Thomsen surfaces in Minkowski geometry. *J. Geom.* **106**(1): 47–61, 2015. DOI: 10.1007/s00022-014-0231-5.

[83] F. Manhart. Die Affinminimalrückungsflächen. German. *Arch. Math. (Basel)* **44**(6): 547–556, 1985. DOI: 10.1007/BF01193996.

[84] L. V. McNertney. One-parameter families of surfaces with constant curvature in Lorentz 3-space. Ph.D. Thesis. Providence, RI: Brown University, 1980.

[85] T. K. Milnor. Entire timelike minimal surfaces in $E^{3,1}$. *Michigan Math. J.* **37**(2): 163–177, 1990. DOI: 10.1307/mmj/1029004123.

[86] I. M. Mladenov. Generalization of Goursat transformation of the minimal surfaces. *C. R. Acad. Bulgare Sci.* **52**(5-6): 23–26, 1999.

[87] C. Müller. Planar discrete isothermic nets of conical type. *Beitr. Algebra Geom.* **57**(2): 459–482, 2016. DOI: 10.1007/s13366-015-0256-4.

[88] J. C. C. Nitsche. *Vorlesungen über Minimalflächen.* Die Grundlehren der mathematischen Wissenschaften, Band 199. Berlin: Springer-Verlag, 1975.

[89] K. Nomizu and T. Sasaki. *Affine Differential Geometry.* Vol. 111. Cambridge Tracts in Mathematics. Geometry of affine immersions. Cambridge: Cambridge University Press, 1994.

[90] A. W. Nutbourne and R. R. Martin. *Differential geometry applied to curve and surface design. Vol. 1.* Chichester: Ellis Horwood Ltd., 1988.

[91] Y. Ogata and K. Teramoto. Duality between cuspidal butterflies and cuspidal S_1^- singularities on maximal surfaces. *Note Mat.* **38**(1): 115–130, 2018. DOI: 10.1285/i15900932v38n1p115.

[92] Z. Olszak. A note about the torsion of null curves in the 3-dimensional Minkowski spacetime and the Schwarzian derivative. *Filomat* **29**(3): 553–561, 2015. DOI: 10.2298/FIL1503553O.

[93] H. Pabel. Deformationen von Minimalflächen. In: *Geometrie und ihre Anwendungen.* O. Giering and J. Hoschek (Eds.). Munich: Hanser, 1994, 107–139.

[94] J. Pérez and A. Ros. Properly embedded minimal surfaces with finite total curvature. In: *The global theory of minimal surfaces in flat spaces (Martina Franca, 1999)*. G. P. Pirola (Ed.). Vol. 1775. Lecture Notes in Math. Berlin: Springer, 2002, 15–66.

[95] H. Pottmann, Y. Liu, J. Wallner, A. I. Bobenko, and W. Wang. Geometry of multi-layer freeform structures for architecture. *ACM Trans. on Graph. (TOG)* **26**(3): 65–1–65–11, 2007. DOI: 10.1145/1276377.1276458.

[96] W. Rossman. *Isothermic surfaces in Möbius and Lie sphere geometry*. Vol. 22. Rokko Lectures in Mathematics. Kobe: Kobe University, 2014. arXiv: math/0602570.

[97] W. Rossman. Minimal surfaces in $\mathbf{R}^3$ with dihedral symmetry. *Tohoku Math. J. (2)* **47**(1): 31–54, 1995. DOI: 10.2748/tmj/1178225634.

[98] W. Rossman, M. Umehara, and K. Yamada. Irreducible constant mean curvature 1 surfaces in hyperbolic space with positive genus. *Tohoku Math. J. (2)* **49**(4): 449–484, 1997. DOI: 10.2748/tmj/1178225055.

[99] W. Rossman and M. Yasumoto. Discrete linear Weingarten surfaces with singularities in Riemannian and Lorentzian spaceforms. In: *Singularities in generic geometry*. S. Izumiya, G. Ishikawa, M. Yamamoto, K. Saji, T. Yamamoto, and M. Takahashi (Eds.). Vol. 78. Adv. Stud. Pure Math. Tokyo: Math. Soc. Japan, 2018, 383–410. DOI: 10.2969/aspm/07810383.

[100] S. D. Santos. Special isothermic surfaces. Ph.D. Thesis. University of Bath, 2008.

[101] R. Sauer and H. Graf. Über Flächenverbiegung in Analogie zur Verknickung offener Facettenflache. *Math. Ann.* **105**(1): 499–535, 1931. DOI: 10.1007/BF01455828.

[102] R. Sauer. *Differenzengeometrie*. Berlin-New York: Springer-Verlag, 1970.

[103] R. Sauer. Parallelogrammgitter als Modelle pseudosphärischer Flächen. *Math. Z.* **52**: 611–622, 1950. DOI: 10.1007/BF02230715.

[104] H. Schaal. Die Ennepersche Minimalfläche als Grenzfall der Minimalfläche von G. Thomsen. German. *Arch. Math. (Basel)* **24**: 320–322, 1973. DOI: 10.1007/BF01228217.

[105] W. K. Schief. On the unification of classical and novel integrable surfaces. II. Difference geometry. *R. Soc. Lond. Proc. Ser. A Math. Phys. Eng. Sci.* **459**(2030): 373–391, 2003. DOI: 10.1098/rspa.2002.1008.

[106] A. H. Schoen. *Infinite periodic minimal surfaces without self-intersections*. Technical Report NASA-TN-D-5541, C-98. Cambridge, MA: NASA Electronics Research Center, May 1970, 100.

[107] Y. Song and P. Wang. On transforms of timelike isothermic surfaces in pseudo-Riemannian space forms. *Results Math.* **71**(3-4): 1421–1442, 2017. DOI: 10.1007/s00025-016-0607-y.

[108] H. Takahashi. Tokuitenwo yurusu sanjigen jikūnaino jikanteki kyokushō kyokumenni tsuite [Timelike minimal surfaces with singularities in three-dimensional spacetime]. Japanese. Master thesis. Osaka University, 2012.

[109] G. Thomsen. Uber affine Geometrie XXXIX. German. *Abh. Math. Sem. Univ. Hamburg* **2**(1): 71–73, 1923. DOI: 10.1007/BF02951850.

[110] M. Umehara and K. Yamada. Maximal surfaces with singularities in Minkowski space. *Hokkaido Math. J.* **35**(1): 13–40, 2006. DOI: 10.14492/hokmj/1285766302.

[111] E. Vessiot. Sur les courbes minima. French. *C. R. Acad. Sci. Paris* **140**: 1381–1384, 1905.

[112] R. Walter. Explicit examples to the H-problem of Heinz Hopf. *Geom. Dedicata* **23**(2): 187–213, 1987. DOI: 10.1007/BF00181275.

[113] P. Wang. Blaschke's problem for timelike surfaces in pseudo-Riemannian space forms. *Int. J. Geom. Methods Mod. Phys.* **7**(7): 1147–1158, 2010. DOI: 10.1142/S0219887810004774.

[114] K. T. Weierstrass. Untersuchungen über die Flächen, deren mittlere Krümmung überall gleich Null ist. *Moatsber. Berliner Akad.* 612–625, 1866.

[115] T. Weinstein. *An introduction to Lorentz surfaces*. Vol. 22. de Gruyter Expositions in Mathematics. Berlin: Walter de Gruyter & Co., 1996.

[116] H. C. Wente. Constant mean curvature immersions of Enneper type. *Mem. Amer. Math. Soc.* **100**(478): vi+77, 1992. DOI: 10.1090/memo/0478.

[117] H. C. Wente. Counterexample to a conjecture of H. Hopf. *Pacific J. Math.* **121**(1): 193–243, 1986. DOI: 10.2140/pjm.1986.121.193.

[118] W. Wunderlich. Zur Differenzengeometrie der Flächen konstanter negativer Krümmung. *Österreich. Akad. Wiss. Math.-Nat. Kl. S.-B. IIa.* **160**: 39–77, 1951.

[119] Y. Xu. Symmetric minimal surfaces in $\mathbf{R^3}$. *Pacific J. Math.* **171**(1): 275–296, 1995. DOI: 10.2140/pjm.1995.171.275.

[120] M. Yasumoto. Weierstrass-type representations for timelike surfaces. In: *Singularities in Generic Geometry*. S. Izumiya, G. Ishikawa, M. Yamamoto, K. Saji, T. Yamamoto, and M. Takahashi (Eds.). Vol. 78. Adv. Stud. Pure Math. Tokyo: Math. Soc. Japan, 2018, 449–469. DOI: 10.2969/aspm/07810449.